

Iterative Learning Control Methods for Hybrid Wearable Robots

by

Vahidreza Molazadeh

Master of Science, Sharif University of Technology, 2015

Submitted to the Graduate Faculty of
the Swanson School of Engineering in partial fulfillment
of the requirements for the degree of

Doctor of Philosophy

University of Pittsburgh

2020

UNIVERSITY OF PITTSBURGH
SWANSON SCHOOL OF ENGINEERING

This dissertation was presented

by

Vahidreza Molazadeh

It was defended on

March 20, 2020

and approved by

Nitin Sharma, PhD, Associate Professor

Department of Mechanical Engineering and Materials Science

William Clark, PhD, Professor

Department of Mechanical Engineering and Materials Science

Jeffery Vipperman, PhD, Professor

Department of Mechanical Engineering and Materials Science

Zhi-Hong Mao, PhD, Professor

Department of Electrical and Computer Engineering and Department of Bioengineering

Dissertation Director: Nitin Sharma, PhD, Associate Professor

Department of Mechanical Engineering and Materials Science

Iterative Learning Control Methods for Hybrid Wearable Robots

Vahidreza Molazadeh, PhD

University of Pittsburgh, 2020

In this dissertation, iterative learning control methods for a hybrid exoskeleton to produce sitting-to-standing and walking in people with paraplegia are investigated. The hybrid exoskeleton combines a lower limb powered exoskeleton and functional electrical stimulation (FES). Limited research has been done to design control methods that provide shared modulation of FES and the powered exoskeleton. A major technical challenge to the implementation of control algorithms is their need to identify a user's musculoskeletal dynamics. Further, currently, setting desired regulation points or desired limb trajectories during sitting-to-standing and walking movements is a daunting task as it requires separate and coordinated design for each lower-limb. An inaccurate regulation of set-points or desired trajectories can possibly cause uncoordinated standing-up movements, potentially destabilizing the user.

Goal: The goal of this research is to design robust and adaptive control algorithms for hybrid exoskeletons that overcome the difficulty in model identification, can dynamically allocate the shared use of FES and the powered exoskeleton, and produce coordinated joint movements.

Objectives: The primary objective of this research is to develop robust control methods that iteratively learn modeling uncertainties in the hybrid exoskeleton (i.e., addressing model identification), while facilitating allocation of FES and motor input (i.e., resolving actuator redundancy) in the hybrid exoskeleton. The proposed control methods are experimentally validated for a sitting to standing task with the hybrid exoskeleton. The experiments are performed on human participants with no disabilities and a participant with spinal cord injury. The tasks that are accomplished to achieve the objectives are listed as:

- 1- Design and implement time-invariant desired joint trajectories by using virtual constraints for sitting-to-standing and walking motion
- 2- Derive and experimentally validate a robust control method that uses an arbitrarily switched allocation strategy to coordinate motor and FES.

3- Derive a control method that iteratively learns the system nonlinear dynamics and control gains.

4- Using an optimal and cooperative model predictive control method, instead of switched control, to allocate between motors and FES.

Table of Contents

Preface	x
1.0 Introduction	1
1.1 Background and Motivation	1
1.2 Existing Methods	2
1.3 Research Description	3
1.4 Contribution	6
2.0 A Switching Super Twisting Sliding Control	8
2.1 Introduction	8
2.2 General Walking Model Equation with Impact Effects	8
2.2.1 Joint Actuation	9
2.2.2 Switched System	10
2.3 Virtual Constraint and Controller Design	11
2.3.1 Virtual Constraint Design	11
2.3.2 Controller Design	12
2.3.3 Optimization Process	16
2.4 Simulation Results	17
2.4.1 Conclusion	17
3.0 A Switching Iterative Learning Control for following Virtual Constraints 23	
3.1 Introduction	23
3.2 General Walking Model Equation with Impact Effects	24
3.2.1 Joint Actuation	25
3.2.2 Switched System	26
3.3 Virtual Constraint and Controller Design	26
3.3.1 Virtual Constraint Design	26
3.3.2 Controller Design	27
3.3.3 Optimization Process	33

3.4	Simulation Results	34
3.5	Conclusion	34
4.0	A Robust Neural-Network Based Iterative Learning Controller for a Hybrid Exoskeleton	38
4.1	Introduction	38
4.2	General hybrid exoskeleton Lower Limb Model	40
4.2.1	Controller	41
4.2.2	Controller Design	42
4.2.3	Stability Analysis and Finite Time Convergence	46
4.3	Experimental Procedure and Results	50
4.4	Walking Simulation Results	58
4.5	Discussion	58
4.6	Conclusion	61
5.0	Shared Control of a Powered Exoskeleton and Functional Electrical Stimulation using Iterative Learning and Fatigue Optimization	63
5.1	Introduction	63
5.2	A Generalized Hybrid Exoskeleton Model	64
5.3	Control Development	65
5.3.1	Top-level Controller	68
5.3.2	Control distribution between FES and Motor	68
5.3.3	Predictive Allocation Strategy	69
5.4	Simulation Results	70
5.5	Experimental Results	75
5.6	Discussion	81
5.7	Conclusion	85
6.0	Summary and Future Works	86
	Bibliography	88

List of Tables

1	RMSE of joints angular position tracking results on Participants 1 and 2 in different iterations where $\iota = 0.1$ and $\varsigma = 0.9$ (RK: right knee, LK: left knee, RH: right hip, LH: left hip)	56
2	RMSE of joints angular position tracking results on Participants 3 and 4 in different iterations where $\iota = 0.1$ and $\varsigma = 0.9$ (RK: right knee, LK: left knee, RH: right hip, LH: left hip)	57
3	Steps of model predictive allocation strategy	71
4	Steps of model predictive allocation strategy	72
5	The fatigue and recovery time constants T_f and T_r for Participants 1, 2, and 3 on both legs	77
6	RMSE of trajectory tracking on each participant in the 1 st and 4 th iterations	83
7	RMSE of inputs from motors and FES on each participant in the 1 st and 4 th iterations	84

List of Figures

1	Schematic of the system	19
2	optimization process block diagram	20
3	FES and Motor control inputs versus time	20
4	Muscle fatigue behavior versus time	21
5	Angle and angular velocities of the linkages versus time	21
6	Identity function and function λ for various v_H^-	22
7	3-D diagram, showing attractive limit cycle of the system	22
8	3-D diagram, showing attractive limit cycle of the system	30
9	Root mean square versus iterations	35
10	Muscle fatigue behavior versus time	35
11	Angle and angular velocities of the linkages versus time	37
12	The hybrid exoskeleton testbed used for the experiments and the diagram of the control algorithm.	51
13	Snapshots of the standing up experiment performed on participant 1.	52
14	Knee joints angular profiles, tracking errors and the control inputs of Participant 1 for the 1 st iteration and the 4 th iteration, where $\iota = 0.2$ and $\varsigma = 0.8$	53
15	Hip joints angular profiles, tracking errors and the control inputs of Participant 1 for the 1 st iteration and the 4 th iteration, where $\iota = 0.2$ and $\varsigma = 0.8$	53
16	The snapshot sequences of participant 4 with complete SCI for a sitting to standing scenario.	54
17	Knee joints angular profiles, tracking errors, and the control inputs of Participant 4 in the 1 st and 4 th iteration	55
18	Hip joints angular profiles, tracking errors and the control inputs of Participant 4 in the 1 st and 4 th iteration	55
19	The linearly parameterizable part estimation, $\hat{\sigma}v_{f_1}$ and the not linearly parameterizable part estimation, \hat{v}_{f_2} of the system dynamic for Participant 4 with complete SCI	56

20	Means of RMSE improvement percentage on both knee and hip joints in different iterations across all participants, where $\iota = 0.1$ and $\varsigma = 0.9$	57
21	RMSE of participant 1 angular positions tracking for 2 impulse switching to allocation ratios.	59
22	Control inputs versus time	59
23	Angle of the linkages versus time	60
24	3-D diagram, showing attractive limit cycle of the system	60
25	FES torque allocation on the knee joint by using MPC	73
26	Normalized fatigue over time	73
27	Joint angles over time	74
28	Root mean square of the joint angles error vs iterations	74
29	The controller structure and the experimental testbed employed in this study	76
30	The snapshots of one successful sitting to standings trial for Participant 4 with paraplegia from a SCI	77
31	Knee and hip joints angular position tracking results of Participant 4 in the 1 st and 4 th iterations	78
32	Angular position tracking errors on both knee and hip joints of Participant 4 in the 1 st and 4 th iterations	78
33	RMSE improvement percentage of both knee and hip joints from the 1 st to the 4 th iterations for each participant	79
34	Changes of F_k , \hat{f}_2 , and $\hat{\sigma}f_1$ in the top level controller for Participant 4 in 4 iterations	80
35	Bottom-level control inputs for Participant 2 allocated by MPC in the 1 st and 4 th iterations	81
36	Forces applied on both walker handles in the 1 st iteration and 4 th iteration during sitting to standing experiments for Participant 4	82

Preface

My PhD study at the University of Pittsburgh was possible by help and support from a group of people. First of all, I greatly appreciate help from my parents and my PhD adviser, Dr. Nitin Sharma. Dr. Sharma's great knowledge and guidance helped me a lot during the research. He also provided scholarship support to accomplish my Ph.D. study. I will keep going, and hopefully make him proud of his student. I should also express my sincere respect and gratitude to the university employees and professors specifically Prof. Zhi-Hong Mao, Dr. Dicianno, Prof. Clark, Prof. Vipperman and Dr. Aaron Johnson for their knowledge and the guidance they shared with me over the years, in and out of the classroom. I'm also thankful to my colleagues in the lab: Dr. Bao, Dr. Alibeji, Mr. Zhiyu Sheng, Mr. Qiang Zhang, Mr. Albert Dodson, Mr. Abdullah Allangawi, Mr. Zunding Xiao, Mr. Ziyue Sun, and Mr. Ashwin Iyer.

I would like to dedicate this dissertation to my parents, Reza Molazadeh and Tahereh Pahlavan, for all the sacrifices they have made for me and my brother, Amirhossein, who helped me through this path. All I have in my life was impossible without god's and my parents support and help.

1.0 Introduction

1.1 Background and Motivation

Across the United States, approximately 3,400 people are diagnosed with complete paraplegia each year due to injuries to the spinal cord[66]. People with paraplegia have lower limb impairments that impede standing and walking activities. Functional electrical stimulation (FES) and powered exoskeleton are two potential technologies that can be used to restore standing and walking functions. FES was used for the first time in the 1960s by Kantrowitz et al. [41] and Liberson et al. [53] to correct drop foot. Since then FES has been shown to restore walking [31, 49, 37] and sitting to standing [17, 24, 70, 25, 1]. Despite the progress, the rapid onset of muscle fatigue during FES remains a huge challenge because it limits duration of standing and walking activities. A powered exoskeleton is an alternative rehabilitation technology for enabling people with paraplegia to regain lower-limb function. However, in the case of a complete paraplegia, the powered exoskeleton only passively moves limbs, unlike FES, which actively contracts the muscle. Active muscle contractions are preferred due to the fact that they increase metabolic energy consumption, and thus may help achieve recommended exercise targets for people with paraplegia[23]. Additionally, exoskeleton training may improve level of physical activity after spinal cord injury (SCI) [28].

Hybrid exoskeletons that constitute a powered exoskeleton and an FES system have recently been proposed to use the potential benefits and overcome the aforementioned shortcomings of FES and a powered exoskeleton, when used solely [23, 22, 45]. Powered exoskeleton and FES can work cooperatively to offset FES-induced fatigue effects. Further, the use of FES can potentially reduce actuator size and power consumption in the powered exoskeleton [36, 48, 44, 23, 22]. Moreover, the use of FES can provide therapeutic benefits such as preventing muscle atrophy, and increasing bone density [21]. Despite these benefits, very limited researches have been done for developing control methods for this type of devices which makes controlling the devices very challenging.

1.2 Existing Methods

One of the challenges in the control of the hybrid exoskeleton is to coordinate both FES and the powered exoskeleton during a lower limb activity. Recently, several different control approaches have been developed to coordinate FES and the powered exoskeleton. In [69], an adaptive control method allocated a portion of control to the FES and the rest was provided by electric motors for weighted leg lifts. In [10], the control strategy combined a PID controller for an active lower limb exoskeleton actuation with an event-based FES stimulation trigger. The hybrid movement was sub divided into pre-extension and extension sub-phases. The quadriceps muscles were activated by FES during the extension sub-phase because large assistive torque is required during this phase. The sub-phase is detected by using the ground reaction forces. In [73], an algorithm was developed that automatically adjusts the intensity of FES and the current delivered to an electric motor in a cycling scenario. Based on the mismatch between the desired and actual cadence, the algorithm switches automatically between resistive, uncontrolled, and assistive modes to accommodate for differences in functional impairment. In [45] a nonlinear model predictive control-based dynamic control allocation method was used to control seated knee extensions with a hybrid exoskeleton. FES and the electric motor were shown to work cooperatively and their respective control allocation were changed based on an FES-induced muscle fatigue model. In [5, 4], the coordination problem was addressed by deriving a controller that is inspired from the muscle synergy principle in the human motor control. In their subsequent works [8, 9], a dynamic surface control method with electromechanical delay compensation [7] was used in conjunction with the muscle synergy-inspired control scheme to overcome the allocation problem. The controllers in [9, 4, 5, 8, 64], require a fewer number of control signals to actuate multiple effectors in a hybrid exoskeleton.

While these techniques do solve the allocation problems in the hybrid exoskeleton, their implementation may depend on the identification of the musculoskeletal model of people with paraplegia. Due to day-to-day variations and inter-person variations in the musculoskeletal models, and the tedious process needed to identify the model [83, 45], it is difficult to implement these controllers in clinics. While numerous papers in FES control exist that use

high-gain controllers [77, 79] to provide robustness to modeling uncertainties or even adapt and learn the model using neural networks (NNs) [2, 3, 72, 78, 12], their implementation may need extensive tuning or offline training of neural networks. Iterative learning control (ILC) is a class of controllers that can help address this issue through online learning of unknown dynamics while improving the performance in consecutive multiple iterations or task cycles. An ILC was developed for a solo FES system for upper limb stroke rehabilitation in [51]. FES was applied to shoulder and elbow muscles of an able bodied participant for showing the learning capabilities of the controller. Authors in [56] developed an iterative learning method with input-dependent muscle fatigue model for a sole FES system, and it was used for the rehabilitation of upper limb. In [27], in a passivity based framework, an iterative learning control method was used to control a motorized cycle-rider rehabilitation system with FES. Their controller uses the concepts of passivity and adaptation so that it compensates for the time varying dynamics of the system. In another paper, [26], a feed forward repetitive learning control with autonomous state-dependent switching is developed for an uncertain, nonlinear cycle-rider system which yielded to lower cadence tracking error. However, the method does not address a way to learn the uncertain terms that are not linearly parameterizable. The uncertainties arise due to the use of FES in the hybrid exoskeleton because musculoskeletal dynamic will be involved.

1.3 Research Description

The goal of this research is to design control algorithms for hybrid exoskeletons that address the device control challenges including difficulty in model identification, resolving actuator redundancy due to the combined use of FES and the exoskeleton, and design of desired joint trajectories that coordinate limbs during standing and walking movements. The primary objective of this research is to develop robust control methods that can learn modeling uncertainties in the hybrid exoskeleton (i.e., addressing model identification), while facilitating allocation of FES and motor input (i.e., resolving actuator redundancy) in the hybrid exoskeleton.

For achieving the objective, in this dissertation, initially, a novel switching super twisting sliding mode is developed. This sliding mode control method development is the foundational controller used for the subsequent development of the set of robust iterative learning control methods in this thesis. In this control method, for avoiding joint miscoordination, we utilize a time independent profile, known as a virtual constraint, as a desired reference for joint angles. The virtual constraints is designed by utilizing the combination of a genetic-particle swarm optimization algorithm and a sequential quadratic programming (SQP) method. The genetic-particle swarm optimization algorithm (GAPSO) finds an acceptable semi-optimal virtual constraint for the system. This algorithm's results are used as a starting point for the SQP algorithm to find an optimal solution without a higher sampling rate and evolution cycles, which are required for GAPSO.

The switching strategy for control allocation between an electric motor and FES is based on the reduced or recovered control effectiveness (due to muscle fatigue and recovery) of user's muscle force output. The controller allows the user's muscles to recover when motors are mainly responsible for moving the limb joints and then when muscles have recovered, the FES can be used to generate walking. Because we used feedback linearization method for controlling the switched control system it has the downside of requiring exact model knowledge (EMK) during its implementation.

Therefore, in the next step, to remove its dependency on EMK, an iterative learning term is used to estimate system linearly parameterizable part of the dynamics. The stability of this new switching+learning controller is proved using the Lyapunov-based stability analysis. The overall stability, to account for impacts at the end of swing phase during walking, was shown numerically by using the Poincare maps. This new switching controller switches between an electric motor and FES based on muscle fatigue and recovery levels as well.

This preliminary version of the developed iterative learning controller could identify only the linearly parameterizable terms. Therefore, my next aim was to design a control method that iteratively learns both linearly parameterizable part of the dynamics and the other parts of the dynamics that can't be linearly parameterized in the human user's musculoskeletal model, thus improving sitting-to-standing tracking performance with minimal tuning. Addressing this problem is significant for clinical implementation, where inter-person and inter-day

variations can negatively affect control performance. The use of NNs is motivated for its ability to compensate or estimate unknown dynamics, including not linearly parameterizable and highly nonlinear terms, by choosing a suitable number of neurons and NN layers [52, 76, 75, 78]. A recurrent NN (RNN) was used due to its capability to capture the system behavior dynamically [76, 74, 11].

Therefore, in chapter 4, I developed an ILC method that uses two NNs. One NN is used to compensate for not linearly parameterizable terms that occur in the state dynamics. The other NN is used to compensate the unknown input gain function due to the use of FES. The NN update laws are developed through a discrete energy-based stability analysis in an iterative fashion.

Specifically, the second NN update law is designed to avoid singularity during its inverse, which is used to cancel the unknown input gain function. The control design is proven to be uniformly stable despite arbitrary switched FES and exoskeleton allocation. For avoiding joints miscoordination, instead of tracking the time-dependent trajectories for joints angles, the proposed ILC tracks time-invariant desired trajectories computed through the virtual constraints.

In the final step, a novel dynamic shared control of a powered exoskeleton and functional electrical stimulation (FES) that can adjust to the rapid onset of FES-induced muscle fatigue and deal with uncertain nonlinear relationships between FES inputs and joint torques is designed. The shared control design is achieved by using a bi-level hierarchical control. A neural network-based iterative learning controller (NNILC) is used as a top-level controller to learn and overcome uncertain nonlinear dynamics. The top level controller gives the total input demand to the bottom-level controller.

Then, a model predictive control (MPC)-based allocation strategy is used as the bottom-level controller to optimally distribute control contributions between FES and the knee motor of the exoskeleton. The MPC strategy uses the muscle fatigue and recovery characteristics of a participant's quadriceps muscles to modulate the shared control. A Lyapunov-like stability analysis is used to prove global asymptotic tracking of self-generated desired joint trajectories. The experimental results show robustness and optimality of the controller despite high model uncertainties.

1.4 Contribution

Chapter 2: I use a more rigorous non-smooth analysis framework described in [18, 20] to prove exponential tracking of the switching control design in [43] under arbitrary switching. Additionally the controller in [43] is extended to a multi-DOF walking plant, and instead of tracking time-based joint angle trajectories, movements of the lower-limb joints follow a self-generated limit cycle in a time-invariant controller that uses virtual constraints [32, 87, 34]. Virtual constraints were designed and implemented for hybrid exoskeletons for the first time in this novel controller. Virtual constraints were designed using a hierarchical hybrid Genetic algorithm-Particle swarm optimization (GAPSO), and sequential quadratic programming (SQP) optimization algorithm for the first time. The control issues a switching second order sliding mode controller to arbitrarily switch between different cases that depend on fatigue and choice of agonist and antagonist muscles. The simulation of the hybrid exoskeleton for a walking scenario showed the stability of the controller despite switching and ground effects. The results were published in [59].

Chapter 3: A new iterative learning switching controller that uses optimal virtual constraint is designed for a hybrid walking exoskeleton in this chapter. The novel synthesis of iterative learning control with sliding-mode control improves tracking performance and accuracy. A generalized switching control method is obtained to switch based on the stimulated muscle fatigue state. The effectiveness of the new iterative learning control for output tracking is tested in a walking model. According to the results, this technique helps the switching controller to decrease the RMS in each iteration. The results exhibit the excellent performance of the proposed technique to track the designed virtual constraints. The results were published in [60].

Chapter 4: A novel robust neural network (NN) based iterative learning controller is derived for a general model of a hybrid neuroprosthesis in the chapter. The controller is designed to track time-invariant profiles. The NN control strategy learns, in multiple iterations, the parametric uncertainties, unknown nonlinear dynamics and unknown input gains during the control of hybrid exoskeletons. The effectiveness of the new control is validated for a sitting to standing scenario. The experimental results are obtained from

human participants including a person with spinal cord injury. In few iterations, the synthesized controller improves root mean square error between desired positions and actual positions of the knee and hip joints by 51.18% and 57.31%, respectively. The sitting-to-standing control remains stable even when FES and electric motor allocation levels are switched. The results are under review as a journal paper in [63].

Chapter 5: A state of the art, hierarchical neural network based iterative learning control method, augmented with an MPC-based allocation strategy is developed. The experimental results for a sitting to standing task on three participants including a person with spinal cord injury validate the effectiveness of the proposed controller. The experimental results demonstrates an optimal dynamic shared control between FES and the powered exoskeleton, despite FES-induced muscle fatigue, modeling uncertainties, and high nonlinearity of the hybrid exoskeleton. Additionally, the proposed controller can help people with SCI to stand and walk with a hybrid neuroprosthesis without extensive tuning of control parameters. The results are published in [61] and under review in [62].

2.0 A Switching Super Twisting Sliding Control

2.1 Introduction

The objective of this chapter is to validate a novel switching super twisting sliding mode control method that is used to robustly do switching control allocating between electric motors and FESs and to elicit a walking motion. This allocation is done based on the amount that muscles are fatigued. This chapter would investigate, problem formulation, optimization for having optimal time invariant manifold known as virtual constraints, algorithm designing and simulation results. This sliding mode control method development is the foundational controller used for the subsequent development of the set of results in this thesis. The controller will be improved and extended to some other versions in the next chapters to deal with different problems and scenarios.

2.2 General Walking Model Equation with Impact Effects

The schematic of the dynamic system is demonstrated in Fig. 1. In this figure m is the mass of linkages and M_T is the mass of torso and M_H is the hip mass. O_1, O_2, O_h and O_T show the centers of mass positions. The complete walking model, N -DOF, including impulse effects of ground impact, can be expressed in the state space form as

$$\begin{cases} \dot{x} = f(x) + g(x)T & x^-(t) \notin S \\ x^+ = \Delta(x^-) & x^-(t) \in S \end{cases} \quad (2.1)$$

where $x = [q, \dot{q}]^T$, $q \in \mathbb{R}^N$ is defined as $q = [\theta_1 \theta_2 \cdots \theta_N]$. θ_i and ω_i are the i -th linkage deflection angle and angular velocity, respectively. $S = \{(\theta, \omega) \in \chi \mid \theta_i = \theta_i^d\}$, θ_i^d is the final value of θ_i in each step, which is used as a criterion for showing that a step is completed, $f(x)$ is the compact form of $\left[\begin{array}{ccc} \left[\begin{array}{cc} \Phi_{N \times N} & I_{N \times N} \end{array} \right]^T & \cdots & \cdots & [D(q)^{-1}(-C(q, \dot{q}) \cdot \dot{q} - G(q) + \tau_p)]^T \end{array} \right]^T$

and $g(x)$ is the compact form of $\left[\begin{array}{cccc} 0 & 0 & \cdots & \cdots \\ & & & [D(q)^{-1}(B(q)T)] \end{array} \right]^T$, where $D \in \mathbb{R}^{N \times N}$ is an inertia matrix, $C \in \mathbb{R}^{N \times N}$ is a Centripetal-Coriolis matrix, $G \in \mathbb{R}^N$ is a gravity vector, $B \in \mathbb{R}^{N \times N-1}$ is a control gain matrix, and $\tau_p(q, \dot{q}) \in \mathbb{R}^N$ is the passive joint moment. The moment at the i -th link is defined as

$$\tau_{p_i} = d_{1_i}(\vartheta_i - \vartheta_{0_i}) + d_{2_i}\dot{\vartheta}_i + d_{3_i}e^{d_{4_i}\vartheta_i} - d_{5_i}e^{d_{6_i}\vartheta_i}, \quad (2.2)$$

where ϑ_i is the anatomical joint angle, the angle between a segment's anatomical position and the position of the interest, of the i -th linkage, and ϑ_{0_i} and d_{j_i} are positive known constants. During the double support phase, the impact model of [38] is implemented under the assumption that the end of stance leg is in contact with the ground surface and is not slipping [86]. Using the law of conservation of angular momentum, the state values after impact, $x^+ = (q^+, \omega^+)$ can be evaluated by a function $\Delta \in \mathbb{R}^{2N \times 1}$ with the state values before impact, $x^- = (q^-, \omega^-)$.

2.2.1 Joint Actuation

Each linkage actuates with an electric motor, an electrical stimulation for the flexor muscles, and an electrical stimulation for the extensor muscles. The joint torque, T_i ($i = 1, 2, N$), can be expressed as

$$T_i = T_{ag_i} - T_{ant_i} + T_{m_i} \quad (2.3)$$

where T_{ag_i} and T_{ant_i} is the torque produced by the electrical stimulation of the agonist muscles and antagonist muscles, respectively and T_{motor} is the torque produced by motor. The motor torque at the i -th link is given as

$$T_{m_i} = k_{m_i}u_{m_i}, \quad (2.4)$$

The torque produced stimulation of agonist or antagonist muscles is given by

$$T_{ag/ant} = \psi_{l_i}(\vartheta_i)\psi_{v_i}(\dot{\vartheta}_i)\mu_i u_i, \quad (2.5)$$

In (2.5), $u_i \in \mathbb{R}$ is the normalized muscle stimulation, $\mu_i \in \mathbb{R}$ is the normalized fatigue variable, and $\psi_{v_i}(\dot{\vartheta}) \in \mathbb{R}^+$ and $\psi_{l_i}(\vartheta) \in \mathbb{R}^+$ are the torque-velocity relationships and torque-length of the flexor/extensor muscles, respectively. As in [70], torque-length and torque-velocity equations can be defined for i -th link as

$$\psi_{l_i}(\vartheta_i) = c_{1_i} e^{\frac{-(\vartheta_i - c_{2_i})^2}{2c_{3_i}}} \quad (2.6)$$

$$\psi_{v_i}(\dot{\vartheta}_i) = c_{4_i} \left[1 + \tanh \left(c_{5_i} \dot{\vartheta}_i + \frac{1}{c_{4_i}} \right) \right] \quad (2.7)$$

For guaranteeing that $\psi_{l_i}(\vartheta)\psi_{v_i}(\dot{\vartheta}) > 0$, the parameters $c_{1_i}; c_{3_i}; c_{4_i}; c_{5_i}$ should be positive and $c_{2_i} \geq 0$. The constraints on these parameters is due to the fact that the muscles can only ever produce a positive (contractile) force. In (2.4) $u_{m_i} \in \mathbb{R}$ is the current amplitude to the electric motor and $k_{m_i} \in \mathbb{R}$ is the torque constant of electric motor.

The normalized muscle fatigue, μ_i , in (2.5) can be calculated with the following differential equation [71]

$$\dot{\mu}_i = \frac{1}{t_{f_i}} (\mu_{min_i} - \mu_i) u_{h_i} + \frac{1}{t_{r_i}} (1 - \mu_i) (1 - u_{h_i}), \quad (2.8)$$

where, $t_{r_i}, t_{f_i} \in \mathbb{R}^+$ are time constants for fatigue recovery and fatigue in the muscle, respectively and $\mu_{min_i} \in (0, 1]$ is the fatigue constant.

2.2.2 Switched System

The switched system can be written as

$$\begin{aligned} D(q)\ddot{q} + C(q, \dot{q})\dot{q} + G(q) + \tau_p \\ = B(q) (a_n \iota_n T - (1 - a_n) \iota_n T + \varsigma_n T), \end{aligned} \quad (2.9)$$

where $a_n \iota_n T - (I_{N-1 \times N-1} - a_n) \iota_n T + \varsigma_n T = T$, $a_n \iota_n T = T_{ag}$, $-(I_{N-1 \times N-1} - a_n) \iota_n T = T_{ant}$, $\varsigma_n T = T_m$, and $\iota_n, \varsigma_n \in R^{+^{N-1 \times N-1}}$ are inside the finite set switch family, Ω , defined as

$$\begin{aligned} \Omega = \\ \{(\iota_1, \varsigma_1, a_1), (\iota_2, \varsigma_2, a_2), \dots, (\iota_{N_\Omega}, \varsigma_{N_\Omega}, a_{N_\Omega}) \dots \\ \dots \left| a_n = \text{diag} \begin{pmatrix} a_{n_1} & a_{n_2} & \dots & a_{n_{N-1}} \end{pmatrix}, \dots \right. \\ \dots \iota + \varsigma_n = I_{N-1 \times N-1}, a_{n_i} \in \{0, 1\}, n = 1, 2, \dots, N_\Omega \} \end{aligned} \quad (2.10)$$

with N_Ω number of combinations. Note that the choice of (ι_n, ς_n) is determined by muscle fatigue variable μ .

Remark. Note that a_{n_i} can be either 0 or 1 depending on the type of muscle being recruited (i.e., flexor or extensor). The above switched family shows the finite set of ratios in which the torque is distributed between FES and the motor.

2.3 Virtual Constraint and Controller Design

2.3.1 Virtual Constraint Design

The output, $y \in \mathbb{R}^{N-1}$, is defined as follows [87]:

$$y = h_0(q) - h_d(\theta(q)) \quad (2.11)$$

The size of y is $N - 1$ because the system has one degree of freedom underactuation for torso. In (2.11), $h_0(q)$ is a function of the independent joint angles is forced to follow $h_d(\theta(q))$, which is a desired virtual constraint function that is defined based on the Bezier polynomials as follows

$$h_d \circ \theta(q) = \begin{bmatrix} b_1 \circ w(q) \\ b_2 \circ w(q) \\ \vdots \\ b_{N-1} \circ w(q) \end{bmatrix}, \quad (2.12)$$

where

$$b_i(w) = \sum_{k=0}^M \alpha_k^i \frac{M!}{k!(M-k)!} w^k (1-w)^{M-k}. \quad (2.13)$$

In (2.13) α_k^i is the optimization parameter, M is an integer, specifying number of terms in Bezier polynomial, and w is defined as follows

$$w(q) = \frac{\theta(q) - \theta^-}{\theta^+ - \theta^-}. \quad (2.14)$$

In (2.14), $\theta(q)$ is a function of hybrid exoskeleton configuration variables and is defined as $\theta(q) = e_1 \theta_1 + e_2 \theta_2 + \dots + e_n \theta_N$. $e_i \in \mathbb{R}$ is chosen such that $\theta(q)$ is monotonically increasing. θ^- and θ^+ are minimum and maximum value of the $\theta(q)$ respectively.

2.3.2 Controller Design

The goal of the controller is to make the output zero or in other words, it forces $h_0(q)$ of the system, to follow the $h_d(q)$. For this purpose, initially, the output is rewritten as (2.15).

$$y = h(q) \quad (2.15)$$

Hence:

$$\frac{d^2y}{dt^2} = L_f^2 h(q, \dot{q}) + L_g L_f h(q) T \quad (2.16)$$

The invertibility of the decoupling matrix, $L_g L_f h$, at a specific point guarantees the zero dynamics existence and uniqueness in that point neighborhood [39]. Considering the output vector $y \in \mathbb{R}^{N-1}$ of the n-link walking model, for each single output y_i , ($i = 1 \dots N - 1$), if $\bar{y}_{1,i}, \bar{y}_{2,i} \in \mathbb{R}$ are chosen as $\bar{y}_{1,i} = y_i$ and $\bar{y}_{2,i} = \dot{y}_i$, (2.16) can be rewritten as the follows

$$\begin{aligned} \dot{\bar{y}}_{1,i} &= \bar{y}_{2,i} \\ \dot{\bar{y}}_{2,i} &= v_i + v_{d,i}, \end{aligned} \quad (2.17)$$

where v_i is the i th row from the $N - 1$ dimensional virtual input vector, $v(q) = L_{\hat{f}}^2 h(q, \dot{q}) + L_{\hat{g}} L_{\hat{f}} h(q) T$, related to the actual signal contributed from both FES and the motor, where \hat{f} and \hat{g} are nominal models of the dynamics in (2.1), $v_{d,i}$ is a corresponding input disturbance term v_i due to model uncertainty. In order to stabilize the system in (2.17), a controller will be designed based on the virtual input, $v_i = \varphi_i(\bar{y}_{1,i}, \bar{y}_{2,i}, t)$, ($i = 1 \dots N - 1$), so that the allocation coefficient pair (ι_n, ς_n) can be arbitrarily changed or switched, without affecting the stability property of the system. In the remaining part of this section, a Variable-Gain Super-Twisting Sliding Mode Control (VGSTSMC) is implemented and the robust exponential stability under the theoretical framework of non-smooth analysis and control theory [18, 20] is described.

For $i = 1 \dots N - 1$, let the sliding surface $s_i \in \mathbb{R}$ be defined as $s_i = \eta_i \bar{y}_{1,i} + \bar{y}_{2,i}$, such that the system in (2.17) will equivalently become

$$\begin{aligned} \dot{\bar{y}}_{1,i} &= -\eta_i \bar{y}_{1,i} + s_i \\ \dot{s}_i &= \eta_i \dot{\bar{y}}_{1,i} + \dot{\bar{y}}_{2,i} = \eta_i \bar{y}_{2,i} + v_i + v_{d,i} \end{aligned} \quad (2.18)$$

Using a Variable-Gain Super-Twisting Algorithm (VGSTA) [82],

$$v_i = -\eta_i \bar{y}_{2,i} - k_{1,i} \phi_{1,i}(s_i) - \int_0^t k_{2,i} \phi_{2,i}(s_i) dt \quad (2.19)$$

where $i = 1 \dots N - 1$, $\phi_{1,i}(s_i) = |s_i|^{\frac{1}{2}} \text{sign}(s_i) + k_{3,i} s_i$, $\phi_{2,i}(s_i) = \frac{1}{2} \text{sign}(s_i) + \frac{3}{2} k_{3,i} |s_i|^{\frac{1}{2}} \text{sign}(s_i) + k_{3,i}^2 s_i$, and $k_{1,i}(\bar{y}_{1,i}, \bar{y}_{2,i}, t)$ and $k_{2,i}(\bar{y}_{1,i}, \bar{y}_{2,i}, t)$ are variable gains. $k_{3,i}$ is a non-negative constant gain. As in [82], the i th disturbance is assumed to be modeled as, $v_{d,i} = v_{d,i_1} + v_{d,i_2}$ satisfying $|v_{d,i_1}| \leq \varrho_{1,i}(\bar{y}_{1,i}, \bar{y}_{2,i}, t) |\phi_{1,i}(s_i)|$ and $|\dot{v}_{d,i_2}| \leq \varrho_{2,i}(\bar{y}_{1,i}, \bar{y}_{2,i}, t) |\phi_{2,i}(s_i)|$, ($\varrho_{1,i}, \varrho_{2,i} > 0$), , and therefore, without loss of generality, can be written as follows

$$v_{d,i_1} = \rho_{1,i}(\bar{y}_{1,i}, \bar{y}_{2,i}, t) \phi_{1,i}(s_i) \quad (2.20)$$

$$\dot{v}_{d,i_2} = \rho_{2,i}(\bar{y}_{1,i}, \bar{y}_{2,i}, t) \phi_{2,i}(s_i), \quad (2.21)$$

where $|\rho_{1,i}(\bar{y}_{1,i}, \bar{y}_{2,i}, t)| \leq \varrho_{1,i}(\bar{y}_{1,i}, \bar{y}_{2,i}, t)$ and $|\rho_{2,i}(\bar{y}_{1,i}, \bar{y}_{2,i}, t)| \leq \varrho_{2,i}(\bar{y}_{1,i}, \bar{y}_{2,i}, t)$. Finally, system in (2.18) yields an exponential stability that is robust to input disturbance from model uncertainty, as long as the sliding surface $s_i = 0$ can be reached in finite time. Therefore, the following stability analysis is equivalent to prove finite time convergence of the subsystem $[\dot{s}_i, \dot{e}_{0,i}]^T = z_i(s_i, e_{0,i}, t)$, $i = 1 \dots N - 1$:

$$\begin{aligned} \dot{s}_i &= -(k_{1,i} - \rho_{1,i}) \phi_{1,i} + e_{0,i} \\ \dot{e}_{0,i} &= -(k_{2,i} - \rho_{2,i}) \phi_{2,i} \end{aligned} \quad (2.22)$$

Definition of proximal sub-differential is firstly reviewed as the following:

Definition: [20] For a lower semi-continuous function $V : \mathbb{R}^2 \rightarrow \mathbb{R}$, $\xi \in \mathbb{R}^2$ is a proximal-sub gradient of V at $\varpi_1 \in \mathbb{R}^2$, if $\exists \sigma, \varepsilon \in (0, +\infty)$ such that, $\forall \varpi_2 \in B(\varpi_1, \varepsilon)$,

$$V(\varpi_1) \geq V(\varpi_2) + \xi(\varpi_1 - \varpi_2) - \sigma^2 \|\varpi_1 - \varpi_2\|_2^2 \quad (2.23)$$

The set $\partial_P V$ of all proximal sub-gradients of V at ϖ_1 is the proximal sub-differential of V at ϖ_1 .

Theorem. [82] $\forall i=1 \dots N-1$, Subsystem in (2.22) can reach the equilibrium point $(s_i, e_{0,i}) = (0, 0)$ in finite time, if the control gains in VGSTA are selected as $k_{1,i} = \delta_i + \frac{1}{\beta_i} \left(\frac{1}{4\epsilon_i} (2\epsilon_i \varrho_{1,i} +$

$\varrho_{2,i})^2 + 2\epsilon_i \varrho_{2,i} + \epsilon_i + (2\epsilon_i + \varrho_{1,i})(\beta_i + 4\epsilon_i^2)$, $k_{2,i} = \beta_i + 4\epsilon_i^2 + 2\epsilon_i k_{1,i}$, $k_{3,i} \geq 0$, where $\beta_i, \epsilon_i, \delta_i$ are positive constants.

Proof: (i) Existence and uniqueness of the solution. According to [20] (Proposition 3) the solution to (2.22) exists in the sense of Filippov, that is, an absolutely continuous map, $[s_i(t), e_{0,i}(t)]^T : [0, +\infty) \rightarrow \mathbb{D} \subseteq \mathbb{R}^2$ satisfying the differential inclusion $K_i[z_i]([s_i, e_{0,i}]^T, t)$, $i = 1 \dots N - 1$, almost everywhere,

$$\begin{aligned} \begin{bmatrix} \dot{s}_i \\ \dot{e}_{0,i} \end{bmatrix} &\in K_i[z_i]([s_i, e_{0,i}]^T, t) : & (2.24) \\ \left\{ \begin{aligned} &= z_i(s_i, e_{0,i}, t), \\ &[s_i, e_{0,i}]^T \in \mathbb{D} \cap \{[s_i, e_{0,i}]^T \mid s_i \neq 0\} \\ &= \overline{co} \left\{ \begin{bmatrix} e_{0,i} \\ -\frac{1}{2}(k_{2,i} - \rho_{2,i}) \end{bmatrix}, \begin{bmatrix} e_{0,i} \\ \frac{1}{2}(k_{2,i} - \rho_{2,i}) \end{bmatrix} \right\}, \\ &[s_i, e_{0,i}]^T \in \mathbb{D} \cap \{[s_i, e_{0,i}]^T \mid s_i = 0\} \end{aligned} \right. \end{aligned}$$

Furthermore, by [20] (Proposition 5), (2.22) has a unique solution, due to the fact that the piece-wise continuous vector fields, near the manifold where discontinuity occurs, are driving the solution trajectories (except for $e_{0,i} = 0$, where trajectories slide along the manifold) transversally cross the manifold. Note that $[0, 0]^T \in K_i[z_i]$.

(ii) Lyapunov stability analysis. As explained in (i), (2.22) has a unique solution. Therefore, weak and strong stability coincide, and it will be sufficient to find a Lyapunov function $V_i(s_i, e_{0,i})$, for i th subsystem (2.22), satisfying the following conditions [20], for $\forall t \in [0, +\infty)$, : *Condition (A)* $V_i(s_i, e_{0,i})$ continuous on \mathbb{D} ; *Condition (B)* $V_i(0, 0) = 0$, $V_i(s_i, e_{0,i}) > 0$, $\forall [s_i, e_{0,i}]^T \in \mathbb{D} \setminus \{[0, 0]^T\}$; *Condition (C)* $\sup \underline{L}_{K_i[z_i]} V_i(s_i, e_{0,i}) \leq 0$, $\forall [s_i, e_{0,i}]^T \in \mathbb{D}$; *Condition (D)* $\sup \underline{L}_{K_i[z_i]} V_i(s_i, e_{0,i}) < 0$, $\forall [s_i, e_{0,i}]^T \in \mathbb{D} \setminus \{[0, 0]^T\}$, such that the system (2.22) is asymptotically stable. For simplicity purpose, index i ($i = 1 \dots N$) referring to i th output will be dropped hereafter in all the corresponding notations. First of all, (A) and (B) can be satisfied by choosing the Lyapunov function [82],

$$V = \zeta^T P_V \zeta \quad (2.25)$$

where, $\zeta = \left[|s|^{\frac{1}{2}}\text{sign}(s) + k_3s \quad e_0 \right]^T$, positive definite matrix $P_V = \begin{bmatrix} p_{11} & p_{12} \\ p_{21} & p_{22} \end{bmatrix}$ which is

equal to $\begin{bmatrix} \beta + 4\epsilon^2 & -2\epsilon \\ -2\epsilon & 1 \end{bmatrix}$. Explicitly, $V = (\beta + 4\epsilon^2)|s| + 2(\beta + 4\epsilon^2)k_3|s|^{\frac{3}{2}} + (\beta + 4\epsilon^2)k_3^2s^2 +$

$e_0^2 - 4\epsilon e_0|s|^{\frac{1}{2}}\text{sign}(s) - 4\epsilon k_3s e_0$. It should be noted that V is smooth (C^∞) everywhere, except $s \neq 0$, continuous but not locally Lipschitz at $s = 0$. Therefore, proximal sub-differential needs to be employed to compute the lower set-valued lie derivative $\underline{L}_{K[z]}V(s, e_0) \triangleq \{a \in \mathbb{R} : \exists \xi \in \partial_P V(s, e_0), \text{ such that } a = \min\{\xi^T r : r \in K[z]\}\}$, where proximal sub-differential is defined in **Definition 1**. Condition (C) and (D), describing a weak monotonic behavior of V , can then be satisfied by showing the following.

$$\partial_P V(s, e_0) : \begin{cases} = \nabla V(s, e_0), \\ [s, e_0]^T \in \mathbb{D} \cap \{[s, e_0]^T \mid s \neq 0\} \\ = \partial_P \left((\beta + 4\epsilon^2)|s| \right. \\ \quad \left. + (\beta + 4\epsilon^2)k_3^2s^2 \right. \\ \quad \left. + 2(\beta + 4\epsilon^2)k_3|s|^{\frac{3}{2}} - 4\epsilon k_3s e_0 \right. \\ \quad \left. + e_0^2 - 4\epsilon e_0|s|^{\frac{1}{2}}\text{sign}(s) \right) \supseteq \Omega, \\ [s, e_0]^T \in \mathbb{D} \cap \{[s, e_0]^T \mid s = 0\} \end{cases} \quad (2.26)$$

where, ∇ is an usual gradient due to the fact that V is smooth at that place, while $\Omega = \left[(\beta + 4\epsilon^2)[-1, 1] - 4\epsilon k_3e_0 - 4\epsilon e_0(+\infty) \quad 2e_0 \right]^T$ is obtained using the sum rule and geometric interpretation of V around $s = 0$. Therefore, lower set-valued lie derivative is computed as

$$\underline{L}_{K[z]}V(s, e_0) : \begin{cases} = \nabla^T V z, \\ [s, e_0]^T \in \mathbb{D} \cap \{[s, e_0]^T \mid s \neq 0\} \\ = \min_{\xi \in \partial_P, r \in K[z]} \{\xi^T r\}, \\ [s, e_0]^T \in \mathbb{D} \cap \{[s, e_0]^T \mid s = 0\} \end{cases} \quad (2.27)$$

When $s = 0, e_0 \neq 0, \{\xi^T r\} \supseteq (\beta + 4\epsilon^2)e_0[-1, 1] - 4\epsilon k_3e_0^2 - 4\epsilon e_0^2(+\infty) + e_0[-(k_2 - \rho_2), (k_2 - \rho_2)]$.

Apparently, $\min_{\xi \in \partial_P, r \in K[z]} \{\xi^T r\} = -\infty < 0$. When $s = 0, e_0 = 0$, since $-4\epsilon 0^2(+\infty)$ is an element

of $\{\xi^T r\}$, $\min \xi^T r$ will be non-positive. When $s \neq 0$, as shown in [82], with $\dot{\zeta} = \phi'_1 \mathcal{A} \zeta$, $\mathcal{A} = \begin{bmatrix} -(k - \rho_1) & 1 \\ -(k_2 - \rho_2) & 0 \end{bmatrix}$, $\phi'_1 = \frac{\partial \phi_1}{\partial s} = \frac{1}{2|s|^{\frac{1}{2}}} + k_3$, $\nabla^T V z = \frac{d}{dt} (V(s(t), e_0(t))) = -\phi'_1 \zeta^T (\mathcal{A}^T P + P \mathcal{A}) \zeta \leq -2\epsilon \left(\frac{1}{2|s|^{\frac{1}{2}}} + k_3 \right) \zeta^T \zeta < 0$, if control gains are selected according to Theorem 2.

(iii) Finite time convergence. It was shown in [65] that $V(s(t), e_0(t))$ is absolutely continuous. Therefore, with the results obtained in (ii) discussing the monotonicity behavior of V , Theorem 2 in [67] can be applied to ensure the finite time convergence. Estimation of the convergence time is given by [82].

To sum up, a second order VGSTSMC is designed to control system (2.17). Equivalently, for $\forall i = 1 \dots N - 1$, output y_i can be stabilized, robust to input disturbance, with proved exponential stability, allowing arbitrary switching. $V(s, e_0)$ given by (2.25) can be regarded as a common Lyapunov function of the switched system (2.9), so that the stability result is consistent with switching system theory [55].

2.3.3 Optimization Process

α_k^i in the Bezier polynomials in (2.13) should be defined in such a way that the walking be with minimum effort. A combination of GAPS0 and SQP method is used. The GAPS0 finds the global optimal convex region that satisfies the constraints and the SQP method finds the absolute optimal solution in that region, which is found by GAPS0. The cost function is defined as the follows

$$J_{Eff} = \frac{1}{2p_2^h(q_0^-)} \int_0^{T_s} \sum_{i=1}^m (u_i(t))^2 dt, \quad (2.28)$$

where $u_i(t)$ is the control input, m is the number of control inputs, p_2^h is the step length and T_s is the step duration time. The block diagram of the optimization process is depicted in Fig. 2. In Fig. 2, J_{Com} is the constraint cost, used in order that the system can satisfy its constraints.

2.4 Simulation Results

The walking simulation was run for 90 seconds for $N = 3$. The results are shown in Fig. 3- 5, which show a robust, optimal, and stable walking despite switching between FES and the motor as the muscle fatigues or recovers.

The motor control inputs and FES control inputs are displayed in Fig. 3 for first 20 seconds of the simulation run. The fatigue behavior which is the main criteria for switching is shown in Fig. (4). Fig. (5) shows the link angles and link angular velocities. In Fig. (5) the abrupt change in angular velocities is due to the impact with walking surface at each step. As it is clear from this figure, the states are renominated after the double support phase. For checking the stability of closed-loop system, controlled by (2.19), the function λ , which maps the system variables to the next step variables, is computed for v_H^- , in the boundary of $[0.5, 1.5]$. v_H^- is the hip horizontal velocity just before impact. The function λ is displayed in Fig. 6. This graph establishes the existence and the limit of the stability for walking motion. From Fig. 6, it can be concluded that λ is undefined for v_H^- less than 0.9180 m/s (In fact, with speeds less than 0.9180 m/s the resulting kinetic energy is less than required energy for making a step). It is also undefined for the speeds more than 1.36 m/s since for the outputs, the walking movement is too fast to converge in a single stride. A fixed point appears at $v_H^- = 1.037m/s$, and corresponds to the walking cycle that system is convergent to that. Fig. 7 represents the limit cycle over several steps with the simulating when $v_H^- = 1.1m/s$. The resulted trajectory is convergent to a limit cycle as shown in Fig. 7 which according to the Poincare map also supporting the stability in both the swing phase and the impact phase. The “flat” portion of the curve in the figure is an instantaneous transition due to the swing leg ground impact, where the star is the initial point of the trajectory.

2.4.1 Conclusion

A two-step optimization method and control design is presented in this chapter in order to design an optimal gait for a hybrid exoskeleton. The exoskeleton controlled based on the zero dynamic concept by using feedback linearization controller cascaded with a

switching second order sliding mode controller. By comparing the obtained results and the results of previous papers, it was observed that not only because of no need for trial and error in optimization phase, the implementation of this method has advantages, but also the recommended response with this method requires less control effort. The exoskeleton which uses this solution, enables people with paraplegia to use that for a longer time. For determining sufficient conditions for asymptotic tracking of the switched system the Lyapunov stability and the Poincare sections methods were used. Further, the obtained results from the hybrid zero dynamic control and the control allocation, based on the fatigue percentage, show that the exoskeleton is capable of walking more than it is possible with other exoskeleton. Finally, results showed that due to the use of virtual constraints, the exoskeleton is much more robust than other exoskeletons which traditionally use time dependent trajectory for guidance.

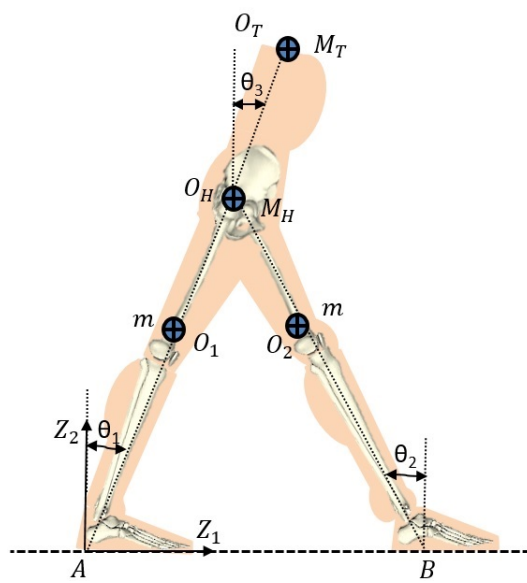


Figure 1: Schematic of the system

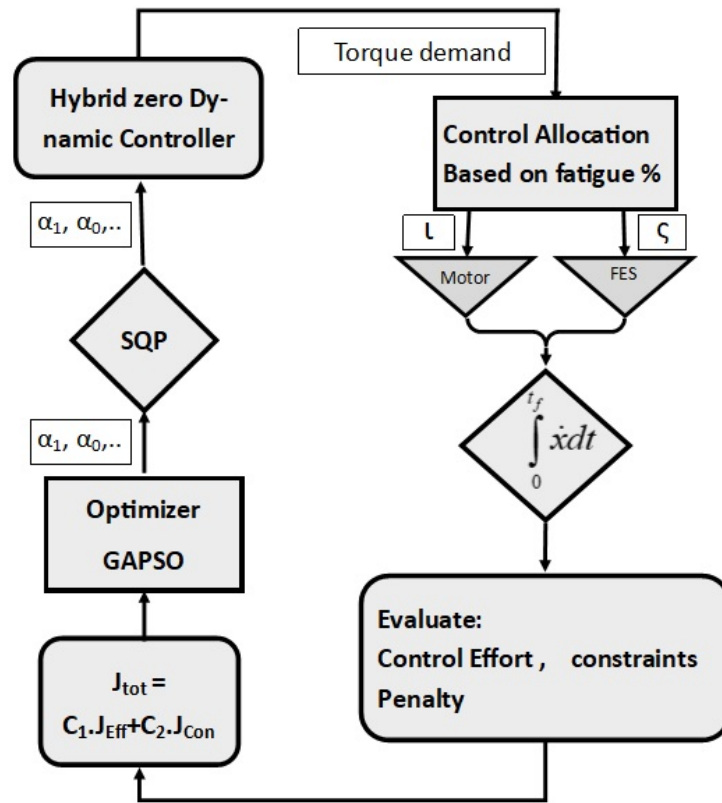


Figure 2: optimization process block diagram

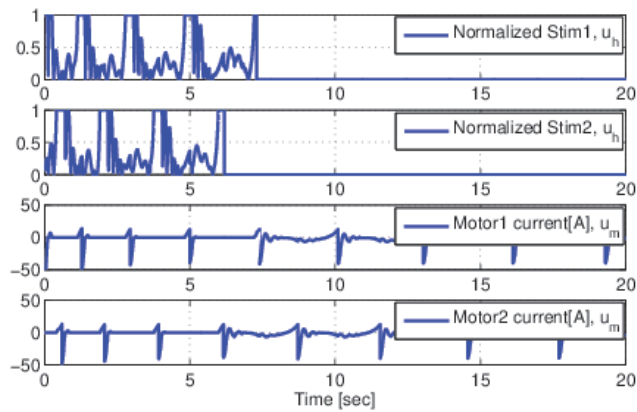


Figure 3: FES and Motor control inputs versus time

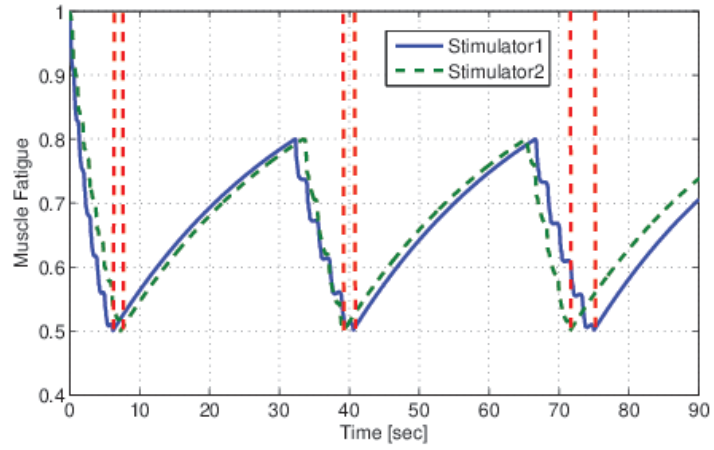


Figure 4: Muscle fatigue behavior versus time

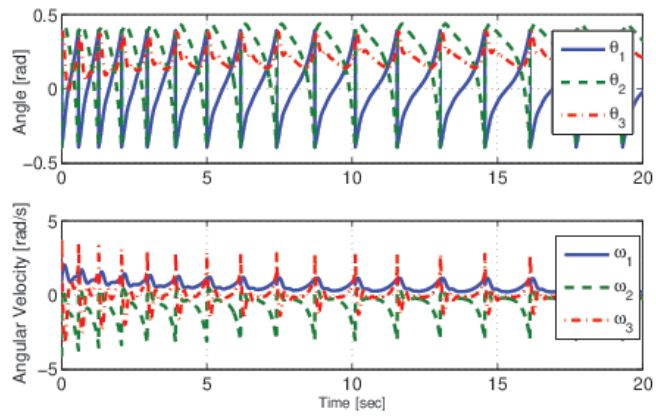


Figure 5: Angle and angular velocities of the linkages versus time

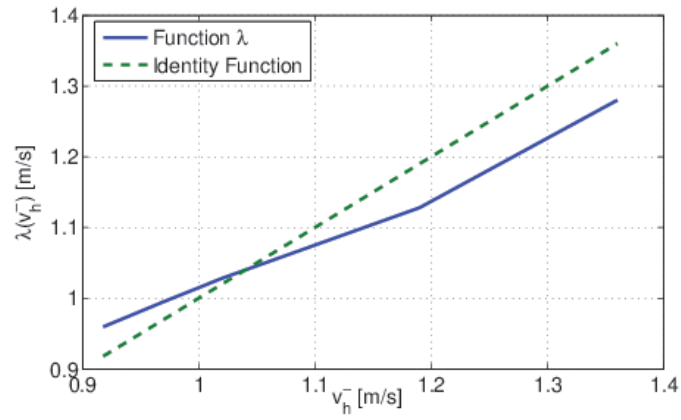


Figure 6: Identity function and function λ for various v_H^-

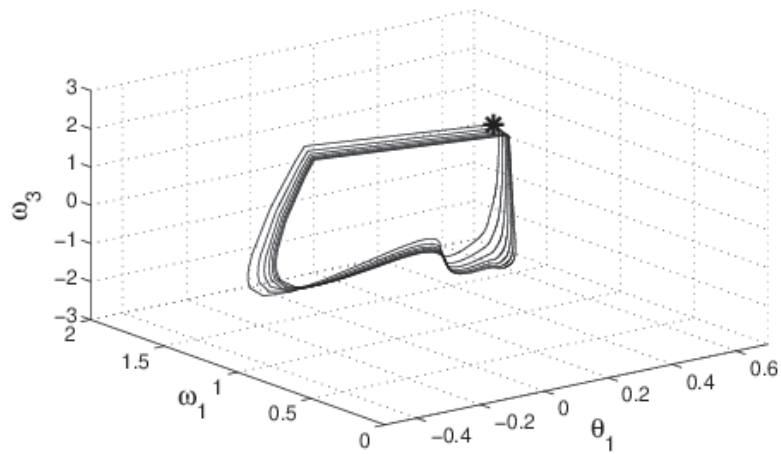


Figure 7: 3-D diagram, showing attractive limit cycle of the system

3.0 A Switching Iterative Learning Control for following Virtual Constraints

3.1 Introduction

This chapter extends the switching control design in the previous chapter, by adding an iteratively learning procedure. The lower-limb joints movement is self-generated via a time-invariant manifold, which is based on virtual constraints concept [87, 34, 33]. Therefore, a unified (virtual constraint + switching + iterative leaning) optimal, and robust controller is designed to achieve walking with the hybrid exoskeleton.

In the previous chapter, we used feedback linearization method for controlling the system, which has a considerable downside due to the requirement of exact model knowledge (EMK). Therefore, in this chapter, an iterative learning term is used to estimate system dynamics. The stability proof of the controller is provided using Lyapunov-like method. A more generalized switched cases family are considered in the design that do switching based on the normalized muscle fatigue variable. By utilizing the combination of sequential quadratic programming (SQP) method and genetic-particle swarm optimization algorithm (GAPSO), the virtual constraints are obtained.

GAPSO is used for achieving an acceptable semi-optimal manifold for system virtual constraints. Then, the results are utilized as a starting point for the SQP in order to find an optimal solution without needing to a high sampling rate and evolution cycles for GAPSO.

Therefore, with this procedure, the optimal solution that satisfies all the constraints can be obtained, and meanwhile, the virtual constraints can be re-planned in semi-real-time, which lets the system to redesign the virtual constraints after few steps if required. Additionally, the solution can get very close to the global optimal solution.

Achieving global optimal solution can have a hug power consumption benefit. This benefit lets the user to use the device for a longer time. In other words, it helps the patient to have his recovered abilities for a longer time. Having recovered abilities for a longer time can improve the patient's hope and enthusiasm for life.

3.2 General Walking Model Equation with Impact Effects

The complete model of walking, N -DOF which includes impulse effects of ground impact, in the state space form, can be written as,

$$\begin{cases} \dot{x} = f(x) + g(x)T & x^-(t) \notin S \\ x^+ = \Delta(x^-) & x^-(t) \in S \end{cases} \quad (3.1)$$

where $x = [q, \dot{q}]^T$, $q \in \mathbb{R}^N$ is defined as $q = [\theta_1 \theta_2 \cdots \theta_N]$. ω_i and θ_i are the i -th linkage angular velocity and deflection angle, respectively. $S = \{(\theta, \omega) \in \chi \mid \theta_i = \theta_i^d\}$, θ_i^d is the final value of θ_i in a step, which is a criterion which shows that a step is completed, $f(x)$ is the compact form of $\left[I_{N \times N} \quad [D(q)^{-1}(-C(q, \dot{q})\dot{q} - G(q) + \tau_p)] \right]^T$ and $g(x)$ is the compact form of $\left[0 \quad 0 \cdots 0 \quad [D(q)^{-1}(B(q)T)]^T \right]^T$, where $B \in \mathbb{R}^{N \times N-1}$ is a control gain matrix, $C \in \mathbb{R}^{N \times N}$ is a Centripetal-Coriolis matrix, $D \in \mathbb{R}^{N \times N}$ is an inertia matrix, $G \in \mathbb{R}^N$ is a gravity vector, $T \in \mathbb{R}^{N-1}$ is the input torque and $\tau_p(q, \dot{q}) \in \mathbb{R}^N$ is the passive joint moment in the musculoskeletal dynamics. The i -th link moment is defined as

$$\tau_{p_i} = d_{1_i}(\vartheta_i - \vartheta_{0_i}) + d_{2_i}\dot{\vartheta}_i + d_{3_i}e^{d_{4_i}\vartheta_i} - d_{5_i}e^{d_{6_i}\vartheta_i} \quad (3.2)$$

where ϑ_i is the joint anatomical angle which is the angle between the position of the interest and a segment's anatomical position, of the i -th linkage, and ϑ_{0_i} and d_{j_i} are positive constants. The double support phase is assumed as instantaneous moment that includes impulsive effect of ground impact, the impact model of [38] is implemented under the assumption that the stance leg end is not slipping and it is in contact with the ground surface [86]. Using the angular momentum conservation law, the post impact state values, $x^+ = (q^+, \omega^+)$ can be obtained by a function $\Delta \in \mathbb{R}^{2N \times 1}$ with the values of state before impact, $x^- = (q^-, \omega^-)$.

3.2.1 Joint Actuation

An electrical stimulation for the extensor muscles, an electrical stimulation for the flexor muscles, and an electric motor, actuate each linkage. The joint torque, T_i ($i = 1, 2, N$), can be defined as

$$T_i = T_{ag_i} - T_{ant_i} + T_{m_i} \quad (3.3)$$

where T_{ant_i} and T_{ag_i} are the torques produced by antagonist muscles and the electrical stimulation of the agonist muscles and, respectively and T_{motor} is the electrical motor torque. The torque of the motor at the i -th link is given as

$$T_{m_i} = k_{m_i} u_{m_i}. \quad (3.4)$$

In (3.4) $u_{m_i} \in \mathbb{R}$ is the current amplitude to the electric motor and $k_{m_i} \in \mathbb{R}$ is the torque constant of electric motor. The torque produced by electrical stimulation of antagonist and agonist muscles is obtained by

$$T_{ag/ant} = \psi_{l_i}(\vartheta_i) \psi_{v_i}(\omega_i) \mu_i u_i. \quad (3.5)$$

In (3.5), $\mu_i \in \mathbb{R}$ is the normalized fatigue variable, $u_i \in \mathbb{R}$ is the normalized muscle stimulation, and $\psi_{l_i}(\vartheta) \in \mathbb{R}^+$ and $\psi_{v_i}(\dot{\vartheta}) \in \mathbb{R}^+$ are the torque-length and torque-velocity relationships of the flexor/extensor muscles, respectively. As in [70], the equations of torque-length and torque-velocity, for i -th link, can be defined as

$$\psi_{l_i}(\vartheta_i) = c_{1_i} e^{\frac{-(\vartheta_i - c_{2_i})^2}{2c_{3_i}}} \quad (3.6)$$

$$\psi_{v_i}(\omega_i) = c_{4_i} \left[1 + \tanh \left(c_{5_i} \omega_i + \frac{1}{c_{4_i}} \right) \right]. \quad (3.7)$$

The parameters c_{1_i} , c_{3_i} , c_{4_i} and c_{5_i} should be positive for guaranteeing that $\psi_{l_i}(\vartheta) \psi_{v_i}(\omega_i) > 0$ and $c_{2_i} \geq 0$. The reason for constraining these parameters is that the muscles can only produce a positive contractile force. Based on [71], the following differential equation is used for deriving the normalized muscle fatigue, μ_i , in (3.5)

$$\dot{\mu}_i = \frac{1}{t_{f_i}} (\mu_{min_i} - \mu_i) u_{h_i} + \frac{1}{t_{r_i}} (1 - \mu_i) (1 - u_{h_i}) \quad (3.8)$$

where, $\mu_{min_i} \in (0, 1]$ is the fatigue constant and $t_{f_i}, t_{r_i} \in \mathbb{R}^+$ are time constants for fatigue and fatigue recovery in the muscle, respectively.

3.2.2 Switched System

The system with switching can be expressed as

$$\begin{aligned} D(q)\ddot{q} + C(q, \dot{q})\dot{q} + G(q) + \tau_p \\ = B(q) (a_n \iota_n T - (I_{N-1 \times N-1} - a_n) \iota_n T + \varsigma_n T) \end{aligned} \quad (3.9)$$

where $T = a_n \iota_n T - (I_{N-1 \times N-1} - a_n) \iota_n T + \varsigma_n T =, T_{ant} = a_n \iota_n T = T_{ag}, -(I_{N-1 \times N-1} - a_n) \iota_n T, T_m = \varsigma_n T,$ and $\iota_n, \varsigma_n \in R^{+^{N-1 \times N-1}}$ belongs to the finite set of switch family,

$$\begin{aligned} \Omega = \\ \{(\iota_1, \varsigma_1, a_1), (\iota_2, \varsigma_2, a_2), \dots, (\iota_{N_\Omega}, \varsigma_{N_\Omega}, a_{N_\Omega}) \dots \\ \dots \left| a_n = \text{diag} \begin{pmatrix} a_{n_1} & a_{n_2} & \dots & a_{n_{N-1}} \end{pmatrix} \right. \dots \\ \dots \iota + \varsigma_n = I_{N-1 \times N-1}, a_{n_i} \in \{0, 1\}, n = 1, 2, \dots, N_\Omega \} \end{aligned} \quad (3.10)$$

where N_Ω is the number of combinations. (ι_n, ς_n) are chosen based on the variable of muscle fatigue, μ .

Remark: Note that based on the type of muscle being recruited (i.e., flexor or extensor), a_{n_i} can be either 0 or 1.

3.3 Virtual Constraint and Controller Design

3.3.1 Virtual Constraint Design

Based on [87], the output, $y \in \mathbb{R}^{N-1}$, can be defined as

$$y = h_0(q) - h_d(\theta(q)). \quad (3.11)$$

The system has one degree of underactuation for torso. Therefore, the size of y is $N - 1$. In (3.11), $h_0(q)$ is a function of the independent joint angles which based on the current

arrangement of the output is obliged to follow $h_d(\theta(q))$, which is a desired virtual constraint function that can be expressed with the Bezier polynomials as

$$h_d(\theta(q)) = \begin{bmatrix} b_1(w(q)) \\ b_2(w(q)) \\ \vdots \\ b_{N-1}(w(q)) \end{bmatrix} \quad (3.12)$$

where

$$b_i(w) = \sum_{k=0}^M \varrho_k^i \frac{M!}{k!(M-k)!} w^k (1-w)^{M-k}. \quad (3.13)$$

In (3.13) M is an integer that shows the number of Bezier polynomial terms, ϱ_k^i is the optimization parameter, and w is obtained according to the following equation.

$$w(q) = \frac{\theta(q) - \theta^+}{\theta^- - \theta^+}. \quad (3.14)$$

In (3.14), θ^- and θ^+ are minimum and maximum value of the $\theta(q)$ respectively. $\theta(q)$ is a function of joints angles and is defined as $\theta(q) = \zeta_1\theta_1 + \zeta_2\theta_2 + \dots + \zeta_n\theta_n$. $\zeta_i \in \mathbb{R}$ are chosen such that $\theta(q)$ is increasing monotonically.

3.3.2 Controller Design

The the controller goal is to make the output zero or in other words, force $h_0(q)$ to follow $h_d(q)$. Therefore, the output should be expressed as follow (3.15).

$$y = h(q) \quad (3.15)$$

and thus

$$\frac{d^2y}{dt^2} = L_f^2 h(q, \dot{q}) + L_g L_f h(q) T \quad (3.16)$$

where $L_g L_f h$ is the decoupling matrix. The invertibility of this matrix at a point guarantees the zero dynamics uniqueness and existence in the neighborhood of that point [39]. For each

output y_i , ($i = 1 \dots N - 1$), if it is considered that $\bar{y}_{1,i} = y_i$ and $\bar{y}_{2,i} = \dot{y}_i$, (3.16) can be rewritten as

$$\begin{aligned}\dot{\bar{y}}_{1,i} &= \bar{y}_{2,i} \\ \dot{\bar{y}}_{2,i} &= \sigma_i^T v_{f,i} + v_{f_{2,i}} + v_{g,i} T_i + v_{d,i}\end{aligned}\quad (3.17)$$

where $\sigma_i^T v_{f,i} + v_{f_{2,i}}$ and $v_{g,i}$ are the i th row from $L_{\hat{f}}^2 h(q, \dot{q})$ and $L_{\hat{g}} L_{\hat{f}} h(q)$ respectively, where \hat{f} and \hat{g} are the dynamics nominal models in (3.1), $\sigma_i^T v_{f,i}$ is linearly parameterizable terms part of the system, $v_{f_{2,i}}$ is not linearly parameterizable terms and σ_i^T is unknown time variant function which is learned by iterative learning method and $v_{d,i}$ is the system and input disturbance term due to model uncertainty. For the system stabilization in (3.17), based on the virtual input, T_i , a controller is designed, so that the pair of allocation coefficient (ι_n, ς_n) can be switched arbitrarily without affecting the stability property of the system. In the next part, an iterative learning continuous integral sliding mode (ILCISM) control technique is implemented and the robust stability is proved.

For $i = 1 \dots N - 1$, let the sliding surface $s_i \in \mathbb{R}$ be defined as $s_i = \lambda_1 e(t) + \lambda_2 \dot{e}(t)$, where $e = (\bar{y}_{i,d} - \bar{y}_i)$, $\lambda_i \in \mathbb{R}$ is a constant number, $\bar{y}_{i,d}$ and \bar{y}_i are the desired and the system output respectively such that the system in (3.17) would equivalently become

$$\dot{s}_{k,i} = \sum_{j=1}^2 \lambda_j \bar{y}_{j,d} - \lambda_1 \bar{y}_{1,i} - \sigma_{k,i}^T v_{f,i} - v_{g,i} T_i - v_{f_{2,i}} - v_{d,i}. \quad (3.18)$$

Using the subsequent stability analysis and ILCISM [82],

$$\begin{aligned}T_{k,i} &= v_{g,i}^{-1} \left(\sum_{j=1}^2 \lambda_j \bar{y}_{j,d} - \lambda_1 \bar{y}_{1,i} - \hat{\sigma}_{k,i}^T v_{f,i} - v_{k,i} - v_{f_{2,i}} \right. \\ &\quad \left. + \alpha_{1,i} |s_{k,i}|^{\frac{2}{3}} \text{sgn}(s_{k,i}) + \frac{4}{3} \alpha_{2,i} \text{sgn}(s_{k,i}) + \alpha_{3,i} s_{k,i} \right)\end{aligned}\quad (3.19)$$

where $i = 1 \dots N - 1$, k is the number of iterations, and $\alpha_{1,i}$, $\alpha_{2,i}$ and $\alpha_{3,i}$ are positive constants. $\hat{\sigma}_{k,i}$ is the recursive part of the control. It is used for learning the unknown term $\sigma_{k,i}$, and based on the next section stability analysis, it can be derived using the following update law,

$$\hat{\sigma}_{k,i} = \hat{\sigma}_{k-1,i} - q\xi \left(\frac{4\eta}{3} |s_{k,i}|^{\frac{1}{3}} \text{sgn}(s_{k,i}) + \gamma s_{k,i} \right) \quad (3.20)$$

where q , η and γ are constants belonged to \mathbb{R}^+ . The variable $v_{k,i}$ in (3.12) is an integral term that is defined as below,

$$\dot{v}_{k,i} = -\beta_1 s_{k,i} - \beta_2 |s_{k,i}|^{\frac{1}{3}} \text{sgn}(s_{k,i}) \quad (3.21)$$

where both β_1 and β_2 are positive constants. By using the ILC law (3.19), the sliding surface dynamic equation can be rewritten as follow,

$$\begin{aligned} \dot{s}_{k,i} = & -\alpha_{3,i} s_{k,i} + \Psi_{k,i}^T v_{f,i} + v_{k,i} - v_{d,k,i} \\ & -\alpha_{1,i} |s_{k,i}|^{\frac{2}{3}} \text{sgn}(s_{k,i}) - \frac{4}{3} \alpha_{2,i} \text{sgn}(s_{k,i}) \end{aligned} \quad (3.22)$$

where $\Psi_{k,i} = \hat{\sigma}_{k,i} - \sigma_{k,i}$.

In order to show the stability of the hybrid system that includes the ground impact phase, the system Poincare map is shown in Fig. 8. As, it can be seen from the figure the gait cycle converges to the limit cycle which was designed by the optimization method in the previous step. According to the figure, the error of the system is reducing after each single ground impact in the compare of previous ground impact. For proving the stability of the learning controller, the following energy function is defined.

$$V_{k,i} = V_{k,i}^{(1)} + V_{k,i}^{(2)} + V_{k,i}^{(3)} + V_{k,i}^{(4)} \quad (3.23)$$

where $V_{k,i}^{(1)} = \frac{v_{k,i} v_{k,i}}{2}$, $V_{k,i}^{(2)} = \eta |s_{k,i}|^{\frac{4}{3}}$, $V_{k,i}^{(3)} = \gamma \frac{s_{k,i} s_{k,i}}{2}$, and $V_{k,i}^{(4)} = \frac{1}{2q} \int_{t_{0,k}}^t \Psi_{k,i}^T(\tau) \Psi_{k,i}(\tau) d\tau$. $t_{0,k}$ is the start time of k-th iteration. The convergence of the tracking error will be evaluated based on the difference between energy function between two iterations in a row according to the follow,

$$\Delta V_{k,i}^{(1)} = V_{k,i}^{(1)} - V_{k-1,i}^{(1)} \quad (3.24)$$

Therefore, using (3.16),

$$\begin{aligned} \Delta V_{k,i}^{(1)} = & -\frac{v_{k-1,i} v_{k-1,i}}{2} - \beta_1 \int_{t_{0,k}}^t v_{k,i} s_{k,i} d\tau \\ & -\beta_2 \int_{t_{0,k}}^t v_{k,i} |s_{k,i}|^{\frac{1}{3}} \text{sgn}(s_{k,i}) d\tau + C_1. \end{aligned} \quad (3.25)$$

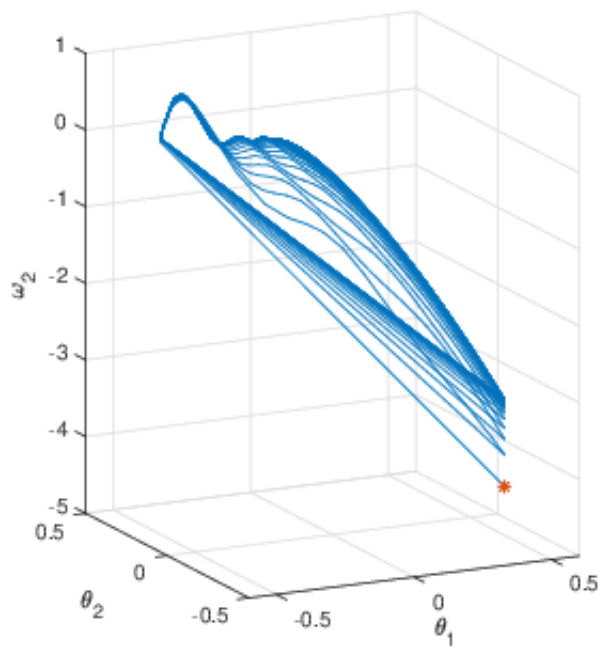


Figure 8: 3-D diagram, showing attractive limit cycle of the system

In a similar way, the difference of k-th and (k-1)-th iteration of the second energy function is obtained,

$$\Delta V_{k,i}^{(2)} = \eta |s_{k,i}|^{\frac{4}{3}} - \eta |s_{k-1,i}|^{\frac{4}{3}}, \quad (3.26)$$

Using the derivative of $|s_{k,i}|^{\frac{4}{3}}$, the above equation can be written in the following alternative way,

$$\Delta V_{k,i}^{(2)} = \frac{4}{3}\eta \int_{t_{0,k}}^t |s_{k,i}|^{\frac{1}{3}} \operatorname{sgn}(s_{k,i}) \dot{s}_{k,i} d\tau + C_2 - \eta |s_{k-1,i}|^{\frac{4}{3}}. \quad (3.27)$$

By substituting (3.22) into (3.27), new form of (3.27) is obtained as,

$$\begin{aligned} \Delta V_{k,i}^{(2)} &= +\frac{4\eta}{3} \int_{t_{0,k}}^t |s_{k,i}|^{\frac{1}{3}} \operatorname{sgn}(s_{k,i}) v_{k,i} d\tau \\ &\frac{-4\alpha_3\eta}{3} \int_{t_{0,k}}^t |s_{k,i}|^{\frac{4}{3}} d\tau + \frac{4\eta}{3} \int_{t_{0,k}}^t |s_{k,i}|^{\frac{1}{3}} \operatorname{sgn}(s_{k,i}) \Psi_{k,i}^T v_{f,i} d\tau \\ &- \frac{4\eta}{3} \int_{t_{0,k}}^t |s_{k,i}|^{\frac{1}{3}} \operatorname{sgn}(s_{k,i}) v_{d,i} d\tau - \frac{4\alpha_1\eta}{3} \int_{t_{0,k}}^t |s_{k,i}| d\tau \\ &- \eta |s_{k-1,i}|^{\frac{4}{3}} - \frac{16}{9}\eta\alpha_{2,i} \int_{t_{0,k}}^t |s_{k,i}|^{\frac{1}{3}} d\tau + C_2 \end{aligned} \quad (3.28)$$

If we consider $|v_{d,i}| \leq b_d$, where b_d is the upper bound of disturbance of the system, (3.28) can be rewritten as

$$\begin{aligned} \Delta V_{k,i}^{(2)} &\leq \frac{-4\alpha_3\eta}{3} \int_{t_{0,k}}^t |s_{k,i}|^{\frac{4}{3}} d\tau - \frac{16}{9}\eta\alpha_{2,i} \int_{t_{0,k}}^t |s_{k,i}|^{\frac{1}{3}} d\tau \\ &+ \frac{4\eta}{3} \int_{t_{0,k}}^t |s_{k,i}|^{\frac{1}{3}} \operatorname{sgn}(s_{k,i}) \Psi_{k,i}^T v_{f,i} d\tau - \frac{4\alpha_1\eta}{3} \int_{t_{0,k}}^t |s_{k,i}| d\tau \\ &- \eta |s_{k-1,i}|^{\frac{4}{3}} + \frac{4b_d\eta}{3} \int_{t_{0,k}}^t |s_{k,i}|^{\frac{1}{3}} d\tau \\ &+ \frac{4\eta}{3} \int_{t_{0,k}}^t |s_{k,i}|^{\frac{1}{3}} \operatorname{sgn}(s_{k,i}) v_{k,i} d\tau + C_2. \end{aligned} \quad (3.29)$$

The difference of k-th and (k-1)-th iteration of the third energy function is obtained as,

$$\begin{aligned} \Delta V_{k,i}^{(3)} &= \gamma \frac{s_{k,i} s_{k,i}}{2} - \gamma \frac{s_{k-1,i} s_{k-1,i}}{2} \\ &= \gamma \int_{t_{0,k}}^t s_{k,i} \dot{s}_{k,i} d\tau + C_3 - \gamma \frac{s_{k-1,i} s_{k-1,i}}{2} \end{aligned} \quad (3.30)$$

By substituting (3.22) into (3.30) and considering the upper bound, b_d for the uncertainties, the following is achieved.

$$\begin{aligned}
\Delta V_{k,i}^{(3)} &= -\gamma \frac{s_{k-1,i} s_{k-1,i}}{2} - \gamma \alpha_3 \int_{t_{0,k}}^t s_{k,i} s_{k,i} d\tau \\
&+ \gamma \int_{t_{0,k}}^t s_{k,i} \Psi_{k,i}^T v_{f,i} d\tau - \frac{4}{3} \alpha_{2,i} \gamma \int_{t_{0,k}}^t |s_{k,i}| d\tau + C_3 \\
&+ \gamma \int_{t_{0,k}}^t s_{k,i} v_{k,i} d\tau + b_d \gamma \int_{t_{0,k}}^t |s_{k,i}| d\tau - \gamma \alpha_1 \int_{t_{0,k}}^t |s_{k,i}|^{\frac{5}{3}} d\tau.
\end{aligned} \tag{3.31}$$

Difference of the last energy function between two iteration in a row can be written as,

$$\Delta V_{k,i}^{(4)} = \frac{1}{2b_q} \int_{t_{0,k}}^t \Psi_{k,i}^T \Psi_{k,i} d\tau - \frac{1}{2b_q} \int_{t_{0,k}}^t \Psi_{k-1,i}^T \Psi_{k-1,i} d\tau \tag{3.32}$$

where $b_q \in \mathbb{R}^+$. Based on (3.20) and [15], the following equation can be derived.

$$\begin{aligned}
&\frac{1}{2b_q} (\Psi_{k,i}^T \Psi_{k,i} - \Psi_{k-1,i}^T \Psi_{k-1,i}) \\
&= \frac{1}{b_q} (\hat{\sigma}_{k,i} - \sigma_i)^T (\hat{\sigma}_{k,i} - \hat{\sigma}_{k-1,i}) \\
&- \frac{1}{2b_q} (\hat{\sigma}_{k,i} - \hat{\sigma}_{k-1})^T (\hat{\sigma}_{k,i} - \hat{\sigma}_{k-1,i}).
\end{aligned} \tag{3.33}$$

Based on (3.20), (3.33) can be rearranged as,

$$\begin{aligned}
&\frac{1}{2b_q} (\Psi_{k,i}^T \Phi_{k,i} - \Psi_{k-1,i}^T \Psi_{k-1,i}) = \\
&\frac{-4\eta}{3} |s_{k,i}|^{\frac{1}{3}} \text{sgn}(s_{k,i}) \Psi_{k,i} v_{f,i} - \gamma s_{k,i} \Psi_{k,i}^T v_{f,i} \\
&- \frac{1}{2b_q} (\hat{\sigma}_{k,i} - \hat{\sigma}_{k-1})^T (\hat{\sigma}_{k,i} - \hat{\sigma}_{k-1,i})
\end{aligned} \tag{3.34}$$

(3.32) can be related to the sliding mode surface as follow,

$$\begin{aligned}
\Delta V_{k,i}^{(4)} &= -\frac{1}{2b_q} \int_{t_{0,k}}^t (\hat{\sigma}_{k,i} - \hat{\sigma}_{k-1})^T (\hat{\sigma}_{k,i} - \hat{\sigma}_{k-1,i}) d\tau \\
&- \gamma \int_{t_{0,k}}^t (s_{k,i} \Psi_{k,i}^T v_{f,i}) d\tau - \frac{4\eta}{3} |s_{k,i}|^{\frac{1}{3}} \text{sgn}(s_{k,i}) \Psi_{k,i} v_{f,i} d\tau.
\end{aligned} \tag{3.35}$$

For proving the convergence of both the output tracking error and sliding surface dynamics, we now combine the difference of energy terms for two iterations as below, based on considering $\beta_1 = \gamma$, $\beta_2 = \frac{4\eta}{3}$, $\alpha_{2,i} = \frac{\alpha_1\eta}{\gamma}$, $\gamma = \frac{4\alpha_1\eta}{3b_d}$ and $C_4 = C_3 + C_2 + C_1$

$$\begin{aligned}
\Delta V_{k,i} &= \Delta V_k^1 + \Delta V_k^2 + \Delta V_k^3 + \Delta V_k^4 \\
&\leq -\frac{v_{k-1}v_{k-1}}{2} - \eta |s_{k-1,i}|^{\frac{4}{3}} - \frac{4\alpha_3\eta}{3} \int_{t_{0,k}}^t |s_{k,i}|^{\frac{4}{3}} d\tau \\
&\quad - \alpha_3\gamma \int_{t_{0,k}}^t s_{k,i}s_{k,i}d\tau - \frac{4}{3}\alpha_1\eta \int_{t_{0,k}}^t |s_{k,i}| d\tau \\
&\quad - \gamma\alpha_1 \int_{t_{0,k}}^t |s_{k-1,i}|^{\frac{5}{3}} d\tau - \gamma \frac{s_{k-1,i}s_{k-1,i}}{2} + C_4
\end{aligned} \tag{3.36}$$

Based on the Poincare map conclusion about ground impact error, $C_4 \in \mathbb{R}^-$. Therefore, 3.36 can be simplified as,

$$\begin{aligned}
\Delta V_k &\leq -\frac{4\alpha_3\eta}{3} \int_{t_{0,k}}^t |s_{k,i}|^{\frac{4}{3}} d\tau \\
&\quad - \alpha_3\gamma \int_{t_{0,k}}^t s_{k,i}s_{k,i}d\tau - \frac{4}{3}\alpha_1\eta \int_{t_{0,k}}^t |s_{k,i}| d\tau,
\end{aligned} \tag{3.37}$$

(3.37) is negative definite whenever $s_{k,i} \neq 0$ at least in one of the moments, $t \in [t_{0,k}, T]$. Therefore, it can be concluded that V_k is convergent. Because $V_k(t) \in \mathbb{R}^+$, This convergence ensures V_k converges to zero. Therefore, it ensures that the sliding surface and Ψ which shows the estimation error of the system dynamics converge to zero. On the other hand, the dynamics of the sliding surface is Hurwitz. Hence, after this convergence, the output error is exponentially convergent to zero. To sum up, a second order ILCISM is designed to control system (3.17). In other word output y_i can be stabilized for $\forall i = 1 \dots N - 1$. It is robust with asymptotic stability to the system disturbance, allowing the system switches arbitrarily. $V(s, e_0)$ given by (3.23) can be regarded as a common switched system Lyapunov function (3.9), hence, the stability result is consistent with the switching system theory [55].

3.3.3 Optimization Process

In the optimization process, the value of α_k^i in the Bezier polynomials in (3.13) should be chosen optimally in order to have a minimum effort movement. GAPSO and SQP

combination method is used for the optimization. The global optimal convex region is found by GAPSO that satisfies the constraints and the absolute optimal solution is found by the SQP method in that region, which is found by GAPSO. For achieving minimum control effort, the following cost function is defined

$$J_{Eff} = \frac{1}{2p_2^h(q_0^-)} \int_0^{T_s} \sum_{i=1}^m (u_i(t))^2 dt, \quad (3.38)$$

where $u_i(t)$ is the control input, T_s is the step time, p_2^h is the length of a step, and m is the number of control inputs.

3.4 Simulation Results

The walking simulation is done for 100 seconds for $N = 3$. Fig. 9- 11 show the results, where a robust, optimal, and stable walking can be seen despite switching between the motor and FES as the muscle recovers or fatigues.

In Fig. 9, the root mean square (RMS) of the output tracking error is displayed during iterations of learning. As it can be seen it is reducing during different iterations. It shows that the learning term, σ_i is making system more robust in each iteration. The behavior of muscles fatigue is shown in Fig. (10) which is the switching main criterion. In the figure, S1-F and S1-S points show the stimulator 1 first and second switching respectively. S2-F and S2-S show the stimulator 2 first and second switching respectively. The angles and angular velocities of linkages are shown in Fig. (11). The abrupt angular velocities change, in Fig. (11), is because of the ground stride in each step. Note that the states are renominated after the double support phase which can be clearly seen in the figure.

3.5 Conclusion

A switching controller that combines iterative learning and sliding mode control has been developed to coordinate FES and the powered exoskeleton. The sliding mode-based iterative

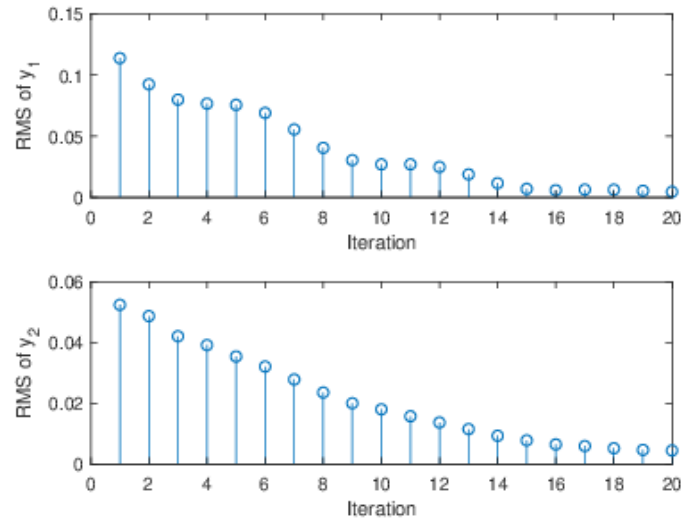


Figure 9: Root mean square versus iterations

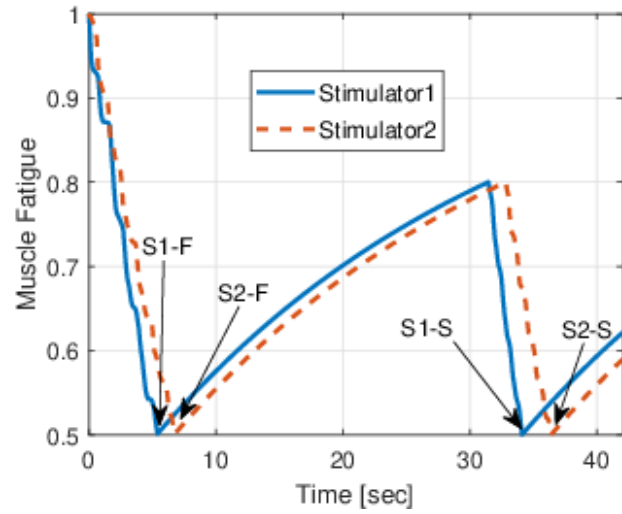


Figure 10: Muscle fatigue behavior versus time

learning control is used to learn the unknown functions in system dynamics. According to the simulated results, this technique helps the switching controller to decrease the RMS in each iteration. The controller stability was proven for using the Lyapunov-based stability analysis. The overall stability to account for impacts was shown numerically by using Poincare maps. The results exhibited the excellent performance of the proposed technique by-tracking the designed virtual constraints .

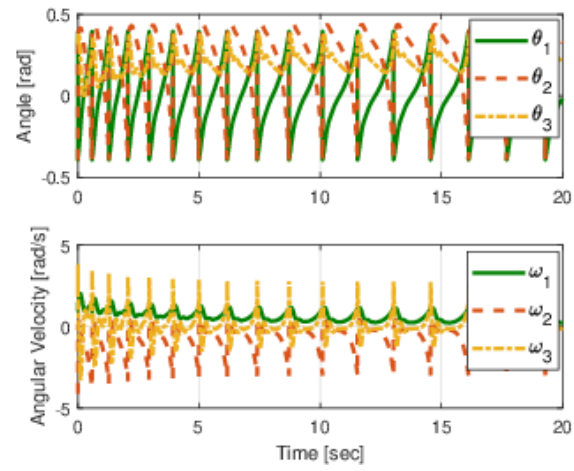


Figure 11: Angle and angular velocities of the linkages versus time

4.0 A Robust Neural-Network Based Iterative Learning Controller for a Hybrid Exoskeleton

4.1 Introduction

The implementation of the controller introduced in the previous chapter, depends on the identification of parameterizable part of the dynamics including the musculoskeletal model. Due to day-to-day variations and inter-person variations in the musculoskeletal dynamics, and the tedious process needed to identify the model [83, 45], it is difficult to implement these controllers in clinics. While numerous papers in FES control exist that use high-gain controllers [77, 79] to provide robustness to modeling uncertainties or even adapt and learn the model using neural networks (NNs) [2, 3, 72, 78, 12], their implementation may need extensive tuning or offline training of neural networks.

Iterative learning control methods are proposed to help address this issue through learning unknown dynamics while improving the performance in consecutive multiple iterations or task cycles. An ILC was developed for a solo FES system for upper limb stroke rehabilitation in [51]. FES was applied to shoulder and elbow muscles of an able bodied participant for showing the learning capabilities of the controller. Authors in [56] developed an iterative learning method with input-dependent muscle fatigue model for a sole FES system, and it was used for the rehabilitation of upper limb. In [27], in a passivity based framework, an iterative learning control method was used to control a cycle-rider system with FES. Their controller uses the concepts of passivity and adaptation so that it compensates for the time varying dynamics of the system.

In another paper [26], a feed forward repetitive learning control with autonomous state-dependent switching is developed for an uncertain cycle-rider system which yielded to lower cadence tracking error. In our recent previous chapter control method that published in [58], an iterative learning term was used to estimate a linearly parameterizable part of the system dynamics. However, the control implementation does not address a way to learn the uncertain terms that are not linearly parameterizable like musculoskeletal dynamic.

The aim of this chapter is to design a control method that enables sitting-to-standing function with a hybrid exoskeleton. The controller must iteratively learn a human user’s musculoskeletal model and improve sitting-to-standing tracking performance with minimal tuning. Addressing this problem is significant for clinical implementation, where inter-person and inter-day variations can negatively affect control performance. The contribution of this chapter is that a robust NN-based controller for a nonlinear hybrid exoskeleton model is proposed that iteratively learns parametric uncertainties.

The use of NNs is motivated for its ability to compensate or estimate unknown dynamics, including not linearly parameterizable and highly nonlinear terms by choosing a suitable number of neurons and NN layers [52, 76, 75, 78]. A recurrent NN (RNN) was used due to its capability to capture the system behavior dynamically [76, 74, 11]. Specifically two NNs are used. One NN is used to compensate for not linearly parameterizable terms that occur in the state dynamics. The other NN is used to compensate the unknown input gain function due to the use of FES. The NN update laws are developed through a discrete energy-based stability analysis in an iterative fashion. Specifically, the second NN update law is designed to avoid singularity during its inverse, which is used to cancel the unknown input gain function. The control design is proven to be uniformly stable despite arbitrary switched FES and exoskeleton allocation.

Desired time-dependent joint trajectories may be designed independently for both legs, and if there is a miscoordination during trajectory tracking it may cause joint misalignment, which can be potentially unsafe for the transition and, consequently, the desired lower-limb task may not be achieved. Using state dependent profiles allows the joints trajectories to self-generate via a time-invariant manifold known as virtual constraints. The concept presented in details in [87, 33, 34].

Therefore, in this study, instead of tracking the time-based trajectories for different joints, the proposed ILC tracks time-invariant desired trajectories computed through the virtual constraints. Walking simulation and extensive experiments are performed with a hybrid exoskeleton for a sitting to standing scenario. The results were obtained from human participants including a person with complete SCI. The results shows the ability of the controller for tracking the virtual constraints and keeping the system stable.

4.2 General hybrid exoskeleton Lower Limb Model

A general N degrees of freedom (N -DOF) of a hybrid exoskeleton can be written as

$$M(q)\ddot{q} + C(q, \dot{q})\dot{q} + G(q) + \tau_p = \tau_{input} \quad (4.1)$$

where $q \in \mathbb{R}^N$ is defined as $q = [\theta_1, \theta_2, \dots, \theta_N]$. θ_i ($i = 1, 2, \dots, N$) is the angular position of the i^{th} linkage. $C(\dot{q}, q) \in \mathbb{R}^{N \times N}$ is the Centripetal-Coriolis matrix, $M(q) \in \mathbb{R}^{N \times N}$ is the inertia matrix, $G(q) \in \mathbb{R}^N$ is the gravitational vector, and

$$\tau_{input} = B_E(q, \dot{q})u_E + B_M u_M$$

where $B_E(q, \dot{q}) \in \mathbb{R}^{N \times N}$ is the FES input matrix and $B_M \in \mathbb{R}^{N \times N}$ is the powered motor input matrix, $u_E \in \mathbb{R}^N$ is the normalized muscle stimulation, $u_M \in \mathbb{R}^N$ is the current amplitude of motor. In (4.1), $\tau_p \in \mathbb{R}^N$ is the passive moment of the targeted joint, which can be defined as

$$\tau_p \triangleq d_1(\vartheta - \vartheta_0) + d_2\dot{\vartheta} + d_3e^{d_4\vartheta} - d_5e^{d_6\vartheta} \quad (4.2)$$

where ϑ is the anatomical joint angle that is the angle between the position of interest and a segment's anatomical position of the linkage, and ϑ_0 and d_j ($j = 1, 2, \dots, 6$) are positive constants. The dynamics in (4.1) can be rewritten in the state space form as

$$\dot{x} = f(x) + g_E(x)u_E + g_M(x)u_M \quad (4.3)$$

where $x = [q, \dot{q}]^T$, $f(x)$ is the compact form of $\left[I_{N \times N} \dot{q}^T, [M^{-1}(\tau_p - G - C\dot{q})] \right]^T$, $g_E(x)$ and $g_M(x)$ are $\left[\Phi_{N \times N}, [M(q)^{-1}(B_E(q, \dot{q}))]^T \right]^T$ and $\left[\Phi_{N \times N}, [M(q)^{-1}(B_M)]^T \right]^T$, respectively.

4.2.1 Controller

A time-invariant sitting to standing movement profile called virtual constraint is designed offline through an optimization process. The desired profile is used later during the controller implementation. In the optimization process a hybrid exoskeleton movement is simulated in a closed control loop with various candidate virtual constraints [87]. The details of the optimization process are provided hereafter.

Firstly, the output error term $e \in \mathbb{R}^N$ is defined as

$$e = h(q) = h_0(q) - h_d(\theta(q)) \quad (4.4)$$

where $h_0(q) \in \mathbb{R}^N$ is an independent joint angle function that is obliged to follow $h_d(\theta(q)) \in \mathbb{R}^N$ [87]. $h_d(\theta(q))$ is a desired virtual constraint function and can be represented with the Bezier polynomials as

$$h_d(\theta(q)) = \begin{bmatrix} b_1(w(q)) \\ b_2(w(q)) \\ \vdots \\ b_N(w(q)) \end{bmatrix} \quad (4.5)$$

where

$$b(w) = \sum_{k=0}^M \varrho_k \frac{M!}{k!(M-k)!} w^k (1-w)^{M-k}. \quad (4.6)$$

In (4.6) M is an integer, showing the number of Bezier polynomial terms, ϱ_k is the parameter that is going to be optimized, and w is calculated according to the following equation

$$w(q) = \frac{\theta(q) - \theta^+}{\theta^- - \theta^+} \quad (4.7)$$

where θ^+ and θ^- are maximum value and minimum value of the $\theta(q)$, respectively, and $\theta(q) = \zeta_1\theta_1 + \zeta_2\theta_2 + \dots + \zeta_n\theta_n$. $\zeta_i \in \mathbb{R}$ is chosen such that $\theta(q)$ is monotonically increasing.

To obtain an optimal movement, the value of ϱ_k in the Bezier polynomials in (4.6) should be chosen optimally by an optimization process. The following cost function is defined based on the minimum control effort criteria

$$\begin{aligned} \min_{\varrho_k} J &= \frac{1}{2L_s} \int_0^{t_f} \left[\tau_{input}^T \tau_{input} + \frac{1}{2} h(q_{d_f})^T P h(q_{d_f}) \right] dt \\ s.t. & \quad M(q)\ddot{q} + C(q, \dot{q})\dot{q} + G(q) + \tau_p = \tau_{input} \end{aligned} \quad (4.8)$$

where t_f is the standing duration time, L_s is a normalizing constant, P is a weight matrix, q_{d_f} is the desired final condition, and q_{t_f} is the final standing angular positions.

4.2.2 Controller Design

In this subsection a robust NN based iterative learning switching control (RNNILSC) is designed. The control objective is to force $h_0(q)$ to follow $h_d(\theta(q))$ or in other words to drive the error e in (4.4) to zero in multiple iterations. After taking the second order time derivative of (4.4), the following differential equation can be obtained

$$\frac{d^2 e}{dt^2} = L_f^2 h(\theta) + L_{g_E} L_f h(\theta) u_E + L_{g_M} L_f h(\theta) u_M \quad (4.9)$$

where $L_f^2 h(\theta)$ is the second order Lie derivative of $h(\theta)$, and $L_{g_M} L_f h$ and $L_{g_E} L_f h$ are the decoupling matrices.

To facilitate the design of an ILC, $\bar{e}_1^{(i)} \in \mathbb{R}$, $\bar{e}_2^{(i)} \in \mathbb{R}$, $u_1^{(i)} \in \mathbb{R}$, and $u_2^{(i)} \in \mathbb{R}$ are defined as $\bar{e}_1^{(i)} = e_i$, $\bar{e}_2^{(i)} = \dot{e}_i$, $u_1^{(i)} = u_{E_i}$, and $u_2^{(i)} = u_{M_i}$, where subscript of i shows i^{th} element of a vector. Using (4.9), these errors due to the ILC in k^{th} iteration can be rewritten as

$$\begin{aligned} \dot{\bar{e}}_{1,k}^{(i)} &= \bar{e}_{2,k}^{(i)} \\ \dot{\bar{e}}_{2,k}^{(i)} &= \sigma^{T(i)} v_{f_{1,k}}^{(i)} + v_{f_{2,k}}^{(i)} + \Omega_k^{(i)} u_{1,k}^{(i)} \\ &\quad + v_g^{(i)} u_{2,k}^{(i)} + v_{d,k}^{(i)} \end{aligned} \quad (4.10)$$

where the subscription of k denotes that a variable is at k^{th} iteration, $v_{f_{2,k}}^{(i)} + \sigma^{T(i)} v_{f_{1,k}}^{(i)}$ is equal to i^{th} element of $L_f^2 h(\theta)$, $v_g^{(i)}$ and $\Omega_k^{(i)}$ are equal to i^{th} element of $L_{g_M} L_f h(\theta)$ and $L_{g_E} L_f h(\theta)$, respectively, for i^{th} input. f , g_M , and g_E were implied in (4.3). $\sigma^{T(i)} v_{f_{1,k}}^{(i)}$ is the linearly parameterizable part of $L_f^2 h(\theta)$ and $v_{f_{2,k}}^{(i)}$ is the not linearly parameterizable part of $L_f^2 h(\theta)$. In (4.10), $v_{d,k}^{(i)}$ is the system disturbance term due to modeling uncertainty and is bounded by

$$\left| v_{d,k}^{(i)} \right| \leq \bar{v}_d \in \mathbb{R}^+. \quad (4.11)$$

Without loss of generality, the superscript i ($i = 1, 2, \dots, N$) will be dropped hereafter in all the corresponding notations. σ^T is an unknown state independent function which is going

to be learned by an iterative learning method, $v_{f_{2,k}}$ and Ω_k are going to be learned by NNs. $v_{f_{2,k}}$ and Ω_k are represented by two NNs as

$$v_{f_{2,k}} = W^T \Theta_k(V_k X_k) + \varepsilon_{1,k}(X_k) \quad (4.12)$$

$$\Omega_k = R^T \phi_k(X_k) + \varepsilon_{2,k}(X_k) \quad (4.13)$$

where $X_k \in \mathbb{R}^{2N+1}$ is the augmented input vector for two NNs and is defined as $X_k = \begin{bmatrix} 1 & x_k \end{bmatrix}^T$. The two NNs ideal weight matrices are $W \in \mathbb{R}^{N_2+1}$ and $R \in \mathbb{R}^{N_\Omega}$. The input layer is made of $2N + 1$ neurons, N_2 and N_Ω are the number of neurons in the hidden layer of the NNs, and N is the number of the output layer neurons. The NN activation function in (4.12) that maps the input layer to the hidden layer is denoted as $\Theta_k : \mathbb{R}^{2N+1} \rightarrow \mathbb{R}^{N_2+1}$. The activation function in (4.13) that maps the input layer to the output layer is denoted as $\phi_k : \mathbb{R}^{2N+1} \rightarrow \mathbb{R}^{N_\Omega}$. The unknown functional reconstruction errors for the two NNs are denoted as $\varepsilon_{1,k} \in \mathbb{R}$ and $\varepsilon_{2,k} \in \mathbb{R}$ and are bounded which can be written as $|\varepsilon_{1,k}| \leq \bar{\varepsilon}_1$ and $|\varepsilon_{2,k}| \leq \bar{\varepsilon}_2$, where $\bar{\varepsilon}_1, \bar{\varepsilon}_2 \in \mathbb{R}^+$. The estimates of the ideal NNs that approximate $v_{f_{2,k}}$ and Ω_k are learned in an iterative fashion. The k^{th} iteration of their estimates, denoted as $\hat{v}_{f_{2,k}}$ and $\hat{\Omega}_k$, are represented as

$$\hat{v}_{f_{2,k}} = \hat{W}_k^T \Theta_k(\hat{V}_k X_k) \quad (4.14)$$

$$\hat{\Omega}_k = \hat{R}_k^T \phi_k(X_k) \quad (4.15)$$

where $\hat{W}_k \in \mathbb{R}^{N_2+1}$ and $\hat{R}_k \in \mathbb{R}^{N_\Omega}$ are the estimates of ideal weights in k^{th} iteration.

A closed loop feedback component, U_k that is going to be used subsequently is defined as

$$U_k = -F_{1,k} - \hat{v}_{f_{2,k}} - \hat{\sigma}_k v_{f_{1,k}} \quad (4.16)$$

where $\hat{\sigma}_k$ is an estimate for σ and $F_{1,k}$ is described as

$$F_{1,k} = \frac{1}{\lambda_2} \left(\lambda_1 \bar{e}_{2,k} + \lambda_2 \left(\alpha_3 s_k + \frac{4}{3} \alpha_2 \text{sgn}(s_k) \right) - \lambda_2 v_k \right) \quad (4.17)$$

where $\alpha_2 \in \mathbb{R}^+$, $s_k \in \mathbb{R}$ is evaluated as $s_k = \lambda_1 \bar{e}_{1,k}(t) + \lambda_2 \bar{e}_{2,k}(t)$, where $\lambda_i \in \mathbb{R}^+$ is a positive constant, and $v_k \in \mathbb{R}$ is an integral term that is defined as

$$\dot{v}_k = -\beta_1 s_k - \beta_2 v_k, \quad (4.18)$$

where β_1 and β_2 are positive constants.

Consider FES input u_1 at the k^{th} iteration

$$u_{1,k} = -\iota_n \psi_k^{-1} U_k \quad (4.19)$$

where ι_n is FES allocation coefficient and ψ_k is defined as

$$\psi_k = \hat{\Omega}_k + \left(\varrho \left(\hat{\Omega}_k \right) + \beta \right) \quad (4.20)$$

ψ_k is designed such that to avoid a singularity in ψ_k^{-1} when $\hat{\Omega}_k$ is equal to zero. The spectral radius of $\hat{\Omega}_k$, $\varrho_k \left(\hat{\Omega}_k \right) \in \mathbb{R}^+$, and a control gain, $\beta \in \mathbb{R}^+$ are added to ψ_k [14, 6].

$u_{2,k}$ is electric motors feedback component and is defined as

$$u_{2,k} = -\varsigma_n v_g^{-1} U_k \quad (4.21)$$

Where ς_n is allocation coefficient for the electric motors. The pair of allocation coefficients (ι_n, ς_n) are introduced to deal with the input redundancy and can be switched arbitrarily as long as the following conditions are satisfied

$$\iota_n + \varsigma_n = 1 \quad (4.22)$$

$$|u_{1,k}| \leq 1. \quad (4.23)$$

Due to the use of NN, iterative learning, and arbitrary allocation switching between feedback components of FES and electric motor, we call the overall robust control strategy as RNNILSC. Using (4.16), (4.17), (4.19), (4.21), (4.22), and adding and subtracting $\psi_k u_{1,k}$ to (4.10) would result in

$$\begin{aligned} \dot{\bar{e}}_{2,k} &= E_{s,k} + \Psi_k v_{f_{1,k}} + \tilde{\Omega}_k u_{1,k} \\ &- \alpha_3 s_k - \frac{4}{3} \alpha_2 \text{sgn}(s_k) + v_k - \frac{\lambda_1}{\lambda_2} \bar{e}_{2,k} + v_{d,k} \end{aligned} \quad (4.24)$$

where $E_{s,k} = v_{f_{2,k}} - \hat{v}_{f_{2,k}}$ is the not linearly parameterizable estimation error for the NN. Besides, $\tilde{\Omega}_k = \Omega_k - \psi_k$ and $\Psi_k = \sigma - \hat{\sigma}_k$. Based on (4.13) and (4.20), $\tilde{\Omega}_k$ can be expressed as

$$\tilde{\Omega}_k = \tilde{R}_k^T \phi(X_k) + \beta_{\varepsilon,k} \quad (4.25)$$

where $\tilde{R}_k = R_k - \hat{R}_k$, $\beta_{\varepsilon,k} = \varepsilon_{2,k} - \left(\varrho_k \left(\hat{\Omega}_k \right) + \beta \right)$ and $\beta_{\varepsilon,k}$ is bounded by

$$|\beta_{\varepsilon,k}| \leq \bar{\beta}_\varepsilon \in \mathbb{R}^+. \quad (4.26)$$

Therefore, (4.24) can be written as

$$\begin{aligned} \dot{\bar{e}}_{2,k} &= E_{s,k} + \Psi_k v_{f_{1,k}} + \left(\tilde{R}_k^T \phi(X_k) + \beta_{\varepsilon,k} \right) u_{1,k} \\ &\quad - \alpha_3 s_k - \frac{4}{3} \alpha_2 \text{sgn}(s_k) + v_k - \frac{\lambda_1}{\lambda_2} \bar{e}_{2,k} + v_{d,k}. \end{aligned} \quad (4.27)$$

By taking the time derivative of s_k , the \dot{s}_k dynamics is given as

$$\begin{aligned} \dot{s}_k &= \lambda_2 \left(-\alpha_3 s_k - \frac{4}{3} \alpha_2 \text{sgn}(s_k) + v_k + v_{d,k} \right. \\ &\quad \left. + \Psi_k v_{f_{1,k}} + \beta_\varepsilon u_{1,k} + \tilde{R}_k^T \phi_k(X_k) u_{1,k} + E_{s,k} \right). \end{aligned} \quad (4.28)$$

Based on the subsequent stability analysis, weight matrices for NNs are calculated using the following method

$$\hat{W}_{k_j} = \hat{W}_{(k-1)_j} - \kappa_1 \frac{\partial E_b}{\partial \hat{W}_{(k-1)_j}} \quad (4.29)$$

$$\hat{V}_{k_j} = \hat{V}_{(k-1)_j} - \kappa_2 \frac{\partial E_b}{\partial \hat{V}_{(k-1)_j}} \quad (4.30)$$

where $\kappa_1 \in \mathbb{R}^+$ and $\kappa_2 \in \mathbb{R}^+$ are user defined positive constants and E_b is defined as

$$E_b = \frac{1}{2} \left(\hat{v}_{f_{2,k}} - \hat{v}_{f_{2,k-1}} + \xi \gamma s_k \right)^2 \quad (4.31)$$

$$\hat{v}_{f_{2,k}} = 0, \text{ when } k = -1 \quad (4.32)$$

where $\xi \in \mathbb{R}^+$ and $\gamma \in \mathbb{R}^+$ are positive constants. Additionally, based on subsequent stability analysis, the following update laws are designed for the rest of estimation functions.

$$\dot{\hat{R}}_k = \phi_k(X_k) u_{1,k} s_k \quad (4.33)$$

$$\hat{\sigma}_k = \hat{\sigma}_{k-1} - b_q v_{f_{1,k}}(\gamma s_k) \quad (4.34)$$

$$\hat{\sigma}_k = 0, \text{ when } k = -1 \quad (4.35)$$

where $b_q \in \mathbb{R}^+$ is a positive constant.

4.2.3 Stability Analysis and Finite Time Convergence

Let $V_k(x, t) : \mathbb{R}^N \times \mathbb{R} \rightarrow \mathbb{R}$ be an energy function where $t \in [t_0, t]$, t_0 is the start time of iterations and t is the elapsed time after the start of an iteration. V_k is defined as

$$V_k = V_k^{(1)} + V_k^{(2)} + V_k^{(3)} + V_k^{(4)} + V_k^{(5)} \quad (4.36)$$

where $V_k^{(1)} = \frac{v_k^2}{2}$, $V_k^{(2)} = \frac{\gamma}{\lambda_2} \frac{s_k^2}{2}$, $V_k^{(3)} = \frac{1}{2b_q} \int_{t_0}^t \Psi_k^2 d\tau$, $V_k^{(4)} = \frac{1}{2\xi} \int_{t_0}^t E_{s,k}^2 d\tau$, and $V_k^{(5)} = \frac{1}{2} \text{tr} \left\{ \tilde{R}_k^T \tilde{R}_k \right\}$. $\gamma, b_q, \xi \in \mathbb{R}^+$ are constants where b_q and ξ are chosen by the user and γ is subsequently defined. The difference between the first energy function in two successive iterations is computed as

$$\Delta V_k^{(1)} = V_k^{(1)} - V_{k-1}^{(1)}. \quad (4.37)$$

Therefore, the following expression is obtained as

$$\begin{aligned} \Delta V_k^{(1)} &= \frac{v_k^2}{2} - \frac{v_{k-1}^2}{2} = \\ &= \int_{t_0}^t v_k \dot{v}_k d\tau + \frac{v_k^2(t_0)}{2} - \frac{v_{k-1}^2}{2}. \end{aligned} \quad (4.38)$$

By substituting (4.18) in equation (4.38), the following equation is derived as

$$\begin{aligned} \Delta V_k^{(1)} &= -\beta_1 \int_{t_0}^t v_k s_k d\tau - \beta_2 \int_{t_0}^t v_k^2 d\tau \\ &\quad + \frac{v_k^2(t_0)}{2} - \frac{v_{k-1}^2}{2}. \end{aligned} \quad (4.39)$$

The difference of successive iterations for the second energy function is obtained as

$$\begin{aligned} \Delta V_k^{(2)} &= \frac{\gamma}{\lambda_2} \frac{s_k^2}{2} - \frac{\gamma}{\lambda_2} \frac{s_{k-1}^2}{2} \\ &= \frac{\gamma}{\lambda_2} \int_{t_0}^t s_k \dot{s}_k d\tau - \frac{\gamma}{\lambda_2} \frac{s_{k-1}^2}{2} + \frac{\gamma}{\lambda_2} \frac{s_k^2(t_0)}{2}. \end{aligned} \quad (4.40)$$

By substituting (4.28) into (4.40), we have

$$\begin{aligned}
\Delta V_k^{(2)} &= -\frac{\gamma}{\lambda_2} \frac{s_{k-1}^2}{2} - \gamma \alpha_3 \int_{t_0}^t s_k^2 d\tau + \frac{\gamma}{\lambda_2} \frac{s_k^2(t_0)}{2} \\
&+ \gamma \int_{t_0}^t s_k \Psi_k v_{f_{1,k}} d\tau - \frac{4}{3} \alpha_2 \gamma \int_{t_0}^t s_k \operatorname{sgn}(s_k) d\tau \\
&+ \gamma \int_{t_0}^t s_k v_{d,k} d\tau + \gamma \int_{t_0}^t s_k \tilde{R}_k^T \phi_k(X_k) u_{1,k} d\tau \\
&+ \gamma \int_{t_0}^t s_k E_{s,k} d\tau + \gamma \int_{t_0}^t s_k \beta_{\varepsilon,k} u_{1,k} d\tau + \gamma \int_{t_0}^t s_k v_k d\tau
\end{aligned} \tag{4.41}$$

Using the upper bound of v_d and β_ε in (4.11) and (4.26) respectively and 4.23, the following inequality is achieved

$$\begin{aligned}
\Delta V_k^{(2)} &\leq -\frac{\gamma}{\lambda_2} \frac{s_{k-1}^2}{2} - \gamma \alpha_3 \int_{t_0}^t s_k^2 d\tau + \frac{\gamma}{\lambda_2} \frac{s_k^2(t_0)}{2} \\
&+ \bar{v}_d \gamma \int_{t_0}^t |s_k| d\tau + \gamma \int_{t_0}^t s_k v_k d\tau + \gamma \bar{\beta}_\varepsilon \int_{t_0}^t |s_k| d\tau \\
&+ \gamma \int_{t_0}^t s_k \Psi_k v_{f_{1,k}} d\tau + \frac{4}{3} \alpha_2 \gamma \int_{t_0}^t |s_k| d\tau \\
&+ \gamma \int_{t_0}^t s_k E_{s,k} d\tau + \gamma \int_{t_0}^t s_k \tilde{R}_k^T \phi_k(X_k) u_{1,k} d\tau
\end{aligned} \tag{4.42}$$

The difference of the third energy function between two iterations in a row can be written as

$$\Delta V_k^{(3)} = \frac{1}{2b_q} \int_{t_0}^t \Psi_k^2 d\tau - \frac{1}{2b_q} \int_{t_0}^t \Psi_{k-1}^2 d\tau \tag{4.43}$$

Based on (4.34) and [16], the following equation can be derived

$$\begin{aligned}
&\frac{1}{2b_q} (\Psi_k^2 - \Psi_{k-1}^2) \\
&= \frac{1}{2b_q} (\hat{\sigma}_k - \hat{\sigma}_{k-1}) (\hat{\sigma}_k + \hat{\sigma}_{k-1} - 2\sigma) \\
&= \frac{1}{b_q} (\hat{\sigma}_k - \sigma) (\hat{\sigma}_k - \hat{\sigma}_{k-1}) \\
&\quad - \frac{1}{2b_q} (\hat{\sigma}_k - \hat{\sigma}_{k-1}) (\hat{\sigma}_k - \hat{\sigma}_{k-1})
\end{aligned} \tag{4.44}$$

Considering (4.34), (4.44) can be rearranged as

$$\begin{aligned}
\frac{1}{2b_q} (\Psi_k^2 - \Psi_{k-1}^2) &= -\gamma \Psi_k s_k v_{f_{1,k}} \\
&\quad - \frac{1}{2b_q} (\hat{\sigma}_k - \hat{\sigma}_{k-1})^2
\end{aligned} \tag{4.45}$$

Therefore, $\Delta V_k^{(3)}$ in (4.43) can be simplified as

$$\begin{aligned} \Delta V_k^{(3)} &= -\frac{1}{2b_q} \int_{t_0}^t (\hat{\sigma}_k - \hat{\sigma}_{k-1})^2 d\tau \\ &\quad - \gamma \int_{t_0}^t (\Psi_k s_k v_{f_{1,k}}) d\tau \end{aligned} \quad (4.46)$$

The difference of the fourth energy function between two iterations is

$$\Delta V_k^{(4)} = \frac{1}{2\xi} \int_{t_0}^t E_{s,k}^2 d\tau - \frac{1}{2\xi} \int_{t_0}^t E_{s,k-1}^2 d\tau. \quad (4.47)$$

Similarly, we can rewrite $\Delta V_k^{(4)}$ as

$$\begin{aligned} \frac{1}{2\xi} (E_{s,k}^2 - E_{s,k-1}^2) &= -\frac{1}{2\xi} (\hat{v}_{f_{2,k}} - \hat{v}_{f_{2,k-1}})^2 \\ &\quad + \frac{1}{\xi} (\hat{v}_{f_{2,k}} - v_{f_{2,k}}) (\hat{v}_{f_{2,k}} - \hat{v}_{f_{2,k-1}}) \end{aligned} \quad (4.48)$$

Based on (4.29), (4.30), and (4.31), we have

$$\begin{aligned} \frac{1}{2\xi} (E_{s,k}^2 - E_{s,k-1}^2) &= -\gamma E_{s,k} s_k \\ &\quad - \frac{1}{2\xi} (\hat{v}_{f_{2,k}} - \hat{v}_{f_{2,k-1}})^2 \end{aligned} \quad (4.49)$$

Hence,

$$\begin{aligned} \Delta V_k^{(4)} &= -\frac{1}{2\xi} \int_{t_0}^t (\hat{v}_{f_{2,k}} - \hat{v}_{f_{2,k-1}})^2 d\tau \\ &\quad - \gamma \int_{t_0}^t (E_{s,k} s_k) d\tau \end{aligned} \quad (4.50)$$

Considering $\tilde{R}_k(t_0) = 0$, the difference of the fifth energy function between two iterations in a row can be written as

$$\Delta V_k^{(5)} = \frac{1}{2} tr \left\{ \tilde{R}_k^T \tilde{R}_k \right\} - \frac{1}{2} tr \left\{ \tilde{R}_{k-1}^T \tilde{R}_{k-1} \right\} \quad (4.51)$$

which can also be rewritten as

$$\Delta V_k^{(5)} = -tr \left\{ \int_{t_0}^t \tilde{R}_k^T \dot{\tilde{R}}_k d\tau \right\} - \frac{1}{2} tr \left\{ \tilde{R}_{k-1}^T \tilde{R}_{k-1} \right\}. \quad (4.52)$$

By substituting (4.33) to (4.51), $\Delta V_k^{(5)}$ can be obtained as

$$\begin{aligned} \Delta V_k^{(5)} &= -\frac{1}{2}tr \left\{ \tilde{R}_{k-1}^T \tilde{R}_{k-1} \right\} \\ &- tr \left\{ \int_{t_0}^t \tilde{R}_k^T (\phi_k(X_k) u_{1,k} s_k) d\tau \right\}. \end{aligned} \quad (4.53)$$

For proving the convergence of both the tracking error and s_k by considering the known values of \bar{v}_d and $\bar{\beta}_\varepsilon$, we now combine the difference of energy terms for two successive iterations, and by defining $\gamma = \beta_1$ and $\alpha_2 = \frac{-3(\bar{v}_d + \bar{\beta}_\varepsilon)}{4}$, then it results to the following ultimate inequality

$$\begin{aligned} \Delta V_k &= \Delta V_k^{(1)} + \Delta V_k^{(2)} + \Delta V_k^{(3)} + \Delta V_k^{(4)} + \Delta V_k^{(5)} \\ &\leq -\frac{v_{k-1}^2}{2} - \frac{\gamma}{\lambda_2} \frac{s_{k-1}^2}{2} - \gamma \alpha_3 \int_{t_0}^t s_k^2 d\tau - \beta_2 \int_{t_0}^t v_k^2 d\tau \\ &- \frac{1}{2b_q} \int_{t_0}^t (\hat{\sigma}_k - \hat{\sigma}_{k-1})^2 d\tau - \frac{1}{2\xi} \int_{t_0}^t (\hat{v}_{f_{2,k}} - \hat{v}_{f_{2,k-1}})^2 d\tau \\ &+ \frac{v_k^2(t_0)}{2} + \frac{\gamma}{\lambda_2} \frac{s_k^2(t_0)}{2} - \frac{1}{2}tr \left\{ \tilde{R}_{k-1}^T \tilde{R}_{k-1} \right\} \end{aligned} \quad (4.54)$$

(4.54) can be more simplified as below by choosing the gains, $\beta_2 > 2$ and $\alpha_3 > \frac{2}{\lambda_2}$.

$$\begin{aligned} \Delta V_k &\leq -\alpha_4 \int_{t_0}^t s_k^2 d\tau - \alpha_5 \int_{t_0}^t v_k^2 d\tau \\ &- \frac{1}{2}tr \left\{ \tilde{R}_{k-1}^T \tilde{R}_{k-1} \right\} - \frac{v_{k-1}^2}{2} - \frac{\gamma}{\lambda_2} \frac{s_{k-1}^2}{2} \\ &- \frac{1}{2b_q} \int_{t_0}^t (\hat{\sigma}_k - \hat{\sigma}_{k-1})^2 d\tau - \frac{1}{2\xi} \int_{t_0}^t (\hat{v}_{f_{2,k}} - \hat{v}_{f_{2,k-1}})^2 d\tau \end{aligned} \quad (4.55)$$

where $\alpha_4 \in \mathbb{R}^+$ and $\alpha_5 \in \mathbb{R}^+$. ΔV_k is negative semi definite which results to

$$V_k \leq V_{k-1}, k = 1, 2, 3, \dots \quad (4.56)$$

It results to the fact that V_k is a non increasing sequence. In order to prove boundedness of V_k , using (4.18), (4.28) and (4.33) time derivative of V_0 is derived as below

$$\begin{aligned} \dot{V}_0 &= -\gamma \alpha_3 s_0^2 - \beta_2 v_0^2 + \frac{1}{b_q} \Psi_0^2 \\ &+ \gamma s_0 \Psi_0 v_{f_{1,0}} + \gamma s_0 E_{s,0} + \frac{1}{\xi} E_{s,0}^2 \end{aligned} \quad (4.57)$$

Based on (4.32) and (4.35), \dot{V}_0 can be further simplified as

$$\dot{V}_0 = -\gamma \alpha_3 s_k^2 - \beta_2 v_k^2 + \frac{1}{b_q} \sigma^2 + \frac{1}{\xi} v_{f_2}^2. \quad (4.58)$$

Therefore, \dot{V}_0 is bounded in the interval of $[t_0, t]$, V_0 is also bounded in $[t_0, t]$ because $V_0(t) = V_0(t_0) + \int_{t_0}^t \dot{V}_0(s) ds$. It follows from (4.55) that V_k is bounded. Accordingly, v_k , \tilde{R}_k , $\hat{\sigma}_k$, Ψ_k , $E_{s,k}$, and s_k are also bounded. Furthermore, based on the (4.55), it can be written that

$$\int_{t_0}^t s_k^2 d\tau \leq \frac{1}{\alpha_4} (V_{k-1} - V_k). \quad (4.59)$$

Because V_k is monotonically decreasing but it is lower bounded by zero which leads to the following conclusion

$$\lim_{k \rightarrow \infty} \int_{t_0}^t s_k^2 d\tau = 0. \quad (4.60)$$

Based on the (4.28) and considering (4.23) and the boundedness of v_k , \tilde{R}_k , $\hat{\sigma}_k$, Ψ_k , $E_{s,k}$, and s_k , \dot{s}_k is also bounded. Accordingly, by Barbalat-like lemma presented in [88, 84], $\lim_{k \rightarrow \infty} s_k = 0$ uniformly on $[t_0, t]$.

To sum up, a second order RNNILSC is designed to control the system in (4.3). It is robust to the system disturbance, allowing the system switches the allocation between motors and FES arbitrarily. Because $V_k(x, t)$ in (4.36) can be regarded as a common energy function in (4.27), it will be stable to arbitrary allocation switching [54].

4.3 Experimental Procedure and Results

The experimental study was approved by the Institutional Review Board (IRB) at the University of Pittsburgh (IRB approval number: PRO 14040419). All participants signed informed consent form to participant. Three participants without any neuromuscular disorders were involved in this study. Participant 1: Age 25, male. Participant 2: Age 25, male. Participant 3: Age 23, male. Additionally, one participant with complete SCI was also involved in this study. Participant 4: Age 51, male injury: T11.

As shown in Fig. 12, the experimental setup and control algorithm are illustrated. The testbed consists of two DC brushless servo motors (Harmonic Drive Company, USA) for both hips, two DC motors (Maxon Motor Inc., Switzerland) for both knees, and two sets of FES

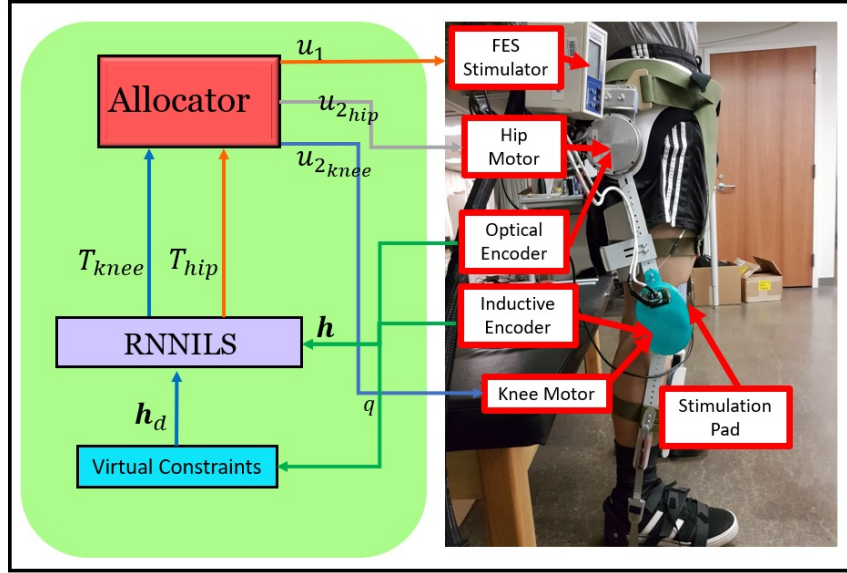


Figure 12: The hybrid exoskeleton testbed used for the experiments and the diagram of the control algorithm.

electrode pads for the quadriceps muscles. An incremental optical encoder with 4000 pulses per revolution (PPR) resolution were used to measure the hip joints angles and an inductive encoder with 4096 PPR resolution were used to measure the knee joints angles. A biphasic stimulation train was applied to the surface electrodes via a RehaStim 8-channel stimulator (Hasomed Inc., DE), where the pulse trains had a frequency of 35 Hz and the stimulation pulse width was chosen as $400 \mu s$. The controller was programmed in Simulink (MathWorks Inc., USA) and implemented using a real-time target machine (Speedgoat Inc., Liebefeld Switzerland) with frequency of 350 Hz, which modulated the stimulation current amplitude and the current amplitudes of the exoskeleton motors during the experiments. Through the entire experimental procedure, the participants were instructed to be relaxed and avoid any voluntary interference with the exoskeleton. Also, the participants were not allowed to view the performance or the desired virtual constraints in real time. Four sets of experiments on each participant were conducted to evaluate the newly proposed ILC. Each experimental set included 4 iterations. Each iteration of the sitting to standing procedure was run for a time

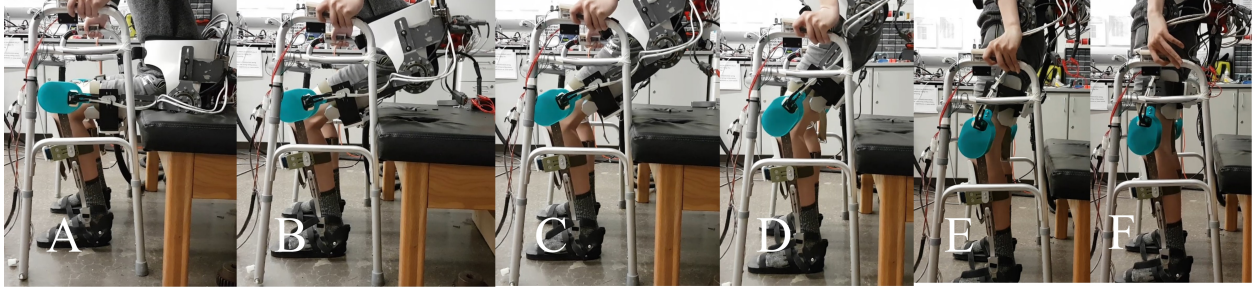


Figure 13: Snapshots of the standing up experiment performed on participant 1.

duration 20 s. This time duration is designed as per participants convenience to use the exoskeleton. The desired movement profile allows a participant to achieve sitting to standing in about 10 seconds. The rest of the 20 seconds are allocated to check control performance in the standing mode. Between two successive iterations, a one minute resting time period was given for the participants. The resting time period was provided to allow the muscles to recover in case of FES-induced fatigue. Fig. 13 demonstrates the snapshots of the sitting-to-standing movement on participant 1, wearing the hybrid exoskeleton. In initial experiments, allocation coefficients of $\iota = 0.2$ and $\varsigma = 0.8$ were chosen. In Fig. 14, knee angle profiles, knee angle tracking errors, and knee control inputs are shown for Participant 1 for the 1st and 4th iterations. In Fig. 15, hip angle profiles, hip angle tracking errors, and hip control inputs are shown for participant 1 for the 1st and 4th iteration. . According to these two figures, in the fourth iteration, the system can track the desired movement profile more accurately. Despite a high model uncertainty, i.e., due to differences between the dynamic model and the real system, and having different participants in the device, the controller could still limit the error and provide a smooth sitting to standing movement for the participant after only 4 iterations. The resulting knee and hip control inputs of the motors and FES of the hybrid exoskeleton are shown in Fig. 14 and Fig. 15 respectively as well. The results of control inputs show that the ILC in the fourth iteration increases the torque to reduce the errors that occur in the first iteration. The control framework was also tested in a participant with SCI. The results in Fig. 16 show the proposed framework could work successfully for the

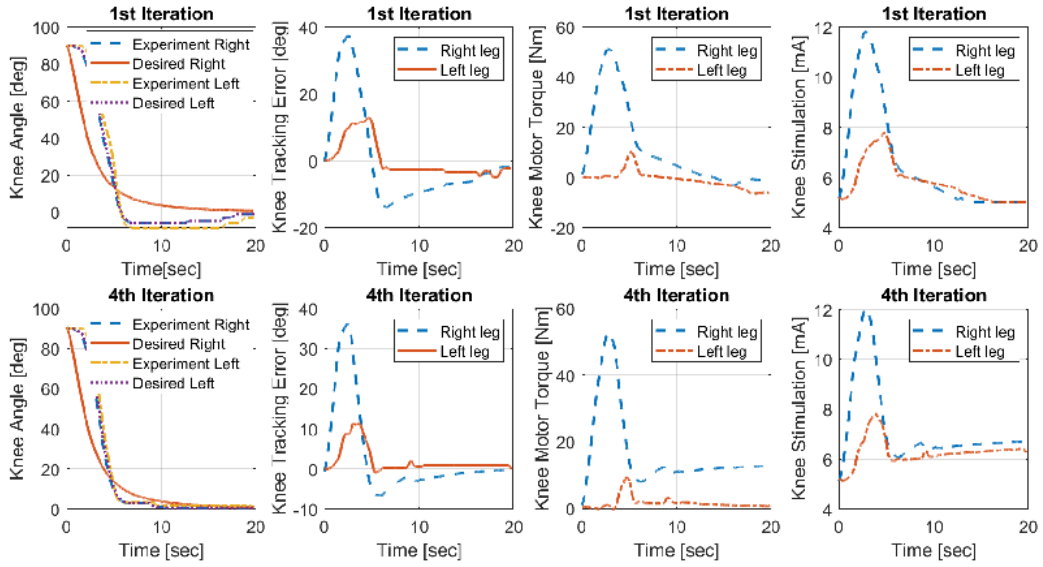


Figure 14: Knee joints angular profiles, tracking errors and the control inputs of Participant 1 for the 1st iteration and the 4th iteration, where $\iota = 0.2$ and $\varsigma = 0.8$.

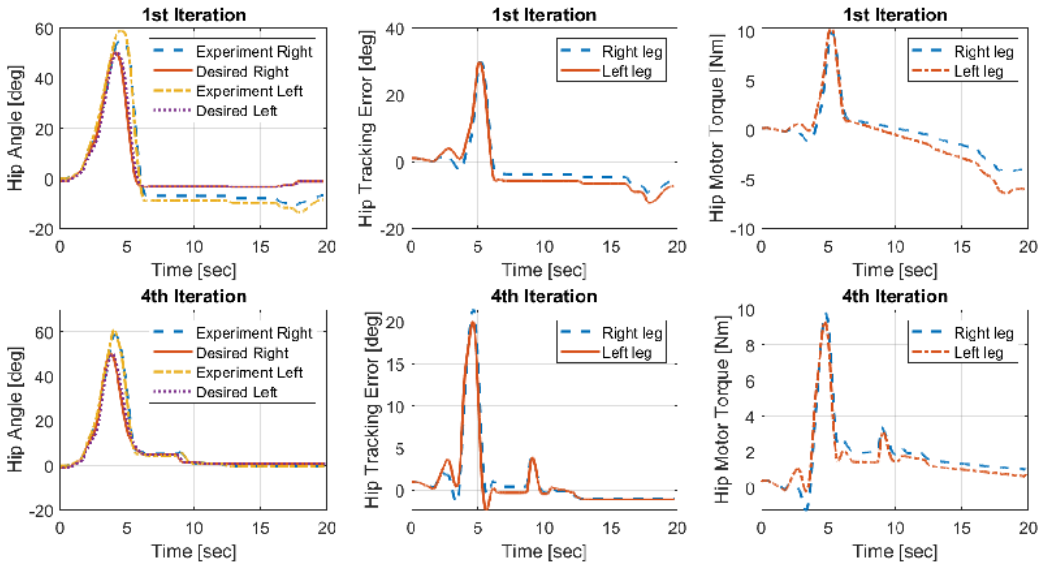


Figure 15: Hip joints angular profiles, tracking errors and the control inputs of Participant 1 for the 1st iteration and the 4th iteration, where $\iota = 0.2$ and $\varsigma = 0.8$.

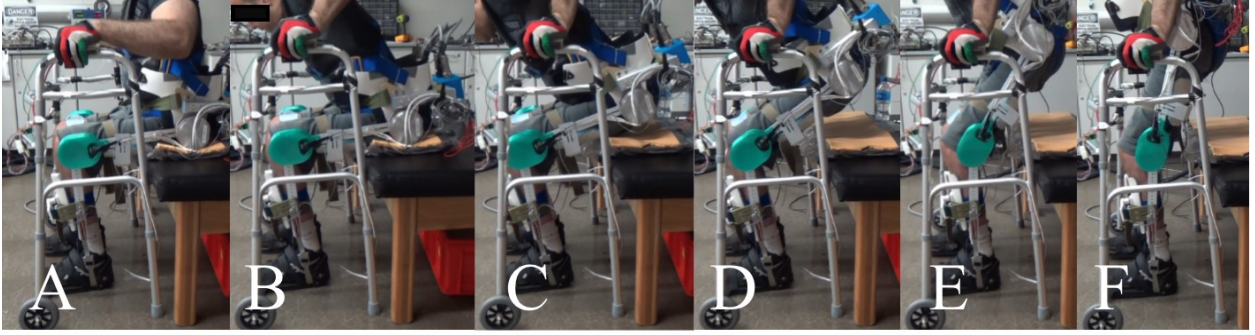


Figure 16: The snapshot sequences of participant 4 with complete SCI for a sitting to standing scenario.

participant with SCI. Fig. 16 shows the snapshots that illustrate the movement produced during the experiments for Participant 4 (the subject with complete SCI). The results in Fig. 17 and 18 illustrate knee joint performance and control inputs and hip joint performance and control inputs, respectively in the 1st and 4th iterations for the participant 4. As it can be seen in the figures, the controller could successfully force the system to track the desired movement profile. The controller used a higher gain to let Participant 4 experience an easier sitting to standing movement. A different movement profile was used for Participant 4 so that it can be matched with his hip joint limitations. These joints angular limitations are due to his spinal cord injury and the long term use of wheelchair. Fig. 19 provides estimation from the linearly parameterizable part, $\hat{\sigma}v_{f_1}$, and estimation of not linearly parameterizable part, \hat{v}_{f_2} , of the system model using neural networks for Participant 4. The root mean square error (RMSE) between the desired angular position and actual trajectory on each joint is listed in Tables 1 and 2 for all four participants, as well as the tracking performance improvement by comparing the 1st iteration and 4th iteration with the allocation ratios $\iota = 0.1$ and $\zeta = 0.9$. Means of the RMSE improvement on each joint across the four participants are plotted in Fig. 20. According to this figure, on average, after four iterations, RMSE of the knee joint and hip joint are improved by 51.18% and 57.31%, respectively. For determining the robustness of the developed control method to the switching allocation between FES and exoskeleton,

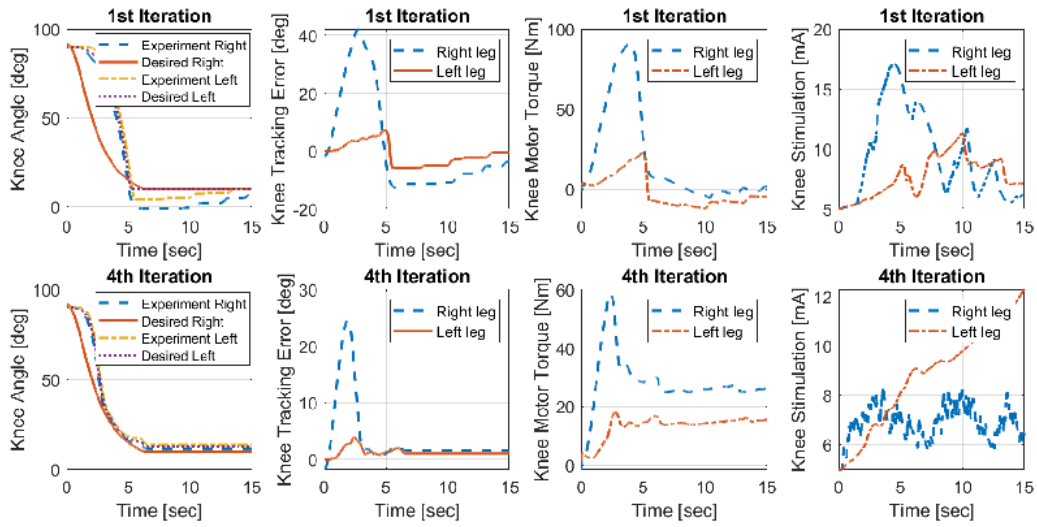


Figure 17: Knee joints angular profiles, tracking errors, and the control inputs of Participant 4 in the 1st and 4th iteration

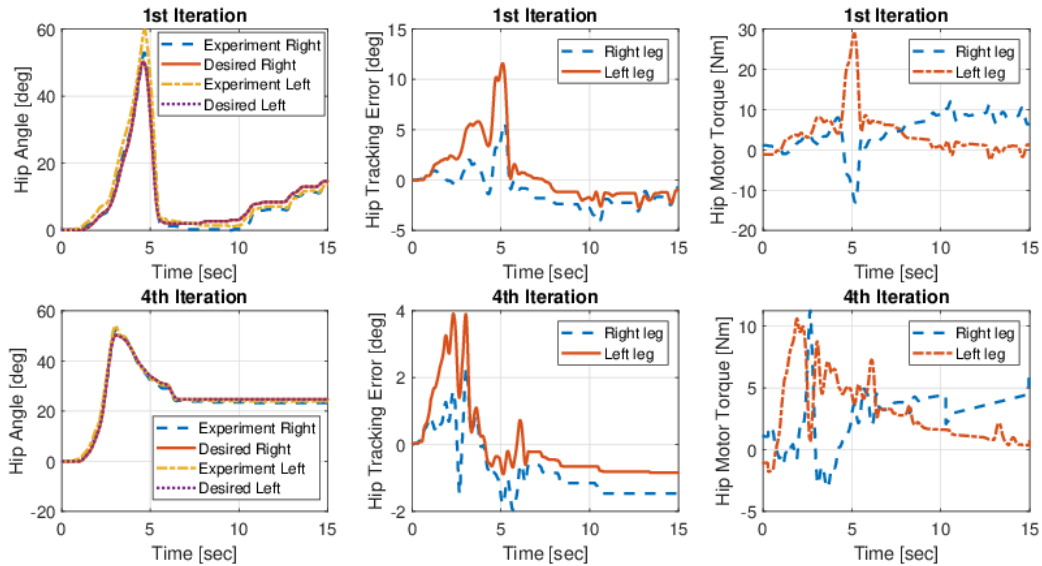


Figure 18: Hip joints angular profiles, tracking errors and the control inputs of Participant 4 in the 1st and 4th iteration

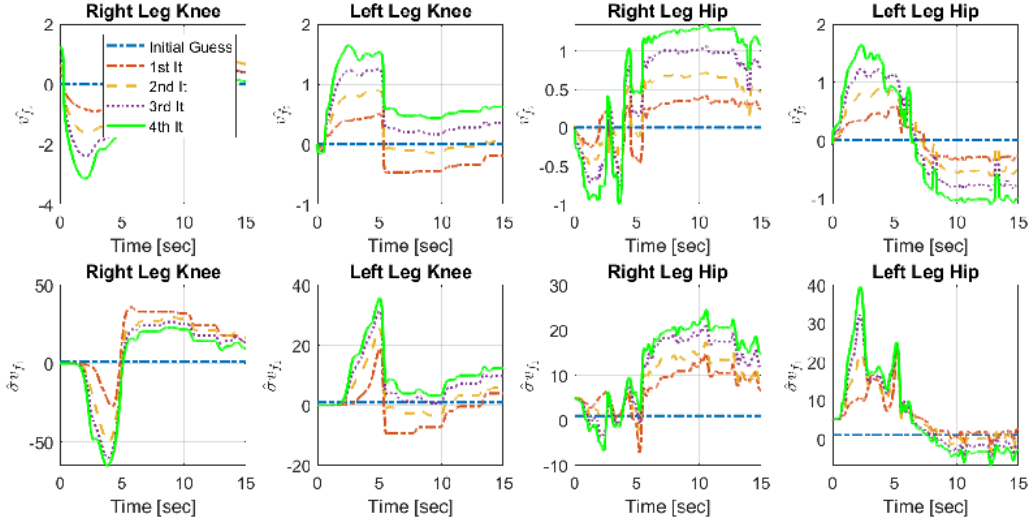


Figure 19: The linearly parameterizable part estimation, $\hat{\sigma}v_{f_1}$ and the not linearly parameterizable part estimation, \hat{v}_{f_2} of the system dynamic for Participant 4 with complete SCI

Table 1: RMSE of joints angular position tracking results on Participants 1 and 2 in different iterations where $\iota = 0.1$ and $\varsigma = 0.9$ (RK: right knee, LK: left knee, RH: right hip, LH: left hip)

RMSE [deg]	Participant 1				Participant 2			
	RK	LK	RH	LH	RK	LK	RH	LH
1 st iteration	10.09	14.35	13.01	14.87	6.72	8.81	11.93	11.43
2 nd iteration	7.90	9.57	9.14	10.36	4.87	5.59	7.74	6.35
3 rd iteration	7.29	8.99	8.85	9.00	3.91	4.75	5.99	5.43
4 th iteration	4.71	5.88	5.24	5.59	3.78	4.70	4.74	4.37
Improvement [%]	53.32	59.02	59.72	62.41	43.75	46.65	60.27	61.77

Table 2: RMSE of joints angular position tracking results on Participants 3 and 4 in different iterations where $\iota = 0.1$ and $\varsigma = 0.9$ (RK: right knee, LK: left knee, RH: right hip, LH: left hip)

RMSE [deg]	Participant 3				Participant 4			
	RK	LK	RH	LH	RK	LK	RH	LH
1 st iteration	9.88	12.31	15.82	15.01	11.84	3.43	1.70	3.13
2 nd iteration	7.61	8.39	10.98	9.72	9.07	3.16	1.49	2.16
3 rd iteration	6.64	7.21	8.19	7.56	5.01	2.21	1.46	1.22
4 th iteration	5.90	6.59	7.43	7.39	4.33	1.91	1.20	1.13
Improvement [%]	40.28	46.47	53.03	50.77	63.43	44.31	41.67	63.90

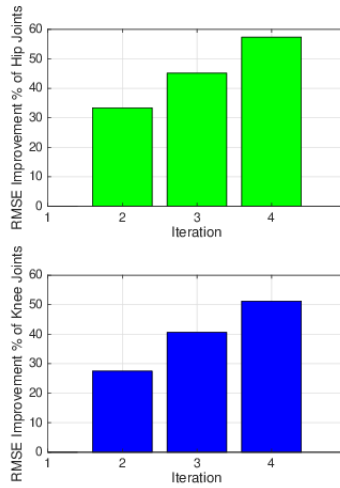


Figure 20: Means of RMSE improvement percentage on both knee and hip joints in different iterations across all participants, where $\iota = 0.1$ and $\varsigma = 0.9$.

the allocation ratio was switched twice during the experiments. We changed the exoskeleton and FES ratio from $\varsigma = 0.7$, $\iota = 0.3$ in the first set of iterations to $\varsigma = 0.8$, $\iota = 0.2$ in the second set of iterations, and then $\varsigma = 0.9$, $\iota = 0.1$ in the final set of iterations. The results of this switching on participant 1 can be seen in Fig. 21. In this figure, RMSE of joint angular positions for different iterations and for the two switching scenarios are shown. It can be observed that after the switching, the system remains stable and the RMSE remains decreasing under the same allocation ratio. Although the errors are increased initially, but the system starts to learn and reduces the error again.

4.4 Walking Simulation Results

The walking simulation was run for 10 steps for $N = 5$. The model has two shanks, two thighs and a trunk and the simulation is done in Matlab Environment. The results are shown in Fig. 22- 23, which show a robust, optimal, and stable walking despite ground effects. The control inputs are displayed in Fig. 22 for first 8 steps of the simulation run. The Fig. (23) shows the link angles. In Fig. (23) the abrupt change in angles is due to the impact with walking surface at each step. As it is clear from this figure, the states are renominated after the ground contact. Fig. 24 represents the limit cycle over 10 steps with the simulating. The resulted trajectory is convergent to a limit cycle as shown in Fig. 24 which according to the Poincare map also supporting the stability in both the swing phase and the impact phase. The “flat” portion of the curve in the figure is an instantaneous transition due to the swing leg ground impact, where the star is the initial point of the trajectory.

4.5 Discussion

A hybrid exoskeleton that uses a combination of FES and a powered exoskeleton can potentially enable people with paraplegia to stand and walk again. We were motivated to design its controller that iteratively learns a participant’s musculoskeletal model and

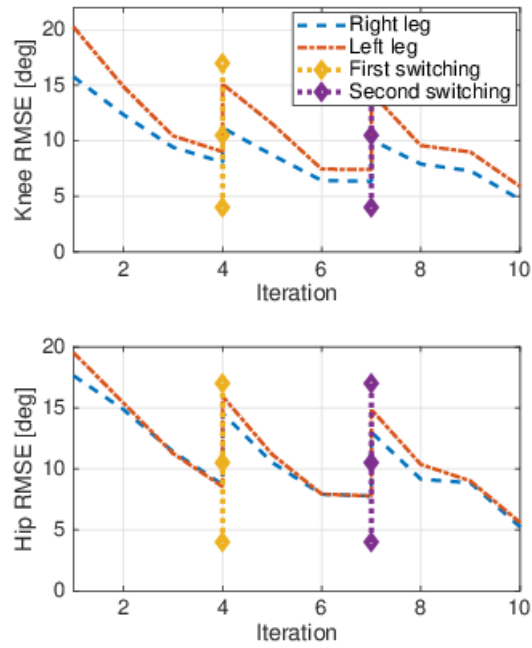


Figure 21: RMSE of participant 1 angular positions tracking for 2 impulse switching to allocation ratios.

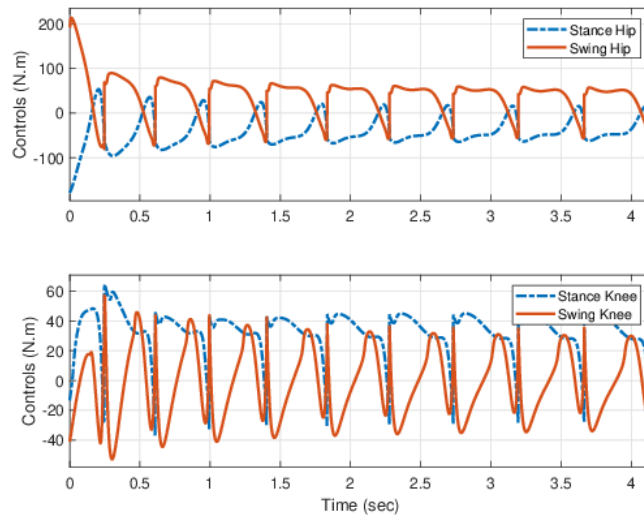


Figure 22: Control inputs versus time

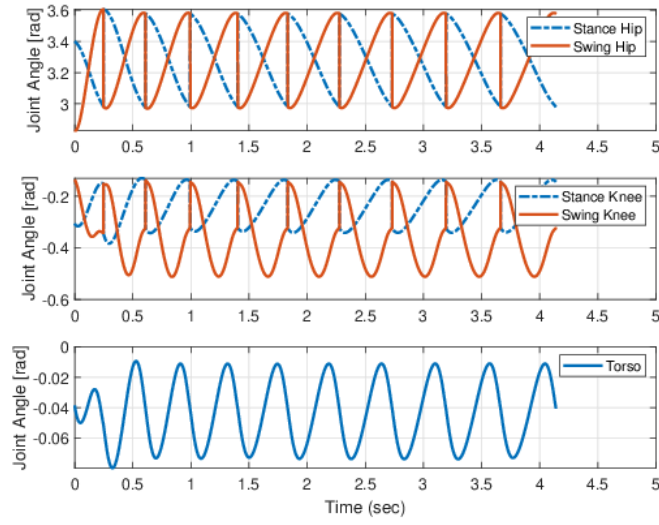


Figure 23: Angle of the linkages versus time

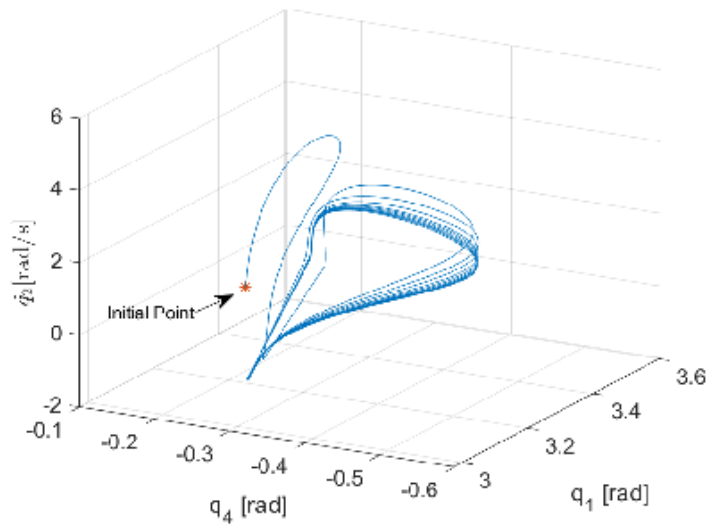


Figure 24: 3-D diagram, showing attractive limit cycle of the system

thus, potentially, ease its implementation in clinics with minimal tuning. Further, we were interested in guaranteeing that task stability and performance are not compromised when FES and the exoskeleton motors allocation levels are switched or changed by a clinician/therapist. To achieve these objectives, a robust NN based ILC was derived and validated through experiments. Due to day-to-day and inter-person variations in the musculoskeletal models, and the tedious process needed to identify the model [83, 45], it is difficult to implement existing controllers for hybrid exoskeletons in clinics. While numerous papers in FES control exist that use high-gain controllers [77, 79] to provide robustness to modeling uncertainties or even adapt and learn the model using neural networks [2, 3, 72, 78] but their implementation may need extensive tuning or offline training of neural networks. This makes the job of a clinician/physical therapist difficult because they may not have a control engineering experience. This problem arises when there are several parameters that they can tune but the parameters may have a coupled performance effects. This control method targeted this problem by tuning some of the control through an iterative learning method. Furthermore, using real time NN estimations as a feed forward component can help the system work adaptively and robustly without requiring the control system to use high gains. Additionally, it allows the physical therapist to change the allocation of the torque between the electric motors and FES arbitrarily, without being afraid of causing instability.

4.6 Conclusion

A robust NN based ILC was designed in this chapter for a hybrid exoskeleton. The controller tracks time-invariant joint trajectories that are determined by virtual constraints. Walking simulation and sitting to standing experiments were performed on four human subjects including one patient with complete SCI. The experimental results showed that RMSE of the angular position tracking on both knee and hip joints in each iteration was reduced, which validated the controller's effectiveness and robustness. The results also showed that the hybrid exoskeleton system followed time-invariant joint trajectories with high accuracy, as well as the robustness when switching allocation ratio between FES and

powered exoskeleton. The proposed controller can help people with SCI to stand and walk with a hybrid exoskeleton without extensive tuning of control parameters. It can also enable changing of FES and the exoskeleton motor allocation levels while a patient is performing standing and walking tasks.

5.0 Shared Control of a Powered Exoskeleton and Functional Electrical Stimulation using Iterative Learning and Fatigue Optimization

5.1 Introduction

Dynamic shared control of FES and the powered exoskeleton is an open research topic. Actuation redundancy due to the simultaneous use of FES and electrical motors and a modulation of the shared effort in view of FES-induced dynamics are challenging control problems. Recent research efforts in this direction certainly inform ways to implement shared control in a hybrid exoskeleton but these control designs do not explicitly account for FES-induced fatigue dynamics. In [69], authors used an adaptive control method for the allocation between motors and FES. In both [22] and [35], a combination of feed forward learning control and proportional-integral-derivative (PID) feedback control were used for controlling electric motors and FES. In [45], a hybrid leg extension machine with one degree of freedom (DOF) was controlled by a nonlinear model predictive control (NMPC) method. The allocation between an electric motor and FES was adjusted by the NMPC method using a gradient projection algorithm. In [80], a switched control approach was derived and simulated based on fixed control allocation ratios that distributed control between FES and the exoskeleton. However, dynamic shared control has not been attempted and also it's not implemented in functionally relevant and multi-DOF lower-limb movements. As a step towards this direction, a model predictive strategy is chosen in this chapter to dynamically optimize allocation between exoskeleton motors and FES.

The objective of this chapter is to improve the performance of the hybrid exoskeleton despite modeling uncertainties in the musculoskeletal dynamics. Nonlinear robust control methods, e.g., sliding mode control [40, 13] and robust integral of sign of the error[79], have been designed specifically to address uncertainties in the nonlinear musculoskeletal model. These approaches, however, inherently rely on high frequency or high gain control to dominate the modeling uncertainties, and thus may cause over-stimulation. A feedforward control strategy is usually recommended along with feedback control to reduce overall control

effort. Neural networks (NN) have been used as feedforward controllers for FES in [50, 68, 42, 3, 57]. The advantage of the NN-based control approach is its universal approximation property that helps to capture unstructured uncertainties in the musculoskeletal dynamics [78]. NN-based control, however, requires training to obtain desired performance. Both offline [50, 68, 42] and online [78] NN training methods have been used for FES control. Motivated by an iterative learning control (ILC) approach that improves a system’s transient performance in multiple iterations, an NN-based ILC method is derived in this chapter. This method also addresses implementation issues in chapter two and three that needed the system model to be known exactly.

In this chapter, a time-invariant manifold, known as virtual constraint [87, 34] is utilized to self-generate desired joint trajectories. In most exoskeleton control results, the desired joint trajectories are time-dependent [36, 19, 9]. These type of trajectories may cause miscoordination due to asymmetric disturbances at limb joints. On the other hand, virtual constraints are desired joint trajectories that are self-generated with state flow. Thus, they may provide a better coordination between the joints, and can be implemented in the controller as a state dependent desired manifold.

To sum up, a unified control framework (MPC based allocation + robust NN-based ILC + Self-generated trajectories computed via virtual constraints) is designed and implemented on a generalized hybrid exoskeleton. The stability of this controller is proven by using a Lyapunov-like stability method. The experimental results on three participants for a sitting to standing task validate the performance of the proposed control framework.

5.2 A Generalized Hybrid Exoskeleton Model

A general N -DOF hybrid exoskeleton that is comprised of FES and a powered exoskeleton is modeled as

$$J\ddot{\theta} + C\dot{\theta} + G + \tau_p = B_F u_{\bar{F}} + B_M u_{\bar{M}} + d, \quad (5.1)$$

where $\theta \in \mathbb{R}^N$, $\dot{\theta} \in \mathbb{R}^N$, and $\ddot{\theta} \in \mathbb{R}^N$ are the vectors that represent the links’ angular position, angular velocity, and angular acceleration, respectively, $J(\theta) \in \mathbb{R}^{N \times N}$ is the inertia

matrix, $C(\dot{\theta}, \theta) \in \mathbb{R}^{N \times N}$ is the Centripetal-Coriolis matrix, $G(\theta) \in \mathbb{R}^N$ is the gravitational vector, $\tau_p \in \mathbb{R}^N$ is the passive viscoelastic moment, $B_F \in \mathbb{R}^{N \times 2N}$ and $B_M \in \mathbb{R}^{N \times N}$ are the FES control gain matrix and the motor control gain matrix, respectively, $u_{\bar{F}} \in \mathbb{R}^N$ is the normalized muscle stimulation input vector, $u_{\bar{M}} \in \mathbb{R}^N$ is the current amplitude vector of powered motors, and $d \in \mathbb{R}^N$ is the system disturbance.

For subsequent control development, the model in (5.1) is rewritten as

$$\dot{x} = f(x) + g_F(x)u_{\bar{F}} + g_M u_{\bar{M}} + D \quad (5.2)$$

where $x \in \mathbb{R}^{2N}$ is $[\theta^T, \dot{\theta}^T]^T$, $f(x) \in \mathbb{R}^{2N}$ is equal to $\left[I_{N \times N} \dot{\theta}^T, \left[J^{-1}(\tau_p - G - C\dot{\theta}) \right]^T \right]^T$, g_F is defined as $\left[\phi_{N \times 2N}, [J^{-1}B_F]^T \right]^T$, g_M is defined as $\left[\phi_{N \times N}, [J^{-1}B_M]^T \right]^T$ and $D \in \mathbb{R}^{2N}$ is defined as $\left[\phi_{1 \times N}, [J^{-1}d]^T \right]^T$

5.3 Control Development

A joint angle function is chosen as $h_0(\theta) = \theta$, where θ is the actual joint angle vector in (5.1). The control objective is to ensure that the independent joint angle function, $h_0(\theta) \in \mathbb{R}^N$, follows a desired virtual constraint function [87], $h_d(\Theta(\theta)) \in \mathbb{R}^N$, where $\Theta(\theta)$ is a polynomial function of the joint angle vector, θ . Note that the virtual constraint function is a function of system state instead of an explicit function of time. The method to design the desired virtual constraint function is given in the previous chapter. The control objective can be expressed as an output, $y \in \mathbb{R}^N$, that must be driven to zero. Thus, the output, y , is defined as

$$y \triangleq h(\theta) = h_0 - h_d. \quad (5.3)$$

Using (5.3), the following output differential equation is derived

$$\frac{d^2 y}{dt^2} = L_f^2 h + L_{g_M} L_f h u_{\bar{M}} + L_{g_F} L_f h u_{\bar{F}} + D_b, \quad (5.4)$$

where $L_f^2 h(\theta)$ is the 2nd-order Lie derivative of $h(\theta)$, $L_{g_M} L_f h(\theta)$ and $L_{g_F} L_f h(\theta)$ are the decoupling matrices, and $D_b \in \mathbb{R}^N$ is the disturbance of the system output.

We consider that $\bar{y}_1^{(i)} = y_i$, $\bar{y}_2^{(i)} = \dot{y}_i$, $u_F^{(i)} = u_{\bar{F}_i}$, and $u_M^{(i)} = u_{\bar{M}_i}$, where subscript i shows i^{th} element of a vector. As the main motivation is to develop an ILC, (5.4) is expressed for a k^{th} iteration as

$$\begin{aligned}\dot{\bar{y}}_{1,k}^{(i)} &= \bar{y}_{2,k}^{(i)} \\ \dot{\bar{y}}_{2,k}^{(i)} &= \sigma^{(i)} f_{1,k}^{(i)} + f_{2,k}^{(i)} + \Omega_k^{(i)} u_{F,k}^{(i)} + b_M^{(i)} u_{M,k}^{(i)} + b_{d,k}^{(i)}\end{aligned}\quad (5.5)$$

where $\sigma^{(i)} f_{1,k}^{(i)} + f_{2,k}^{(i)}$ is equal to i^{th} element of $L_f^2 h(\theta)$ and is expressed as a sum of structured and unstructured uncertain nonlinear terms. Specifically, $\sigma^{(i)} f_{1,k}^{(i)}$ is the linearly parameterizable (structured uncertainty) part of i^{th} element of $L_f^2 h(\theta)$, where $\sigma^{(i)}$ is an unknown parameter function and $f_{1,k}^{(i)}$ is a known regressor function, and $f_{2,k}^{(i)}$ is the remaining not linearly parameterizable (unstructured uncertainty) part of i^{th} element of $L_f^2 h(\theta)$. In (5.5), $b_M^{(i)}$ and $\Omega_k^{(i)}$ are equal to i^{th} element of $L_{g_M} L_f h(\theta)$ and $L_{g_F} L_f h(\theta)$, respectively, for i^{th} input. Here, $b_M^{(i)}$ is the motor control constant gain and is assumed to be known. $\Omega_k^{(i)}$ is an unknown control gain (unstructured uncertainty) associated with control inputs due to FES. In (5.5), $b_{d,k}^{(i)}$ is the system disturbance term, corresponding to the disturbance vector D_b in (5.4). For simplicity purposes, the superscript i ($i = 1, 2, \dots, N$) will be dropped hereafter in all the corresponding notations.

It is clear that (5.5) contains different types of unknown functions that must be approximated for control implementation. In the next steps, we provide update laws to estimate these unknown functions. These update laws were designed using the subsequent stability analysis. Let $\hat{\sigma}_k$ is an estimate of σ , which is the structured uncertain term. Its update law is expressed as

$$\hat{\sigma}_k = \hat{\sigma}_{k-1} - b_q f_{1,k}(\gamma s_k) \quad (5.6)$$

$$\hat{\sigma}_k = 0 \quad \text{when } k = -1, \quad (5.7)$$

where γ is a positive constant and the sliding surface $s_k \in \mathbb{R}$ is designed as

$$s_k = \lambda_1 e_{1,k} + \lambda_2 e_{2,k} \quad (5.8)$$

where λ_1 and λ_2 are positive constants and $e_{1,k} = \bar{y}_{1,d,k} - \bar{y}_{1,k}$, $e_{2,k} = \bar{y}_{2,d,k} - \bar{y}_{2,k}$, $\bar{y}_{1,d,k}$ and $\bar{y}_{2,d,k}$ are the desired system outputs, and $\bar{y}_{1,k}$ and $\bar{y}_{2,k}$ are actual system outputs.

Both $f_{2,k}$ and Ω_k are unstructured uncertain nonlinear terms, therefore, these terms are represented using NNs as follows

$$f_{2,k} = W^T \Lambda_k(P^T X_k) + \varepsilon_{1,k}(X_k) \quad (5.9)$$

$$\Omega_k = Q^T \phi_k(X_k) + \varepsilon_{2,k}(X_k) \quad (5.10)$$

where $X_k \in \mathbb{R}^{2N+1}$ is the augmented input vector for the aforementioned two NNs and is defined as $X_k = \begin{bmatrix} 1 & x_k^T \end{bmatrix}^T$. $W \in \mathbb{R}^{N_2+1}$ is the ideal weight vector for term $f_{2,k}$ and $Q \in \mathbb{R}^{N_\Omega}$ is the ideal weight vector for Ω_k . The input layer is made of $2N+1$ neurons. N is the output layer neurons number, and the hidden layer numbers of neurons in the two NNs are N_{in} and N_Ω . $\Lambda_k : \mathbb{R}^{N_{in}} \rightarrow \mathbb{R}^{N_2+1}$ is the first NN activation function in (5.9) that maps the input layer to the hidden layer, where $P \in \mathbb{R}^{(2N+1) \times N_{in}}$ is the weight matrix corresponding to the augmented input. $\phi_k : \mathbb{R}^{2N+1} \rightarrow \mathbb{R}^{N_\Omega}$ is the activation function in (5.10) that maps the input layer to the output layer. $\varepsilon_{1,k} \in \mathbb{R}$ and $\varepsilon_{2,k} \in \mathbb{R}$ are the unknown functional reconstruction errors for the two NNs, which are bounded with $|\varepsilon_{1,k}| \leq \bar{\varepsilon}_1$ and $|\varepsilon_{2,k}| \leq \bar{\varepsilon}_2$, respectively, where $\bar{\varepsilon}_1, \bar{\varepsilon}_2 \in \mathbb{R}^+$. Let $\hat{f}_{2,k}$ and $\hat{\Omega}_k$ be the approximations of the ideal NNs, $f_{2,k}$ and Ω_k , in (5.9) and (5.10), respectively. These approximations are represented as

$$\hat{f}_{2,k} = \hat{W}_k^T \Lambda_k(\hat{P}_k^T X_k) \quad (5.11)$$

$$\hat{\Omega}_k = \hat{Q}_k^T \phi_k(X_k) \quad (5.12)$$

where $\hat{W}_k \in \mathbb{R}^{N_2+1}$, $\hat{P}_k \in \mathbb{R}^{(2N+1) \times N_{in}}$ and $\hat{Q}_k \in \mathbb{R}^{N_\Omega}$ are the ideal weight estimates in the k^{th} iteration.

5.3.1 Top-level Controller

The estimated terms in (5.6), (5.11), and (5.12) can be combined together to design the top-level controller, U . Because this controller is based on NNs and updates itself every iteration, we call it: NN-based ILC. The controller is given as

$$U_k = -\hat{f}_{2,k} - \hat{\sigma}_k f_{1,k} - F_k \quad (5.13)$$

where $F_k \in \mathbb{R}$ is an additional feedback input

$$F_k = \frac{1}{\lambda_2} \left(-\lambda_1 \bar{y}_{1,d,k} - \lambda_2 \bar{y}_{2,d,k} + \lambda_1 \bar{y}_{2,k} - \lambda_2 \left(\alpha_3 s_k + \frac{4}{3} \alpha_2 \text{sgn}(s_k) \right) + \lambda_2 v_k \right). \quad (5.14)$$

In (5.14) $\alpha_2 \in \mathbb{R}^+$ and $\alpha_3 \in \mathbb{R}^+$ are control gains, $\lambda_1, \lambda_2 \in \mathbb{R}^+$ are constant values, $\bar{y}_{2,k}$ is defined in (5.5), $\bar{y}_{j,d,k}$ is the desired output, and v_k is an integral term that is designed as

$$\dot{v}_k = -\beta_1 s_k - \beta_2 v_k \quad (5.15)$$

where β_1 and β_2 are positive constants.

5.3.2 Control distribution between FES and Motor

To distribute control effort between FES and the powered motor, we introduce $\iota_k(t), \varsigma_k(t) \in [0, 1]$ as a pair of control allocation coefficients. Based on the subsequent stability analysis, k^{th} iteration of the normalized FES virtual input, $u_{F,k}$, is

$$u_{F,k} = \iota_k \psi_k^{-1} U_k \quad (5.16)$$

where U is defined in (5.13) and ψ_k is given by

$$\psi_k = \hat{\Omega}_k + \varrho \left(\hat{\Omega}_k \right) + \beta \quad (5.17)$$

where the spectral radius of $\hat{\Omega}_k$, $\varrho \left(\hat{\Omega}_k \right) \in \mathbb{R}^+$, and a control gain, $\beta \in \mathbb{R}^+$, are added to ψ_k in order to avoid a singularity, when $\hat{\Omega}_k$ is equal to zero [14]. Similarly, based on the stability analysis in the previous chapter, the motor virtual input $u_{M,k}$ is given as

$$u_{M,k} = \varsigma_k b_M^{-1} U_k. \quad (5.18)$$

5.3.3 Predictive Allocation Strategy

In subsection 5.3.2, controllers (5.16) and (5.18) are designed to track the desired trajectories at the top-level. In this subsection, the lower-level controller is formulated that determines the control allocation coefficients, ι_n and ς_n , in (5.16) and (5.18). An MPC allocation strategy based on dynamic optimization is used. These constraints should be chosen in a way that always satisfy the following constraints

$$\iota_k(t) + \varsigma_k(t) = 1, \quad |u_{F,k}| \leq 1. \quad (5.19)$$

The constraints in (5.19) are enforced using MPC. The strategy is also designed to consider the muscle fatigue level by including a fatigue variable as a weighting variable in the cost function. The optimization determines optimal allocation of the coefficients, ι_k and ς_k . The optimization objective is to determine ι_k and ς_k by minimizing a cost functional $J_{mpc}(t_k) \in \mathbb{R}$

$$\min_{\bar{\tau}_{M,k}, \bar{\tau}_{F,k}} J_{mpc}(t_k) = \int_{t_k}^{t_k+T_p} \left\{ \bar{\tau}_{M,k}^2 + \frac{w}{\bar{\mu}+\epsilon} \bar{\tau}_{F,k}^2 \right\} dt \quad (5.20)$$

$$\text{s.t. } J(\bar{\theta}_k) \ddot{\bar{\theta}}_k + C(\bar{\theta}_k, \dot{\bar{\theta}}_k) \dot{\bar{\theta}}_k + G(\bar{\theta}_k) + \bar{\tau}_{p,k} = \bar{\tau}_{M,k} + \bar{\tau}_{F,k}$$

$$\bar{\tau}_{M,k} + \bar{\tau}_{F,k} = \bar{U}_k \quad (5.21)$$

$$\bar{u}_{F,k} \in \mathcal{U} \quad (5.22)$$

where the terms with a bar, e.g., \bar{x} , represents the nominal variable that is evaluated in the prediction horizon, $\epsilon > 0$ is a constant, and $w > 0$ is a predefined weight. $\mathcal{U} \in [0, 1]$ is the input constraint[45, 85]. In (5.20) the motor torque $\bar{\tau}_{M,k}$ in the prediction horizon is evaluated using (5.23).

$$\bar{\tau}_{M,k} = b_M \bar{u}_{M,k} \quad (5.23)$$

where b_M is the known constant defined in (5.5), and $\bar{u}_{M,k}$ is the k^{th} iteration of \bar{u}_M in (5.18). $\bar{\tau}_F$ in (5.20) is defined as [47]

$$\bar{\tau}_{F,k} = \varphi(\bar{x}_k) \bar{\mu}_k \bar{u}_{F,k}. \quad (5.24)$$

where $\bar{\tau}_{F,k}$ is the torque input of FES in the prediction horizon and $\bar{u}_{F,k}$ is the k^{th} iteration of \bar{u}_F in (5.16). $\varphi(\bar{x}_k) = (c_2 \bar{\theta}_{1,k}^2 + c_1 \bar{\theta}_{1,k} + c_0) \left(1 - c_3 \dot{\bar{\theta}}_{1,k} \right)$, $\bar{\theta}_{1,k}$ is the nominal value of the

knee joint angle, and $c_0 \in \mathbb{R}^+$, $c_1 \in \mathbb{R}^+$, $c_2 \in \mathbb{R}^+$, and $c_3 \in \mathbb{R}^+$ are muscle parameters. $\bar{\mu}_k$ is evaluated using $\Phi_\mu(\dot{\bar{\mu}}_k, \bar{\mu}_k, \bar{u}_{F,k}) = 0$, which is a differential equation, used for estimation of the current fatigue level. Φ_μ can be represented as [71, 47]

$$\Phi_\mu : \dot{\bar{\mu}}_k = \frac{(\mu_{min} - \bar{\mu}_k) \bar{u}_{F,k}}{T_f} + \frac{(1 - \bar{\mu}_k)(1 - \bar{u}_{F,k})}{T_r} \quad (5.25)$$

where $\mu_{min} \in [0, 1)$ is the minimum fatigue level of the targeted muscle, $T_f \in \mathbb{R}^+$ is the fatigue time constant, and $T_r \in \mathbb{R}^+$ is the recovery time constant.

The objective index $J_{mpc}(t_k) \in \mathbb{R}^+ \cup \{0\}$ in (5.20) depends on control allocation between $\bar{\tau}_{M,k}$ and $\bar{\tau}_{F,k}$ along the time horizon $[t_k, t_k + T_p]$, where T_p is the time horizon length and t_k is the current time. When the optimal solution, $u_{F,k}^*(t | : t \in [t_k, t_k + T_p]) = \operatorname{argmin}\{J_{mpc}(t_k)\}$, is found, $u_{F,k} = u_{F,k}^*(t | : t = t_k \rightarrow t_k + \varepsilon)$ is applied to the system, where ε is an infinitesimal time constant that makes $t_{k+1} = t_k + \varepsilon$ [30]. The details of steps of the model predictive allocation algorithm can be found in Tables 3 and 4.

5.4 Simulation Results

After implementing the controller on the system for sitting to standing and standing to sitting scenarios, the MPC algorithm allocates the knee FES torque according to the Fig. 25. This allocation causes a normalized fatigue trend which is shown in the Fig. 26. The desired and actual trajectories of hip and knee joints are demonstrated in Fig. 27. In this figure, θ_1 is the knee joint angle and θ_2 is the hip joint angle. According to Fig. 28, compared to the first iteration, the 10th iteration of the algorithm could reduce 86% of root mean square (RMS) error of the knee joint angle tracking performance and 57% of RMS error of the hip joint angle tracking performance.

Table 3: Steps of model predictive allocation strategy

-
- 1 Initialization:** $j = 0$
- (1a) The convergence tolerance is set to ε_j .
- (1b) $\theta(t_k), \dot{\theta}(t_k)$ are measured.
- (1c) Feedback controller and virtual constraint are used to get $h_d(\tau), \bar{h}(\tau)$, and total torque demand, where $\tau \in [t_k, t_k + T_p]$.
- (1d) An initial control trajectory is chosen $\bar{u}_F(\tau) \in \mathcal{U}_{[t_k, t_k + T_p]}$, where $\tau \in [t_k, t_k + T_p]$.
- (1e) $\bar{u}_F(\tau)$ and $\bar{h}(\tau)$ are used for obtaining $\bar{\tau}_F(\tau)$ and $J_{mpc}^{(j)}(t_k)$, where $\tau \in [t_k, t_k + T_p]$.
-

Table 4: Steps of model predictive allocation strategy

2 Optimal Solution Searching:

(2a) For solving the costates,

integration backward in time is done for $l^{(j)}(\tau)$

$H = J_{mpc}^{(j)} + l^{(j)T} \Phi_\mu$, so the optimal solution is given

$$\dot{l}^{(j)}(\tau) = -\frac{\partial H(z, l^{(j)}, \bar{u}_F)}{\partial z}, \text{ where } z = [\bar{x}, \bar{\mu}].$$

(2b) The search direction, $a^{(j)}(\tau)$, is computed from the Hamiltonian

$$a^{(j)}(\tau) = -\frac{\partial H(z, l^{(j)}, \bar{u}_F)}{\partial \bar{u}_F}.$$

(2c) The optimal step size, $\sigma^{(j)}$, is computed with the adaptive setting in [29].

(2d) The control trajectory is updated.

$$\bar{u}_F^{(j+1)}(\tau) = \psi(\bar{u}_F^{(j)} + \sigma^{(j)} a^{(j)}),$$

where the constraints are denoted by ψ .

(2e) $\bar{u}_F^{(j+1)}$ is used to get $J_{mpc}^{(j+1)}(t_k)$.

(2f) Quit conditions are checked

(i) if $\left| J_{mpc}^{(j+1)}(t_k) - J_{mpc}^{(j)}(t_k) \right| \leq \varepsilon_j$, quit.

(ii) if j has exceeded the max iteration limit, N_t , quit.

(iii) otherwise $j = j + 1$ and reiterate gradient step from (1a).

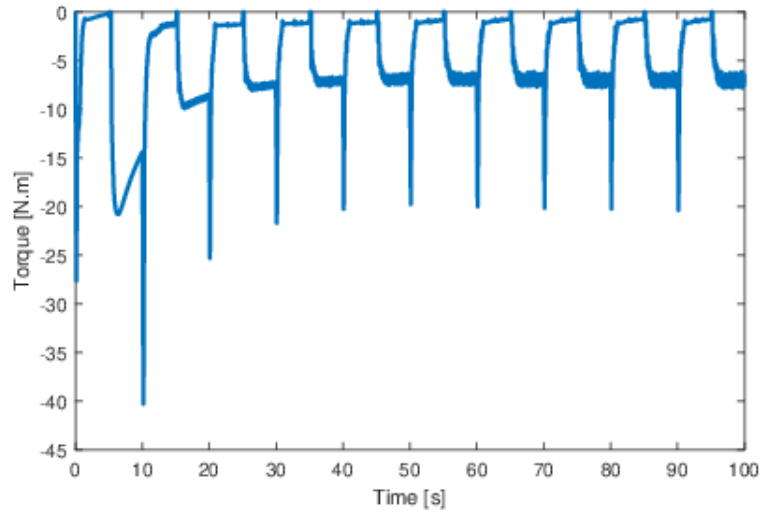


Figure 25: FES torque allocation on the knee joint by using MPC

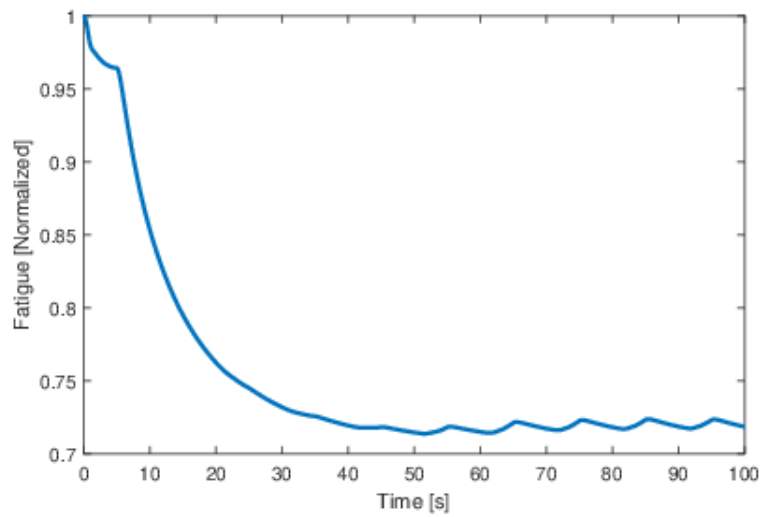


Figure 26: Normalized fatigue over time

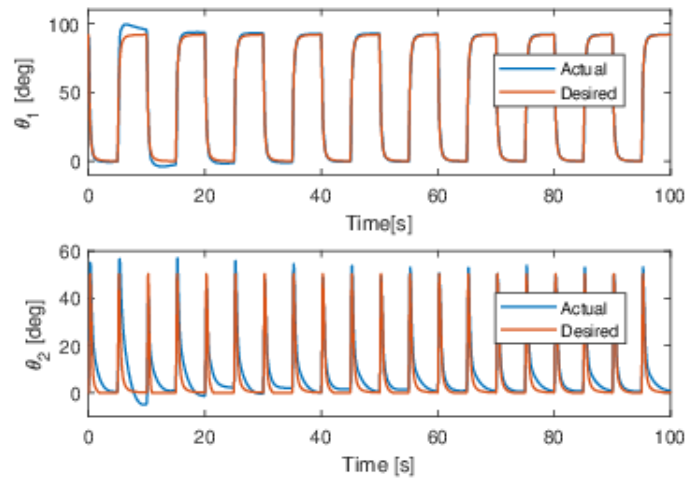


Figure 27: Joint angles over time

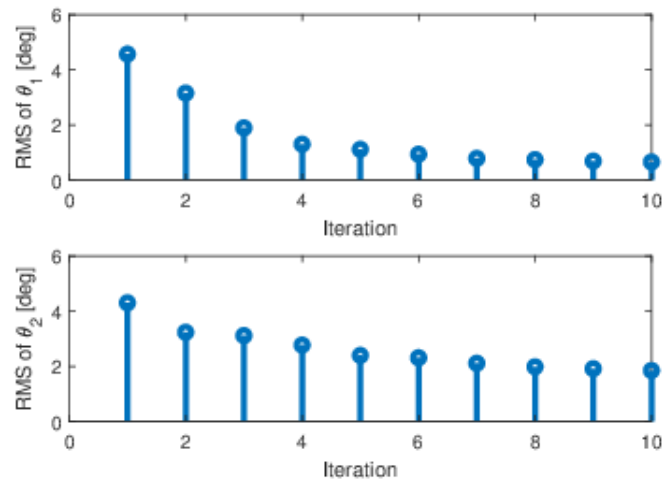


Figure 28: Root mean square of the joint angles error vs iterations

5.5 Experimental Results

The Institutional Review Board (IRB) at the University of Pittsburgh approved the experimental study (IRB approval number: PRO 14040419). Before each experiment, every participant signed an informed consent form. Four participants were recruited in the study, including three without any neuromuscular disorders and one participant with paraplegia from a SCI. Participant 1: Age 23, male. Participant 2: Age 25, male. Participant 3: Age 23, male. Participant 4: Age 51, male, injury: T11, paraplegia from a SCI. Participants wore the lower-limb exoskeleton, developed in our lab [9], during the entire sitting to standing tasks. The exoskeleton is shown in Fig. 29. The hip joints of the powered exoskeleton were actuated by two LPA-17-100-SP electric motors (Harmonic Drive, US). These two motors have a maximum speed of 30 revolutions per minute (RPM) and a peak torque of 54 Nm. Two 90-watt EC Flat Maxon motors (Maxon Motor, Sachseln, Switzerland) were used to actuate the knee joints of the exoskeleton. During the sitting to standing task, a walker was used to assist the participant's balance. Four force sensors were installed on the walker's handles. Sensor 1 and sensor 2 were located at the front and back end of the right handle, while sensor 3 and sensor 4 were located at the front and back end of the left handle. The sensors were used to measure the forces that a participant applied on the walker in the vertical direction. A pair of FES electrodes (Chattanooga Medical Supply, Inc, US) were placed on the participants thighs to stimulate the quadriceps muscles. A biphasic pulse train was delivered to the electrodes by an FES stimulator (RehaStim 8-channel stimulator, Hasomed Inc., DE). A current modulating protocol was chosen at a stimulation frequency of 35 Hz and pulse width of 400 μs . A real-time target machine (Speedgoat Inc., Liebefeld, Switzerland) running at a control frequency of 350 Hz was used to control the exoskeleton and FES. The control implementation was programmed in Simulink (MathWorks Inc., USA). For the execution of the MPC allocator, fatigue and recovery constants: T_f and T_r given in equation 5.25 were identified through a set of experiments, prior to the main sitting-to-standing experiments. In addition, each participant's muscle model parameters were identified. The procedures for model parameters identification are reported in our previous work [46]. The fatigue and recovery constants for the first 3 participants on both legs are

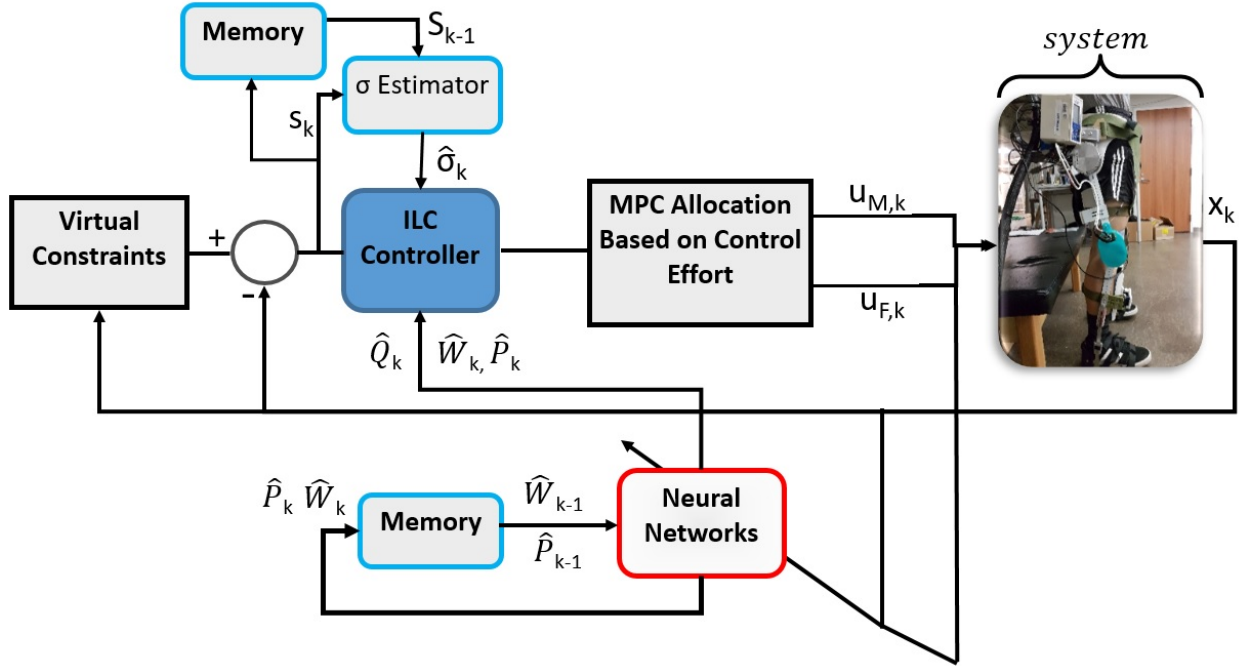


Figure 29: The controller structure and the experimental testbed employed in this study

given in Table 5. S1, S2, and S3 represent the first, second, and third participant. The constants for the Participant 4 are not provided in Table 5 because his quadriceps muscles did not respond to the electrical stimulation. In the main experiment, the developed control framework was validated in a sitting to standing task. A common desired virtual constraint function for the joints of both legs was used. The function was designed such that the sitting to standing task is achieved in 5-6 seconds. After the transition, the standing position was held up to 15 seconds to further validate the controller stability. The controllers were implemented separately for each leg but the controllers used the same virtual constraint function to maintain coordination between the two legs. The control schematic is depicted in Fig. 29. As can be seen in this figure, the top-level ILC controller block uses three inputs: NN estimates $\hat{f}_{2,k}$ and $\hat{\Omega}_k$, linearly parameterizable adaptive component $\hat{\sigma}_k$, and a feedback component F_k . The total torque demand at the knee joint is allocated optimally using the low-level MPC method.

Table 5: The fatigue and recovery time constants T_f and T_r for Participants 1, 2, and 3 on both legs

	S1 Left	S1 Right	S2 Left	S2 Right	S3 Left	S3 Right
T_f [sec]	24.6	23.0	20.2	17.9	25.2	21.6
T_r [sec]	38.6	47.0	50.8	42.0	43.3	49.1

Successful sitting to standing experiments on the four participants were performed using the developed control framework. Fig. 30 demonstrates the snapshots of the sitting to standing experiment from one of the successful trials for Participant 4, who is the participant with paraplegia from a SCI. The trajectory tracking results on both knee and hip joints for Participant 4 are illustrated in Fig. 31. The figure includes the desired trajectories that are based on the virtual constraint function, and the actual trajectories on both legs in the 1st and 4th iterations. The joint angle tracking errors of Participant 4 in the 1st iteration and 4th iteration are shown in Fig. 32. The improvement percentage of the root mean square error (RMSE) of the joints trajectories tracking performance for four participants are plotted in Fig. 33. The results show that from the 1st iteration to the 4th iteration, for each participant, the RMSE values for both knee and hip joints are decreasing. These results indicate that the ILC method improves the joint trajectory tracking performance in successive iterations. In Fig. 34, components of the top level controller, U_k , in (5.13) for

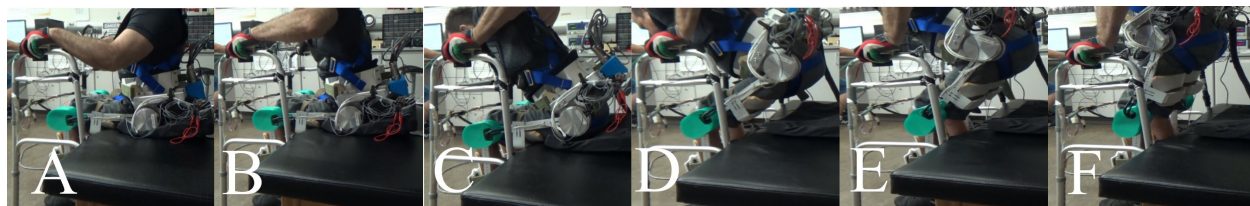


Figure 30: The snapshots of one successful sitting to standings trial for Participant 4 with paraplegia from a SCI

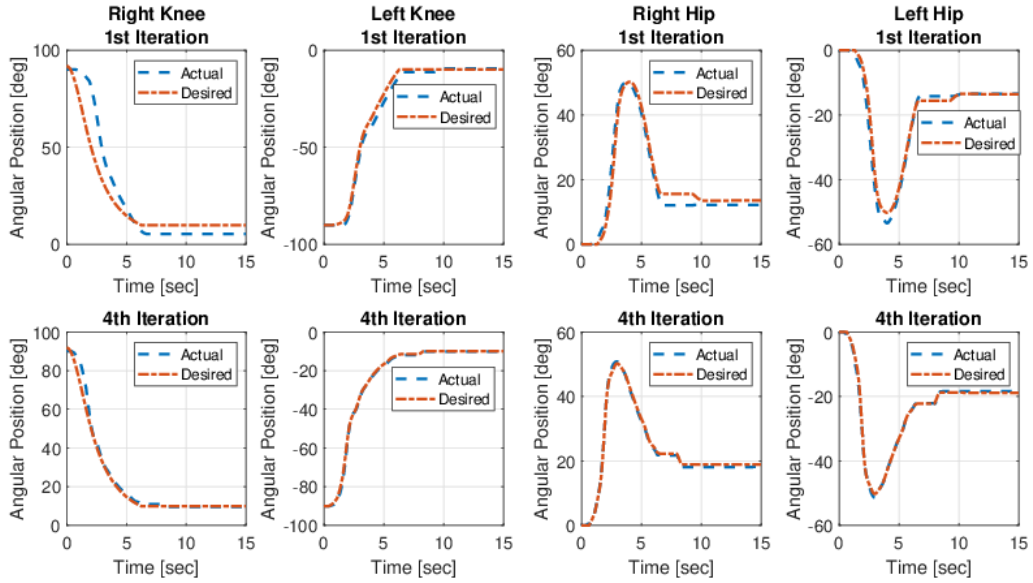


Figure 31: Knee and hip joints angular position tracking results of Participant 4 in the 1st and 4th iterations

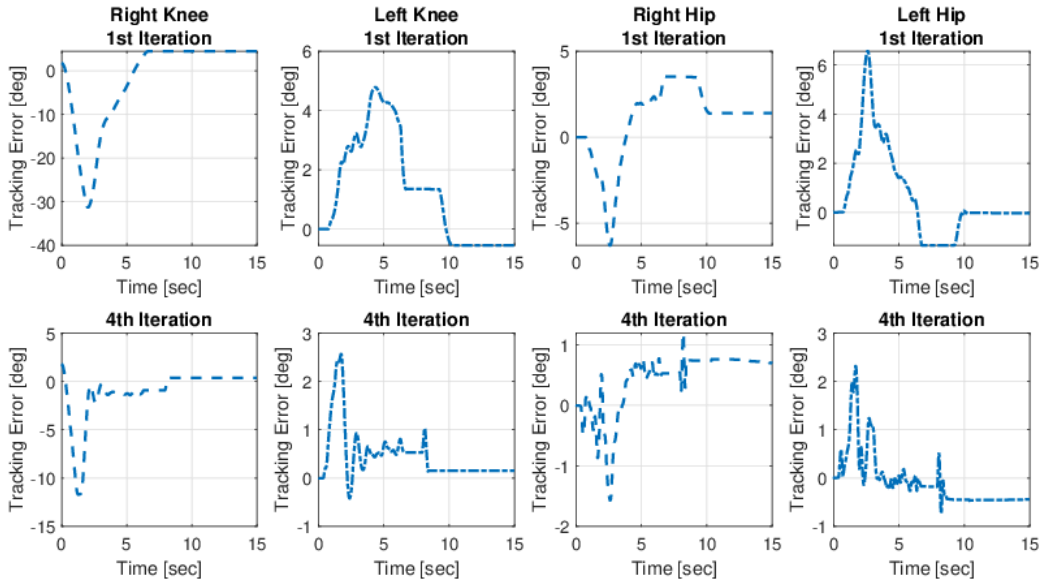


Figure 32: Angular position tracking errors on both knee and hip joints of Participant 4 in the 1st and 4th iterations

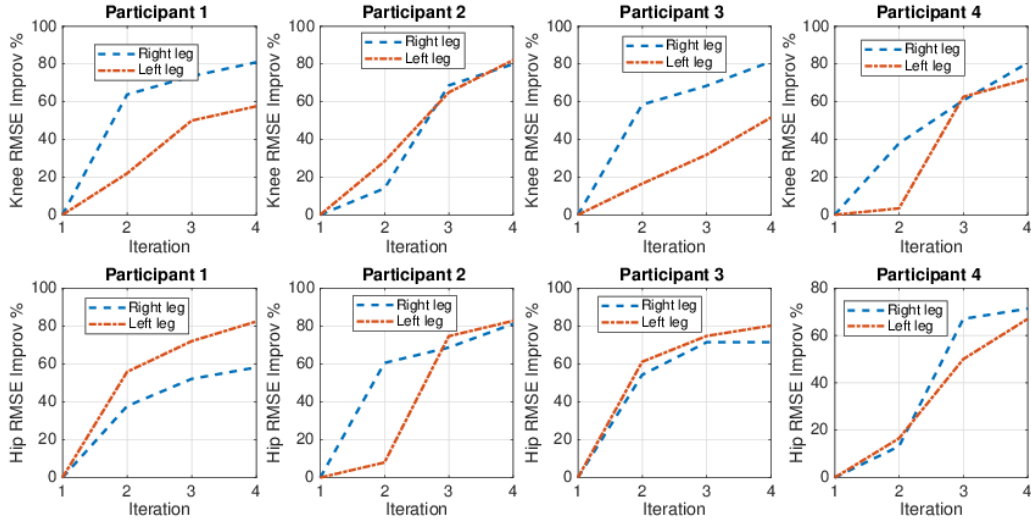


Figure 33: RMSE improvement percentage of both knee and hip joints from the 1st to the 4th iterations for each participant

Participant 4 in four iterations are shown. The components include F_k , $\hat{f}_{2,k}$, and $\hat{\sigma}_k f_{1,k}$. In this figure, F_k represents the additional feedback input and $\hat{f}_{2,k}$ and $\hat{\sigma}_k f_{1,k}$ represent the not linearly parameterizable and linearly parameterizable elements in the system dynamics learned through iterative fashion. As depicted in this figure, the magnitude of F_k decreases while the magnitudes of $\hat{f}_{2,k}$ and $\hat{\sigma}_k f_{1,k}$ increase along with the iterations. Those changes indicate that the contribution of the feedback term F_k in the top level controller is reduced and the contribution of the learning terms is increased. The bottom-level control inputs for 1st and 4th iterations for Participant 2 are shown in Fig. 35. In this figure, ι_k shows the allocation ratio for FES in the k^{th} iteration. At $t = 10$ s, knee motor torque magnitude is 0 and $\iota = 1$, which shows that the constraint on the sum of the allocation ratios is satisfied; i.e., if motor contribution is 0 then FES allocation ratio is 1. Fig. 36 shows the forces applied on the walker handles by Participant 4 in the 1st iteration and the 4th iteration. The results show that the main support forces in the vertical direction were applied on sensor 2 and sensor 4, respectively. The average value of the total forces applied on sensor 2 and sensor 4 in the 1st iteration is 134.18 N, and in the 4th iteration 113.92 N. It is interesting to note that,

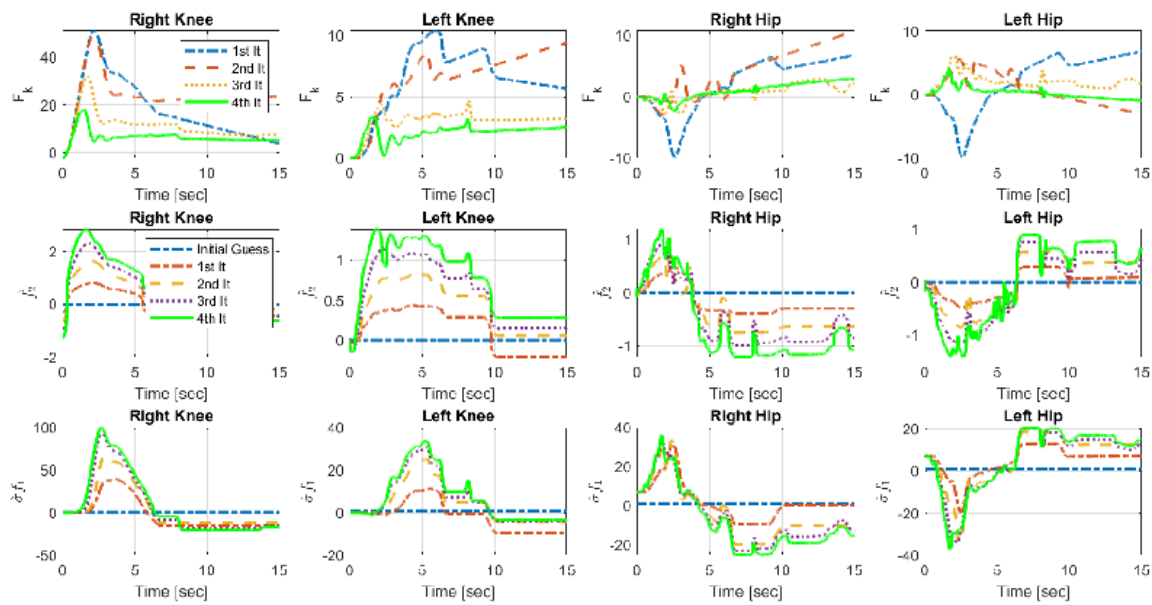


Figure 34: Changes of F_k , \hat{f}_2 , and $\hat{\sigma}f_1$ in the top level controller for Participant 4 in 4 iterations

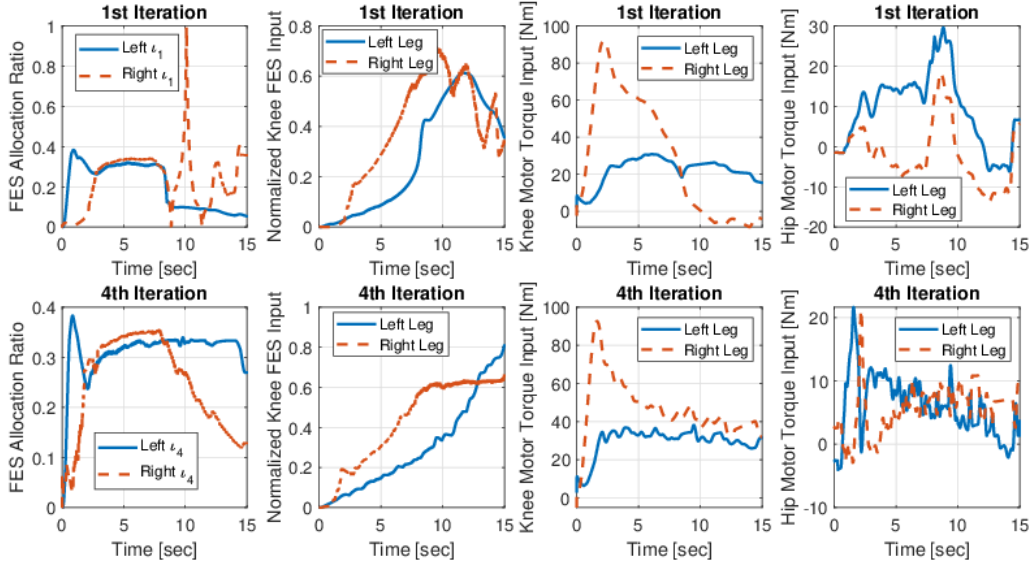


Figure 35: Bottom-level control inputs for Participant 2 allocated by MPC in the 1st and 4th iterations

for Participant 4, through iterative learning, the total force applied on the handles' back ends in the 4th iteration is 15% lower compared to the 1st iteration. Detailed experimental results for all 4 participants are provided in Tables 6 and 7, where $\dot{u}_M^{1st It}$ and $\dot{u}_M^{4th It}$ show absolute mean values of motors control effort in the 1st and 4th iterations, respectively, \dot{u}_F shows mean value of the normalized FES control effort and “Improv” stands for improvement.

5.6 Discussion

A hybrid exoskeleton is a promising rehabilitation intervention that has the potential to assist people with paraplegia during standing and walking activities. A NN-based controller was developed in this chapter to enable a sitting-to-standing task with the hybrid exoskeleton. The results show that the controller improves the tracking performance through an iterative learning process. These results are potentially significant because the clinical implementation

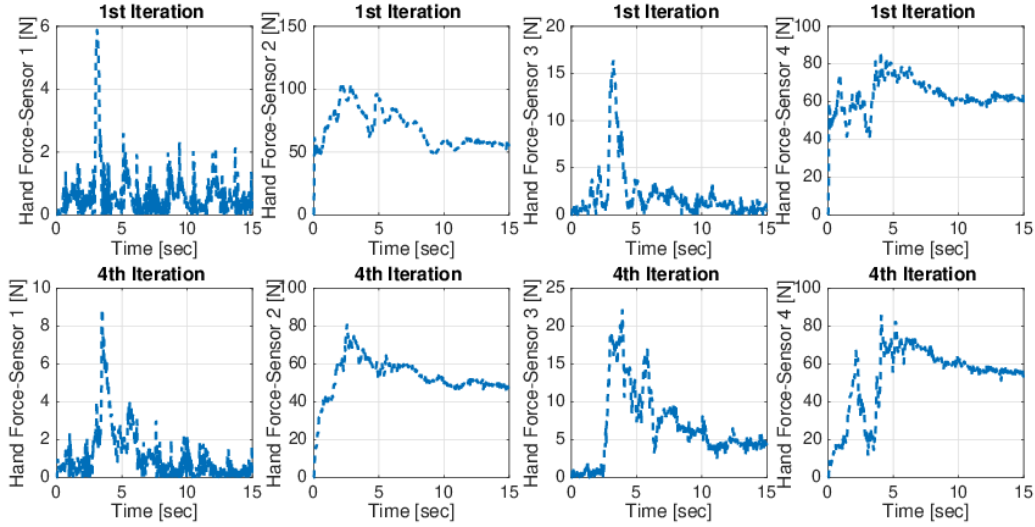


Figure 36: Forces applied on both walker handles in the 1st iteration and 4th iteration during sitting to standing experiments for Participant 4

of existing FES controllers is non-trivial due to inter-person and day-to-day variations in the musculoskeletal models. Most nonlinear control techniques for FES use high-gain controllers [77, 79], while optimal control approaches often involve a tedious process of identifying the model [83, 45]. Alternatively, NNs [2, 3, 72, 78] can be used to learn the model but their implementation needs offline training, which again may be a tedious process in clinics. The proposed NNILC in this chapter learns a participant’s musculoskeletal model in successive iterations. This capability eases its implementation in clinics by reducing gain tuning effort. Additionally, the optimal MPC-based allocator automates the need to specify an allocation ratio between the motor and FES. The proposed control framework eases the parameter tuning process for a clinician/physical therapist. The tuning process can be a daunting task, especially when the tuning process has coupled performance effects and given that a clinician/physical therapist may lack control engineering experience. To validate the control schematic proposed in this chapter, the experiments were performed on three participants without a disability and a participant with SCI.

Table 6: RMSE of trajectory tracking on each participant in the 1st and 4th iterations

Joints RMSE [deg]	RMSE 1 st It	RMSE 4 th It	RMSE Improv %
Participant 1 Right knee	23.11	4.42	80.86
Participant 1 Left knee	3.32	1.41	57.52
Participant 1 Right hip	1.74	0.72	58.14
Participant 1 Left hip	4.14	0.73	82.34
Participant 2 Right knee	9.66	1.94	79.91
Participant 2 Left knee	3.13	0.56	82.01
Participant 2 Right hip	2.04	0.38	81.09
Participant 2 Left hip	2.56	0.44	82.68
Participant 3 Right knee	23.31	4.39	81.17
Participant 3 Left knee	3.33	1.62	51.5
Participant 3 Right hip	2.48	0.71	71.45
Participant 3 Left hip	4.36	0.87	80.15
Participant 4 Right knee	7.44	1.45	80.51
Participant 4 Left knee	1.65	0.46	71.89
Participant 4 Right hip	2.10	0.60	71.29
Participant 4 Left hip	2.21	0.40	66.95

Table 7: RMSE of inputs from motors and FES on each participant in the 1st and 4th iterations

Joints RMSE [deg]	\dot{u}_M^{1st}	\dot{u}_M^{4th}	\dot{u}_F^{1st}	\dot{u}_F^{4th}
Participant 1 Right knee	56.43	52.59	0.44	0.41
Participant 1 Left knee	27.96	26.01	0.26	0.21
Participant 1 Right hip	6.48	6.64	–	–
Participant 1 Left hip	7.73	8.89	–	–
Participant 2 Right knee	36.22	52.43	0.38	0.42
Participant 2 Left knee	22.22	29.72	0.27	0.29
Participant 2 Right hip	6.41	5.90	–	–
Participant 2 Left hip	10.93	6.38	–	–
Participant 3 Right knee	49.45	56.67	0.28	0.35
Participant 3 Left knee	24.67	26.58	0.51	0.25
Participant 3 Right hip	10.85	5.88	–	–
Participant 3 Left hip	8.20	7.66	–	–
Participant 4 Right knee	57.13	94.66	0.43	0.66
Participant 4 Left knee	38.83	26.02	0.36	0.14
Participant 4 Right hip	3.35	5.86	–	–
Participant 4 Left hip	8.15	9.09	–	–

5.7 Conclusion

A novel NNILC augmented with an MPC-based allocation strategy was developed to control a hybrid exoskeleton in this work. A Lyapunov-like based stability analysis was used to prove that the unified control framework yielded asymptotic tracking performance despite of uncertain dynamics and disturbances. Time-invariant trajectories, instead of time-dependent trajectories, were used as desired joint trajectories. The experiments on participants without a disability and a participant with SCI demonstrated that the controller enabled sitting-to-standing task, where the tracking performance was shown to improve in each iteration. The results also showed that the optimal allocation between FES and powered exoskeleton can be achieved by the MPC strategy.

6.0 Summary and Future Works

In this dissertation, switched and iterative control methods to control a hybrid exoskeleton were investigated. A hybrid exoskeleton (HES) is one of the rehabilitation technologies that has the potential of restoring a person's lost standing and walking ability after paraplegia. It provides benefits of both functional electrical stimulation (FES) and a powered exoskeleton. For example, additional therapeutic benefits of FES such as muscle growth and increased bone density can be gained through the use of an HES. Additionally, the size and weight of bulky motors and batteries that are deployed in sole powered exoskeletons can be reduced. The powered exoskeleton can also be used to compensate for the effects of FES-induced muscle fatigue. However controlling this type of devices faces several challenges. Firstly, to control the HES, an allocation strategy is needed to coordinate FES and the powered exoskeleton based on the onset of FES-induced muscle fatigue. Nonlinearity and uncertainty in the dynamic model of HES are another set of challenges that may impede its day-to-day implementation in a clinical setting.

In this dissertation, for addressing the actuation coordination and redundancy problems, novel switching controls that let the system to arbitrary switch the allocation and a model predictive control (MPC) strategy for optimal shared control inputs from motor and FES were used. In this dissertation, a new approach of designing time-invariant desired joint angle trajectories using virtual constraints were used for addressing the problem of joint miscoordination, when time dependent trajectories are utilized. To implement the virtual constraint design, firstly, a novel switching controller that uses a super twisting sliding mode control is developed. However exact model knowledge is required for implementing the method. For addressing this problem, in the next step, a sole switching ILC method was used to learn a linearly parameterizable part of the system dynamics. However it was not able to estimate *not-linearly* parameterizable part of the dynamics. Therefore, in the next study, we developed a novel NN based ILC method that can learn the HES nonlinear dynamics during its operation for overcoming the problem of uncertain HES dynamics. The method was tested in experiments for a sitting to standing task for human participants with no

disabilities and a human participant with SCI. The results showed the effectiveness and ability of the controller for learning the system dynamics and keeping the system stable during the operation. For having a more energy efficient device, next step was to keep the main structure of NN based ILC and do the allocation based on a MPC strategy. Therefore, in the next developed method, a unified (virtual constraint + robust NN based ILC + MPC based allocation) was designed. The control method implemented in several experiments for a sitting to standing task. The experiments on both able bodied and SCI subjects proved that the optimal allocation between FES and powered exoskeleton can be achieved by the MPC strategy.

In the future experiments should validate the ILC _switching framework for producing walking with the hybrid exoskeleton. This may require augmenting the control method with an intent estimation algorithm based the human arm force while using the device. This intention estimation can also be combined with a dynamic movement primitive method so that the desired movement of a task can be dynamically defined by the user. Future work also can focus on using a more rigorous estimation of fatigue using ultrasound imaging-derived fatigue signals [81] so that the controller can switch or change allocation with more precision. A contribution of this thesis, is the use of time-invariant (virtual constraints) desired trajectories. This technique can be extended to our research group's previous work on synergy-inspired control of multiple FES-driven muscles and multiple electric motors of the powered exoskeleton. The muscle synergy-inspired control is especially useful for achieving walking with the hybrid exoskeleton.

Bibliography

- [1] J. J. Abbas and H. J. Chizeck. Feedback control of coronal plane hip angle in paraplegic subjects using functional neuromuscular stimulation. *IEEE Trans. Biomed. Eng.*, 38(7):687–698, 1991.
- [2] James J Abbas and Howard J Chizeck. Neural network control of functional neuromuscular stimulation systems: computer simulation studies. *IEEE Trans. Biomed. Eng.*, 42(11):1117–1127, 1995.
- [3] Arash Ajoudani and Abbas Erfanian. A neuro-sliding-mode control with adaptive modeling of uncertainty for control of movement in paralyzed limbs using functional electrical stimulation. *IEEE Transactions on Biomedical Engineering*, 56(7):1771–1780, 2009.
- [4] N. Alibeji, N. Kirsch, and N. Sharma. A muscle synergy-inspired adaptive control scheme for a hybrid walking neuroprosthesis. *Front. Bioeng. Biotechnol.*, 2015.
- [5] N. Alibeji, N. Kirsch, and N. Sharma. An adaptive low-dimensional control to compensate for actuator redundancy and fes-induced muscle fatigue in a hybrid neuroprosthesis. *Control Eng. Pract.*, 59:204–219, 2017.
- [6] Naji Alibeji, Brad E Dicianno, and Nitin Sharma. Bilateral control of functional electrical stimulation and robotics-based telerehabilitation. *Int. J. Intell. Robot. Appl.*, 1(1):6–18, 2017.
- [7] Naji Alibeji, Nicholas Kirsch, Brad E Dicianno, and Nitin Sharma. A modified dynamic surface controller for delayed neuromuscular electrical stimulation. *IEEE/ASME Trans. Mechatronics*, 22(4):1755–1764, 2017.
- [8] Naji A. Alibeji, Vahidreza Molazadeh, Brad E. Dicianno, and Nitin Sharma. A control scheme that uses dynamic postural synergies to coordinate a hybrid walking neuroprosthesis: Theory and experiments. *Front. Neurosci.*, 12:159, 2018.
- [9] Naji A Alibeji, Vahidreza Molazadeh, Frank Moore-Clingenpeel, and Nitin Sharma. A muscle synergy-inspired control design to coordinate functional electrical stimulation

- and a powered exoskeleton: Artificial generation of synergies to reduce input dimensionality. *IEEE Control Syst. Mag.*, 38(6):35–60, 2018.
- [10] Mohamed Amine Alouane, Weiguang Huo, Hala Rifai, Yacine Amirat, and Samer Mohammed. Hybrid fes-exoskeleton controller to assist sit-to-stand movement. *IFAC-PapersOnLine*, 51(34):296–301, 2019.
- [11] X. Bao, Z. Sun, and N. Sharma. A recurrent neural network based mpc for a hybrid neuroprosthesis system. In *IEEE CDC, Melbourne, Australia*, 2017.
- [12] Xuefeng Bao, Zhi-Hong Mao, Paul Munro, Ziyue Sun, and Nitin Sharma. Sub-optimally solving actuator redundancy in a hybrid neuroprosthetic system with a multi-layer neural network structure. *IJIRA*, pages 1–16, 2019.
- [13] Rihab Bkekri, Anouar Benamor, Mohamed Amine Alouane, Georges Fried, and Hassani Messaoud. Robust adaptive sliding mode control for a human-driven knee joint orthosis. *Industrial Robot: An International Journal*, 45(3):379–389, 2018.
- [14] Mou Chen, Shuzhi Sam Ge, and Bernard Voon Ee How. Robust adaptive neural network control for a class of uncertain mimo nonlinear systems with input nonlinearities. *IEEE Trans. Neural Networks*, 21(5):796–812, 2010.
- [15] Wen Chen, Yang-Quan Chen, and Chih-Ping Yeh. Robust iterative learning control via continuous sliding-mode technique with validation on an srv02 rotary plant. *Mechatronics*, 22(5):588–593, 2012.
- [16] Wen Chen, Yang-Quan Chen, and Chih-Ping Yeh. Robust iterative learning control via continuous sliding-mode technique with validation on an srv02 rotary plant. *Mechatronics*, 22(5):588–593, 2012.
- [17] HJ Chizek, R Kobetic, EB Marsolais, JJ Abbas, IH Donner, and EASE Simon. Control of functional neuromuscular stimulation systems for standing and locomotion in paraplegics. *Proc. IEEE*, 76(9):1155–1165, 1988.
- [18] F. H. Clarke, Y. S. Ledyev, R. J. Stern, and P. R. Wolenski. *Nonsmooth analysis and control theory*, volume 178. Springer, 2008.
- [19] J. Contreras-Vidal, N. Bhagat, J. Brantley, J. Cruz-Garza, Y. He, Q. Manley, S. Nakagome, K. Nathan, S. Tan, and F. Zhu. Powered exoskeletons for bipedal locomotion after spinal cord injury. *J. Neural Eng.*, 13(3), 2016.

- [20] J. Cortes. Discontinuous dynamical systems. *IEEE Control Syst.*, 28(3), 2008.
- [21] Christian A Cousin, Courtney A Rouse, Victor H Duenas, and Warren E Dixon. Position and torque control via rehabilitation robot and functional electrical stimulation. In *ICORR*, pages 38–43. IEEE, 2017.
- [22] A. del Ama, Á. Gil-Agudo, J. Pons, and J. Moreno. Hybrid FES-robot cooperative control of ambulatory gait rehabilitation exoskeleton. *J. NeuroEng. Rehabil.*, 11(1):27, 2014.
- [23] Antonio J del Ama, Aikaterini D Koutsou, Juan C Moreno, Ana de-los Reyes, A Gil-Agudo, and José L Pons. Review of hybrid exoskeletons to restore gait following spinal cord injury. *J. Rehabil. Res. Dev.*, 49(4):497–514, 2012.
- [24] N de N Donaldson and C-N Yu. Fes standing: Control by handle reactions of leg muscle stimulation (chrelms). *IEEE Trans. Rehabil. Eng.*, 4(4):280–284, 1996.
- [25] Nick Donaldson and Chung-Huang Yu. A strategy used by paraplegics to stand up using fes. *IEEE Trans. Rehabil. Eng.*, 6(2):162–167, 1998.
- [26] Victor H Duenas, Christian A Cousin, Anup Parikh, Paul Freeborn, Emily J Fox, and Warren E Dixon. Motorized and functional electrical stimulation induced cycling via switched repetitive learning control. *IEEE Trans. Control Syst. Technol.*, 27(4):1468–1479, 2018.
- [27] Vahideh Ghanbari, Victor H Duenas, Panos J Antsaklis, and Warren E Dixon. Passivity-based iterative learning control for cycling induced by functional electrical stimulation with electric motor assistance. *IEEE Trans. Control Syst. Technol.*, 2018.
- [28] Ashraf S Gorgey, Rodney Wade, Ryan Sumrell, Lynette Villadelgado, Refka E Khalil, and Timothy Lavis. Exoskeleton training may improve level of physical activity after spinal cord injury: a case series. *Topics in spinal cord injury rehabilitation*, 23(3):245–255, 2017.
- [29] K. Graichen and B. Käpernick. *A real-time gradient method for nonlinear model predictive control*. INTECH Open Access Publisher, 2012.
- [30] K. Graichen and A. Kugi. Stability and incremental improvement of suboptimal MPC without terminal constraints. *IEEE Trans. Automat. Contr.*, 55(11):2576–2580, 2010.

- [31] M. Granat, A. Ferguson, B. Andrews, and M. Delargy. The role of functional electrical stimulation in the rehabilitation of patients with incomplete spinal cord injury - observed benefits during gait studies. *Spinal Cord*, 31(4):207–215, 1993.
- [32] R. D. Gregg, T. Lenzi, N. P. Fey, L. J. Hargrove, and J. W. Sensinger. Experimental effective shape control of a powered transfemoral prosthesis. In *2013 IEEE ICORR*, Jun 2013.
- [33] R. D. Gregg, T. Lenzi, N. P. Fey, L. J. Hargrove, and J. W. Sensinger. Experimental effective shape control of a powered transfemoral prosthesis. In *2013 IEEE ICORR*, Jun 2013.
- [34] R. D. Gregg and J. W. Sensinger. Towards biomimetic virtual constraint control of a powered prosthetic leg. *IEEE Trans. Control Syst. Technol.*, 22(1):246–254, Jan 2014.
- [35] K. Ha, S. Murray, and M. Goldfarb. An approach for the cooperative control of FES with a powered exoskeleton during level walking for persons with paraplegia. *IEEE Trans. Neural Syst. Rehabil. Eng.*, 2015.
- [36] K. Ha, H. Quintero, R. Farris, and M. Goldfarb. Enhancing stance phase propulsion during level walking by combining FES with a powered exoskeleton for persons with paraplegia. In *IEEE EMBC*, pages 344–347, 2012.
- [37] E. Hardin, R. Kobetic, L. Murray, M. Corado-Ahmed, G. Pinault, J. Sakai, S. Bailey, C. Ho, and R. Triolo. Walking after incomplete spinal cord injury using an implanted FES system: a case report. *J. Rehabil. Res. Dev.*, 44(3):333–346, 2007.
- [38] Y. Hurmuzlu and D. B. Marghitu. Rigid body collisions of planar kinematic chains with multiple contact points. *INT J ROBOT RES*, 13(1):82–92, 1994.
- [39] Alberto Isidori. *Nonlinear control systems*. Springer Science & Business Media, 2013.
- [40] Sašo Jezernik, Ruben GV Wassink, and Thierry Keller. Sliding mode closed-loop control of FES controlling the shank movement. *IEEE Trans. Biomed. Eng.*, 51(2):263–272, 2004.
- [41] A Kantrowitz. Electronic physiologic aids. *Report of the Maimonides Hospital*, pages 4–5, 1960.

- [42] S. Kim, MD Fairchild, A. Iarkov, JJ Abbas, and R. Jung. Adaptive control for neuromuscular stimulation-assisted movement therapy in a rodent model. *IEEE Trans. Biomed. Eng.*, 56:452–461, 2008.
- [43] N. Kirsch, N. Alibeji, B. E. Dicianno, and N. Sharma. Switching control of functional electrical stimulation and motor assist for muscle fatigue compensation. In *ACC*, Jul 2016.
- [44] N. Kirsch, N. Alibeji, L. Fisher, C. Gregory, and N. Sharma. A semi-active hybrid neuroprosthesis for restoring lower limb function in paraplegics. In *IEEE EMBC*, 2014.
- [45] N. Kirsch, X. Bao, N. Alibeji, B. Dicianno, and N. Sharma. Model-based dynamic control allocation in a hybrid neuroprosthesis. *IEEE Trans. Neural Syst. Rehabil. Eng.*, 26(1):224–232, 2018.
- [46] N. Kirsch, N. and Alibeji and N. Sharma. Nonlinear model predictive control of functional electrical stimulation. *Control Eng. Practice*, 58:319–331, 2017.
- [47] Nicholas Kirsch, Naji Alibeji, Brad E Dicianno, and Nitin Sharma. Switching control of functional electrical stimulation and motor assist for muscle fatigue compensation. In *American Control Conference (ACC), 2016*, pages 4865–4870. IEEE, 2016.
- [48] Nicholas Kirsch, Naji A Alibeji, and Nitin Sharma. Optimized control of different actuation strategies for FES and orthosis aided gait. In *Proc. ASME DSCC*, 2013.
- [49] R. Kobetic, R. Triolo, and E. Marsolais. Muscle selection and walking performance of multichannel FES systems for ambulation in paraplegia. *IEEE Trans. Rehabil. Eng.*, 5(1):23–29, 1997.
- [50] K. Kurosawa, R. Futami, T. Watanabe, and N. Hoshimiya. Joint angle control by FES using a feedback error learning controller. *IEEE Trans. Neural Syst. Rehabil. Eng.*, 13:359–371, 2005.
- [51] Mustafa Kutlu, Chris Freeman, Ann-Marie Hughes, and Matthew Spraggs. A home-based fes system for upper-limb stroke rehabilitation with iterative learning control. *IFAC-PapersOnLine*, 50(1):12089–12094, 2017.
- [52] Frank L Lewis, Darren M Dawson, and Chaouki T Abdallah. *Robot manipulator control: theory and practice*. CRC Press, 2003.

- [53] WT Liberson, HJ Holmquest, David Scot, and Margot Dow. Functional electrotherapy: stimulation of the peroneal nerve synchronized with the swing phase of the gait of hemiplegic patients. *Arch. Phys. Med.*, 42:101–105, 1961.
- [54] D. Liberzon. *Switching in Systems and Control*. Birkhauser, 2003.
- [55] Daniel Liberzon. *Switching in systems and control*. Springer, 2012.
- [56] Fons Luijten, Bing Chu, and Eric Rogers. Iterative learning control for stroke rehabilitation with input dependent muscle fatigue modeling. In *ACC*, pages 6396–6401. IEEE, 2018.
- [57] J Luis Lujan and Patrick E Crago. Automated optimal coordination of multiple-dof neuromuscular actions in feedforward neuroprostheses. *Biomedical Engineering, IEEE Transactions on*, 56(1):179–187, 2009.
- [58] V. Molazadeh, Z. Sheng, X Bao, and N. Sharma. A robust iterative learning switching controller for following virtual constraints: Application to a hybrid neuroprosthesis. In *CPHS. IFAC*, 2018.
- [59] V. Molazadeh, Z. Sheng, and N. Sharma. A within-stride switching controller for walking with virtual constraints: Application to a hybrid neuroprosthesis. In *ACC 2018*. IEEE, Accepted.
- [60] Vahidreza Molazadeh, Zhiyu Sheng, Xuefeng Bao, and Nitin Sharma. A robust iterative learning switching controller for following virtual constraints: Application to a hybrid neuroprosthesis. *IFAC-PapersOnLine*, 51(34):28–33, 2019.
- [61] Vahidreza Molazadeh, Qiang Zhang, Xuefeng Bao, and Nitin Sharma. Neural-network based iterative learning control of a hybrid exoskeleton with an mpc allocation strategy. In *ASME 2019 Dynamic Systems and Control Conference*. American Society of Mechanical Engineers Digital Collection, 2019.
- [62] Vahidreza Molazadeh, Qiang Zhang, Xuefeng Bao, and Nitin Sharma. Preliminary results from shared control of a powered exoskeleton and functional electrical stimulation via iterative learning and fatigue optimization. *IEEE Transactions on robotics*, (submitted).

- [63] Vahidreza Molazadeh, Qiang Zhang, Xuefeng Bao, and Nitin Sharma. A robust neural-network based iterative learning switching controller for a hybrid neuroprosthesis system. *IEEE Transactions on Cybernetics*, (submitted).
- [64] Frank Moore-Clingenpeel, Vahidreza Molazadeh, and Nitin Sharma. An active-subspace-based algorithm for reducing redundancy in a hybrid neuroprosthesis. In *IEEE CDC*, pages 4849–4854. IEEE, 2018.
- [65] J. A. Moreno and M. Osorio. Strict lyapunov functions for the super-twisting algorithm. *IEEE Trans. Autom. Control*, 57(4):1035–1040, 2012.
- [66] National Spinal Cord Injury Statistical Center (NSCISC). Spinal cord injury (SCI) facts and figures at a glance. *National Spinal Cord Injury Statistical Center: Birmingham, AL.*, 2016.
- [67] B. Paden and S. Sastry. A calculus for computing Filippov’s differential inclusion with application to the variable structure control of robot manipulators. *IEEE Trans. Circuits Syst.*, 34 no. 1:73–82, 1987.
- [68] A. Pedrocchi, S. Ferrante, E. De Momi, and G. Ferrigno. Error mapping controller: a closed loop neuroprosthesis controlled by artificial neural networks. *J. Neuroeng. Rehabil.*, 3(1):25, 2006.
- [69] Hugo Quintero, Ryan Farris, Kevin Ha, and Michael Goldfarb. Preliminary assessment of the efficacy of supplementing knee extension capability in a lower limb exoskeleton with FES. In *IEEE Eng. Med. Biol. Soc.*, volume 2012, pages 3360–3, 2012.
- [70] R. Riener and Thomas Fuhr. Patient-driven control of FES-supported standing up: A simulation study. *IEEE Trans. Rehabil. Eng.*, 6:113–124, 1998.
- [71] R. Riener, J. Quintern, and G. Schmidt. Biomechanical model of the human knee evaluated by neuromuscular stimulation. *J. Biomech.*, 29:1157–1167, 1996.
- [72] J. A. Riess and J. J. Abbas. Adaptive neural network control of cyclic movements using functional neuromuscular stimulation. *IEEE Trans. Neural Syst. Rehabil. Eng.*, 8:42–52, 2000.
- [73] C. Rouse, R. J. Downey, C. M. Gregory, C. Cousin, V. H. Duenas, and W. E. Dixon. Fes cycling in stroke: Novel closed-loop algorithm accommodates differences in functional impairments. *IEEE Trans. Biomed. Eng.*, pages 1–1, 2019.

- [74] A. Schäfer, S. Udluft, and H. Zimmermann. The recurrent control neural network. In *ESANN*, pages 319–324. Citeseer, 2007.
- [75] A. Schäfer and H. Zimmermann. Recurrent neural networks are universal approximators. In *ICANN*, pages 632–640. Springer, 2006.
- [76] Jü. Schmidhuber. Deep learning in neural networks: An overview. *Neural networks*, 61:85–117, 2015.
- [77] N. Sharma, C. Gregory, and W. E. Dixon. Predictor-based compensation for electromechanical delay during neuromuscular electrical stimulation. *IEEE Trans. Neural Syst. Rehabil. Eng.*, 19(6):601–611, 2011.
- [78] N. Sharma, C. Gregory, M. Johnson, and W. Dixon. Closed-loop neural network-based NMES control for human limb tracking. *IEEE Trans. Control Syst. Technol.*, 20(3):712–725, 2012.
- [79] N. Sharma, K. Stegath, C. M. Gregory, and W. E. Dixon. Nonlinear neuromuscular electrical stimulation tracking control of a human limb. *IEEE Trans. Neural Syst. Rehabil. Eng.*, 17(6):576–584, 2009.
- [80] Zhiyu Sheng, Vahidreza Molazadeh, and Nitin Sharma. Hybrid dynamical system model and robust control of a hybrid neuroprosthesis under fatigue based switching. In *2018 Annual American Control Conference (ACC)*, pages 1446–1451. IEEE, 2018.
- [81] Zhiyu Sheng, Nitin Sharma, and Kang Kim. Quantitative assessment of changes in muscle contractility due to fatigue during nmes: An ultrasound imaging approach. *IEEE Transactions on Biomedical Engineering*, 2019.
- [82] Yuri Shtessel, Christopher Edwards, Leonid Fridman, and Arie Levant. *Sliding mode control and observation*. Springer, 2014.
- [83] R. Stein, E. Zehr, M. Lebedowska, D. Popovic, A. Scheiner, and H. Chizeck. Estimating mechanical parameters of leg segments in individuals with and without physical disabilities. *IEEE Trans. Rehabil. Eng.*, 4(3):201–211, 1996.
- [84] Mingxuan Sun. A barbalat-like lemma with its application to learning control. *IEEE Trans. Autom. Control*, 54(9):2222–2225, 2009.

- [85] Ziyue Sun, Xufeng Bao, and Nitin Sharma. Lyapunov-based model predictive control of an input delayed functional electrical simulation. In *2nd IFAC Conference on Cyber-Physical & Human-System*, Miami, FL, USA, 2018.
- [86] E. R. Westervelt, J. W. Grizzle, and D. E. Koditschek. Hybrid zero dynamics of planar biped walkers. *IEEE Trans. Autom. Control*, 48(1):42–56, jan 2003.
- [87] Eric R Westervelt, Jessy W Grizzle, Christine Chevallereau, Jun Ho Choi, and Benjamin Morris. *Feedback control of dynamic bipedal robot locomotion*, volume 28. CRC press, 2007.
- [88] Jian-Xin Xu, Ying Tan, and Tong-Heng Lee. Iterative learning control design based on composite energy function with input saturation. *Automatica*, 40(8):1371–1377, 2004.